NTNU
Norwegian University of
Science and Technology

Heat to H$_2$

Hydrogen production in a closed loop RED-system

Ida Johanne Molvik Haga

NTNU

Norwegian University
of Science and Technology

Department of Energy
and Process Engineering

EPT-M-2018-34

MASTER THESIS

for

Student Ida Johanne Molvik Haga

Spring 2018

Heat to H_2

Fra restvarme til hydrogen

Background and objective

Among important research areas for meeting the worlds energy demand and climate challenges are energy storage, renewable energy and efficient resource utilization. These three areas are all integrated in the concept of H_2 production through waste-heat-driven reverse electrodialysis (RED).

RED converts the energy of mixing two solutions with different concentrations to electricity. If the potential produced by the system is high enough, H_2 can be produced directly in the RED cell. For a closed-loop RED system the solutions must be reversed to their original state before re-entering the cell. In this system waste heat is utilized for this reversion.

The goal of the project is to prove the concept of producing H_2 from waste heat using RED.

Two methods for reversal of solutions by heating has been suggested. KNO_3 is an interesting candidate for at least one of these methods and investigating the possibility of using KNO_3 in RED will be an important part of the project.

The following tasks are to be considered:

1. Measuring the transport number of KNO_3 in the membranes used in the RED stack at relevant temperatures and concentrations.
2. Conductivity measurements of membranes soaked in KNO_3 solutions of different concentrations.
3. Electrochemical tests for a RED stack with KNO_3 solutions.
4. Thermodynamic considerations for the two methods of utilizing waste heat for reversal of solution concentrations.

-- " --

Within 14 days of receiving the written text on the master thesis, the candidate shall submit a research plan for his project to the department.

When the thesis is evaluated, emphasis is put on processing of the results, and that they are presented in tabular and/or graphic form in a clear manner, and that they are analyzed carefully.

The thesis should be formulated as a research report with summary both in English and Norwegian, conclusion, literature references, table of contents etc. During the preparation of the text, the candidate should make an effort to produce a well-structured and easily readable report. In order to ease the evaluation of the thesis, it is important that the cross-references are correct. In the making of the report, strong emphasis should be placed on both a thorough discussion of the results and an orderly presentation.

The candidate is requested to initiate and keep close contact with his/her academic supervisor(s) throughout the working period. The candidate must follow the rules and regulations of NTNU as well as passive directions given by the Department of Energy and Process Engineering.

Risk assessment of the candidate's work shall be carried out according to the department's procedures. The risk assessment must be documented and included as part of the final report. Events related to the candidate's work adversely affecting the health, safety or security, must be documented and included as part of the final report. If the documentation on risk assessment represents a large number of pages, the full version is to be submitted electronically to the supervisor and an excerpt is included in the report.

Pursuant to "Regulations concerning the supplementary provisions to the technology study program/Master of Science" at NTNU §20, the Department reserves the permission to utilize all the results and data for teaching and research purposes as well as in future publications.

The final report is to be submitted digitally in DAIM. An executive summary of the thesis including title, student's name, supervisor's name, year, department name, and NTNU's logo and name, shall be submitted to the department as a separate pdf file. Based on an agreement with the supervisor, the final report and other material and documents may be given to the supervisor in digital format.

☒ Work to be done in lab (Water power lab, Fluids engineering lab, Thermal engineering lab, Renewable energy lab)
☐ Field work

Department of Energy and Process Engineering, 15. January 2018

_____   _____
Odne Burheim   Ellen Synnøve Skilbred
Academic Supervisors

Research Advisor:

Preface

This report is composed of thesis work performed throughout the spring of 2018, at the Norwegian University of Science and Technology (NTNU). It constitutes the final 30 credits in the Master's degree in Energy Use and Energy Planning at the Department of Energy and Process Engineering (EPT). The Master's thesis is a continuation of a specialisation project of 15 credits conducted in the fall semester of 2017 [1].

The project is written as part of ongoing research within the strategic research area ENERSENSE at NTNU. Funding for necessary laboratory equipment and stock has been provided by ENERSENSE.

Parts of the thesis work conducted have been compiled in a scientific paper, titled "Heat to H_2 - Using Waste Heat to Set Up Concentration Differences for Reverse Electrodialysis Hydrogen Production". The paper is submitted to ECS Transactions (ECTS), the official conference proceedings publication of The Electrochemical Society. First authorship is shared with Ellen Synnøve Skilbred and Kjersti Wergeland Krakhella, and the paper may be seen in its entirety in Appendix D.

Excellent supervision and support in the project period have been provided by prof. Odne Burheim at EPT. Kjersti Krakhella, PhD candidate at EPT and Department of Materials Science and Engineering, and Ellen Synnøve Skilbred, PhD candidate at EPT, have both been invaluable as co-supervisors. All three deserve great appreciation and gratitude both on a personal and on a professional level.

Several others have been important for the accomplishment of this thesis. The ENERSENSE team, with the additions of Asle Handro Nybakk and Fredrik Heimstad, have been vital both with practical matters and as mental support and cheerleaders. Prof. Svein Sunde at Department of Materials Science and Engineering has provided guidance through the mysterious realms of electrochemistry. Håvard Karoliussen, Associate Professor at the Department of Energy and Process Engineering has been there all along, and has set his mark not only on this thesis, but on all my five years in higher education. My greatest thanks to all of you.

Trondheim, 28.06.2018

Ida J Haga

Abstract

Reverse electrodialysis (RED) in an alternative for production of storable, renewable energy for the future. In the context of climate change, fossil fuel scarcity and international agreements such as the Paris Treaty, innovation to secure a sustainable and reliable energy supply is more important than ever.

RED is a technology that takes advantage of salinity gradient power (SGP), or the release of free energy that occurs whenever two solutions containing different concentrations of a salt meet. Ion exchange membranes divide the ions by charge, thus converting chemical potential to electrical potential. The desired final output in this project is hydrogen gas.

A novel use of this technology is proposed, where heat is added to a system as fuel in order to recharge it. The system is otherwise a closed loop, where traditional disposable electrolytes are replaced with recycled KNO_3. The recycling is enabled by a separation system, where the electrolytes are restored to their initial states by the addition of low quality heat.

Conductivity measurements on membrane samples clarifies the membrane behaviour in KNO_3. Three membranes from Fumatech (Germany) are tested, FAS-50, FAS-30 and FKE-50. The FAS-50 membrane does not display representative conductivity values. FAS-30 and FKE-50 have respective conductivities of 4.3 ± 1.2 mS/cm and 4.5 ± 0.5 mS/cm at 25 °C, and 6.5 ± 2 ms/cm and 6.6 ± 1.3 mS/cm at 40 °C.

A bench-scale RED system is planned, realised and tested under operating conditions suitable for the suggested separation systems. Established membrane potentials are maximum 400 mV for a stack containing 4 unit cells, but some of the tested membranes show unsatisfying performance. Higher potentials are expected for membranes with a normal behaviour.

A theoretical model for RED systems is developed. The model shows that ideal execution of the system may yield power densities above 13 W/m^2 membrane area, a previously unachieved feat. Further iterations of model parameters and practical application should be performed until the model serves as a true representation of an optimised system.

Sammendrag

Revers elektrodialyse (RED) er et alternativ som potensielt kan bidra til produksjon av fornybar, lagret energi for fremtiden. I en kontekst der klimaendringer, knapphet på fossile brensler og internasjonale samarbeidsavtaler som Parisavtalen gjør seg gjeldende, er innovasjon som sikrer en bærekraftig og pålitelig energiforsyning mer aktuell enn noen gang.

RED er en teknologi som utnytter saltgradienter, eller energien som frigjøres hver gang to løsninger med forskjellig konsentrasjon av samme salt møtes. Ioneledende membraner skiller ioner i løsningene etter ladning, og konverterer dermed kjemisk potensial til elektrisk potensial. Det ønskede sluttproduktet i dette prosjektet hydrogengass.

En ny måte å bruke RED-teknologi på er foreslått, der varmeenergi er tilført til et system for å lade det opp. Systemet forøvrig er en lukket krets, der tradisjonelle elektrolytter til engangsbruk er skiftet ut med resirkulert KNO_3. Denne resirkuleringen er mulig ved hjelp av et separasjonssystem som tilbakefører elektrolyttene til starttilstanden ved hjelp av lavkvalitets restvarme.

Målinger av ledningsevne i membranprøver er utført for å kartlegge egenskapene til membraner i KNO_3. Tre membraner fra Fumatech (Tyskland) er undersøkt, FAS-50, FAS-30 og FKE-50. Membranen av typen FAS-50 viser ikke representative konduktivitetsverdier. FAS-30 og FKE-50 har respektive målte ledningsevner på 4.3 ± 1.2 mS/cm og 4.5 ± 0.5 mS/cm ved 25 °C, and 6.5 ± 2 ms/cm og 6.6 ± 1.3 mS/cm ved 40 °C.

Et RED-system i laboratorieskala er planlagt, realisert og testet ved forhold som passer godt i de foreslåtte separasjonssystemene. Oppnådde membranpotensialer er maksimum 400 mV for et system som inneholder 4 enhetsceller, men noen av membranene som er brukt har avvikende oppførsel fra det som er forventet. Det antas at høyere potensialer kan nås med feilfrie membraner.

En teoretisk modell for RED-systemer er utviklet. Modellen viser at ved ideelle forhold kan systemet levere over 13 W/m^2 membranareal, en verdi som ikke tidligere er oppnådd. Videre iterasjoner av modellparametre og praktisk ytelse bør gjennomføres, til modellen fungerer som en nøyaktig representasjon av et optimisert system.

Contents

List of Figures

List of Tables

Nomenclature

Abbreviations

AEM	Anion Exchange Membrane
CEM	Cation Exchange Membrane
CP	Concentration polarisation
DBL	Diffusion boundary layer
DH	Debye-Hückel
DI	Deionised (ultrapure) water
ED	Electrodialysis
EDL	Electric double layer
EIS	Electrochemical Impedance Spectroscopy
IEC	Ion exchange capacity
IEM	Ion Exchange Membrane
OCP	Open circuit potential
PEEK	PolyEther Ether Ketone
RED	Reverse electrodialysis
REN-BTL	Integration of RENewable energy resources for improving current Bio-To-Liquid systems
SGP	Salinity Gradient Power

For IEC: $\frac{mequiv.}{g\ dry\ membrane}$

Constants

F	Faraday constant	96 485 C/mol
N_a	Avogadro's constant	$6.0021 \cdot 10^{23}$ 1/mol

R	Universal gas constant	8.314 J/(mol · K)

Variables

α	Permselectivity of an ion exchange membrane	-
α	Symmetry factor	-
β	Debye length	m
δ	Thickness	m
ϵ	Permittivity	pF/m
ϵ	Spacer porosity	-
η	Reaction overpotential	V
γ	Activity coefficient	-
κ	Conductivity	S/m
ρ	Resistivity	$\Omega \cdot m$
σ	Standard deviation	
A	Effective membrane area	m^2
a	Activity	-
c	Concentration	g salt/100 g solvent
g	Specific gravity	kg/m^3
j	Current density	A/m^2
j_0	Exchange current density	A/m^2
L	Cell length	m
N	Number of membrane pairs	-
P	Power	W
p	Power density	W/m^2
q	Flow rate	m^3/s
R	Resistance	Ω
r	Area resistance	$\Omega \cdot m^2$
R_c	Ionic radius	m
T	Temperature	K
t	Transport number	-
w	Specific weight	kg/m^2

z	The number of electrons transferred in the reaction	-

Sub- and superscripts

Δc	Concentration difference
$\pm$	Mean
an	Anode
app	Apparent
avg	Average
cat	Cathode
$elec$	Electrode
ext	External
$reac$	Reaction
uc	Unit cell
$cons$	In concentrated electrolyte
dil	In dilute electrolyte

Chapter 1

Introduction

The following is in part gathered through the specialisation project work. [1]

Presently, 80 % of the world's total primary energy is obtained from fossil, chemical fuels like oil, gas and coal [2]. Scarcity, negative health impacts and climate impacts make this practice increasingly problematic, and the demand for clean, renewable energy is growing. The Paris agreement, negotiated by 196 parties in 2015, states that the global average temperature should be kept "well below 2 °C above pre-industrial levels", and preferably also limit the temperature increase to 1.5 °C [3]. Although this goal is ambitious, a drastic change in the global energy supply will help to reduce the impact we have on the environment.

Energy for the future needs to be rapidly provided, consistent and with as little negative impacts as possible. The most commercial renewable energy technologies developed so far, like wind and solar power, delivers energy intermittently. The supply fluctuations do not necessarily match the consumption patterns, and to make sure society has access to energy at the right time and the right place, some form of energy storage is required. More than 20 % unadjustable electricity in the supply with no balancing storage present may destabilise the grid [4]. Reliable storage will increase the flexibility and application range of clean energy technologies. This could also contribute to phasing out polluting thermal plants faster by relieving them of the responsibility for the uninterrupted base load.

Efficient and sustainable energy storage may be achieved through the use of hydrogen as an energy carrier. If produced from the right sources, the gas is emission-free regarding CO_2. It is also energy-rich, storable and abundant, and may be produced both centrally and distributed. When comparing energy content, hydrogen performs very well on energy density per weight, but poorer than liquid fuels when it comes to volumetric energy density [5]. Hydrogen carries chemical energy, thus having the benefit of familiarity with society as it is already widely used. However, while chemical energy is well suited for storage and transport, conversion to thermal or electric energy is required before practical utilisation.

RED , or reverse electrodialysis, is a technology that covers the gap between stored and used energy. In a RED system, concentration gradients will create electrical potentials of exploitable magnitudes. This is achieved through the use of ion-conducting membranes, separating solutions with different chemical potentials. When the two solutions are supplied on each side of a membrane, ions will seek to even out the concentration difference and travel through the membrane. This, in turn, establishes an electrical potential, which increases when several membranes are combined in a stack. This is analogous to connecting traditional batteries in series. An electrode rinse solution, containing an ion couple that may be reduced and oxidised on the respective electrodes, is circulated to convert the ionic potential to an electron potential and thus force electrons through the external circuit. [6, 7]

If the potential established by the reversed electrodialysis is higher than the potential required for water splitting, hydrogen evolution is possible. This has traditionally been something to avoid, as high overpotentials have previously been observed [7]. However, this is in the case where the hydrogen gas has not been collected and put to use, while hydrogen harvesting will significantly increase the energy efficiency. If hydrogen is produced indirectly, through an external electrolysis cell running on the RED - produced power, the reported hydrogen produced is only about 1/3 to 1/2 of what is achieved through direct evolution within the stack [7, 8].

Low-quality waste heat is a very large and readily available resource. Enova and McKinsey [9] found in 2009 the potential for available low-quality heat by 2020 to be 13.3 TWh from Norwegian land-based industry alone. The premise for this number is technological possibilities to utilize heat of temperatures down to 60 °C. If the range for usable heat can be expanded to even lower temperatures, the total worldwide potential is presumably of great proportions. An example is the gas processing plant at Nyhamna, Norway, where it is estimated that 313 MW of heat is released at 47 °C [10].This project aims to take advantage of this unused heat potential, in combination with RED, to create flexible and storable energy of high quality. The addition of heat is done to separate solid salt from the aqueous salt solution, thus resetting the electrolytes. Two ways of doing this are proposed, one where the natural precipitation of a saturated solution is utilised, and one where the pure water content of the solution is vaporised. Depending on contexts, such as the expected energy output from the system, the temperature of the available heat and the heat of vaporisation of a substance, both may be viable alternatives. Modelling is required to make the best decision for a specific system.

As the spent electrolytes are not thrown away but rather recharged and reused, the full process will happen in a closed system. Batteries with a continuous supply of electrolyte (flow batteries) have the redox couple directly in the electrolyte and are usually charged by adding current, reversing the reducing and oxidising of the components and thus bringing them to their initial states [11]. In the investigated RED system there is no current added. Instead, the charging process is performed without a redox reaction, exclusively through the addition of heat to the electrolytes.

A RED system is an independent energy technology that may well be used as a stand-alone appliance, converting waste heat to hydrogen where a heat supply is present. However, process benefits may be achieved when it is implemented in a larger industrial process to

serve a specific purpose. The RED setup investigated is intended as part of a novel technology for the production of jet-fuel from biomaterial, where a steady heat supply along with a constant need for the produced hydrogen will ensure a high degree of utilisation.

The process in question is developed by a research group called REN-BTL at the Norwegian University of Science and Technology. The project aims to significantly improve parameters of production of liquid bio-fuels, such as carbon efficiency, energy efficiency, economics and environmental performance. This is done by implementing two systems for renewable production of hydrogen, reverse electrodialysis being one of them. Simultaneously, the heat required for phase separation will be provided from a Fischer-Tropsch synthesis process. With this in mind, a functional mapping of the behaviour of the RED system is crucial. This includes both a model for energy and temperature requirements in the separation process, as well as expected performance regarding hydrogen evolution.

The goal of this project is to investigate a RED system with KNO_3 as electrolyte and hydrogen production as the desired output. Both theoretical and practical approaches are pursued in order to clarify and further develop knowledge about the system and its processes.

Experimentally, both system components and the system itself are investigated. Membrane conductivity is measured for samples soaked in KNO_3 solutions of different concentrations. In addition, the electrochemical performance of a functional system is tested. This includes planning and implementation of a bench-scale reverse electrodialysis rig, including the selection and purchase of components as well as the physical installation. This research includes measurements of open circuit potential (OCP) and polarisation curves, as well as apparent permselectivity and electrode kinetics.

A theoretical calculation model is established for accurate prediction of system performance for different conditions. The results are used for first-tier evaluations of the proposed separation systems.

1.1   Problem formulation

How are key parameters of RED system components altered for various operation conditions, and what consequences do these conditions imply for the total system performance? Is the proposed system a viable energy production alternative?

The goal of the project is experimental research on reverse electrodialysis. Low grade heat will be used as a resource rather than waste, and the end goal is renewable hydrogen production. To reach this target, key parameters for system performance should be established, and obtained through practical experiments.

Chapter 2

Theoretical background

2.1 Literature review

The following is in part gathered through the specialisation project work. [1]

The first attempts of utilising the electrical potential from salinity gradients are more than half a century old. Already in 1954 did Pattle succeed in harvesting power from the osmotic pressure building up when sea and river water mix [12]. His apparatus was called the "hydroelectric pile", and was in essence the first iteration of reverse electrodialysis. The hydroelectric pile was very similar in geometry and construction to the stacks used in salinity gradient power today, with alternating compartments of concentrated and diluted salt solutions separated by anion and cation exchange membranes. The total power density reported was about 200 mW/cm^2. [12]

In the seventies, salinity gradients gained increased attention as an unused power source with high potential [13–15]. Wick and Isaacs (1978) [15] suggest several sources of salts and brines as energy sources, such as salt domes from oil wells, hypersaline lakes and salt ponds along coast lines, in addition to the already recognized mixing at river mouths. The processes involved in electrodialysis were further investigated and improved, with resulting progress in terms of more efficient stack components and polarisation properties as well as continuous operation [16]. Several iterations of theoretical models and equations to predict stack performance has been carried out in parallel with the practical development, performed amongst others by Lacey (1958, 1962, 1965), Weinstein and Leitz (1976), Belfort and Guter (1968) and Forgacs (1975, 1978) [17–22].

Lacey conducted a very thorough investigation of the technology in the beginning of the 1980s, including a model for system performance. He concluded that in order for RED to be an established technology, internal stack resistance would have to decrease, while the power output still needed to increase. [22]

Throughout the 80s and 90s, several groups did research on RED , focusing on improving the power output. A steady increase was obtained, and by 1992 the achieved power density reached 0.40 W/m^2. Although renewed interest favoured reverse electrodialysis in the new millenium, progress was slow, with Turek and Bandura reaching 0.46 W/m^2 in 2007. [23]

Veerman et al.(2008) did a study on the behaviour of the stack with commercially available membranes in 2008, combining 50 unit cells. Now, increased focus was also given to the energy efficiency, not purely the power density. The group found that the main parameters influencing the two was current density and the resistance of the membranes and spacers, in addition to the feed flow rate. They achieved power density of 0.93 W/m^2. [24]

While hydrogen evolution on the cathodes was traditionally seen as disadvantageous due to high overpotentials, Hatzell et al. (2014) suggested that if the hydrogen is harvested as a main product, there was a potential for higher energy efficiency. RED had not been intentionally used for this purpose before. [7]

In 2015, Kingsbury et al. recognised the potential in RED for use as an energy storage technology, as a closed, rechargeable system was constructed. This system relies on applied current through regular (not reversed) electrodialysis (ED) to bring the concentrations of the electrolytes back to their initial states. This technology also achieved the feat of being able to scale membrane area and electrolyte volume (power and energy capacity, respectively) independently of each other. [25]

Some research has been done in order to create a closed loop RED system running on low grade heat, predominantly with ammonium bicarbonate as the charge-carrying electrolyte [7]. However, to the authors knowledge, there has not yet been made systems where both charging by low-grade heat and energy storage is combined in a closed system.

The highest power density to date was achieved by Tufa et al. in 2015, amounting to 2.4 W/m^2. [26]

2.2 Reverse Electrodialysis

The driving force in a RED system, as in any concentration cell, is the difference in chemical potential between solutions that differ in ionic concentrations, but have the same components. Ions seek to even out the concentration differences, and the stronger solution diffuse into the dilute. If a selective barrier is put in place, ensuring that only ions of either positive or negative charge may pass, an electrical potential is established. [27]

Fig. 2.1 is a principle sketch of RED. As solutions flow through the low and high salinity compartments, ions move through the membranes. Anions diffuse towards the anode (left), and cations move towards the cathode. At either end of the stack, electrode rinse solution is circulating. This contains atoms or molecules that undergo reduction and oxidation processes when exposed to adequate potentials, releasing electrons at one electrode and removing them from the other. When a load is connected to the system, the electrons will travel through the external circuit and may produce work. [8]
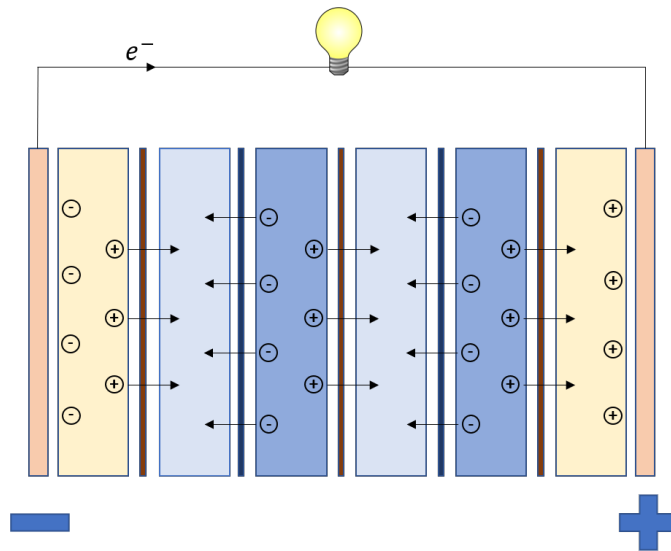
Figure 2.1: The principle of a RED-stack. Dilute and concentrated solutions flow in alternating compartments between ion exchange membranes. Electrode rinse solution circulates at the electrodes, converting ionic potential to electron current.

The combination of one anion selective membrane, one cation selective membrane, dilute solution and concentrated solution, is called a unit cell. Fig. 2.1 depicts two unit cells, in addition to an extra closing membrane at the anode. Combining several unit cells to a stack will increase the potential, analogous to connecting traditional batteries in series.

If the potential established in the stack is sufficiently high, water splitting is possible. This means that the reduction reaction taking place in the stack is in fact hydrogen evolution, while O^{2-} is oxidised to oxygen gas at the anode. Some of, or all, the available potential will then be spent in the gas evolution reactions, and the free energy from the stack is converted to storable chemical energy rather than being immediately spent as work.

2.3 Components and parameters of the RED-stack

The main components of a unit cell are as described in the previous section. In addition, some supporting elements are also present. This includes gaskets, that prevent leaks and maintain the desired flow pattern within the stack, and spacers. Spacers separate the membranes, creating compartments where the electrolytes flow as well as providing mixing to avoid pile-ups of charges at the membrane surfaces.

Fig. 2.2 presents an overview of a complete stack with one unit cell. Feed solutions enter at the bottom end plate, and gaskets control the flow. Electrode rinse solution, also called redox solution, is directed to the electrode compartments, while the electrolytes flow in

alternating layers throughout the stack. Spacers are present in all compartments, shaped to match the gaskets without overlaps.
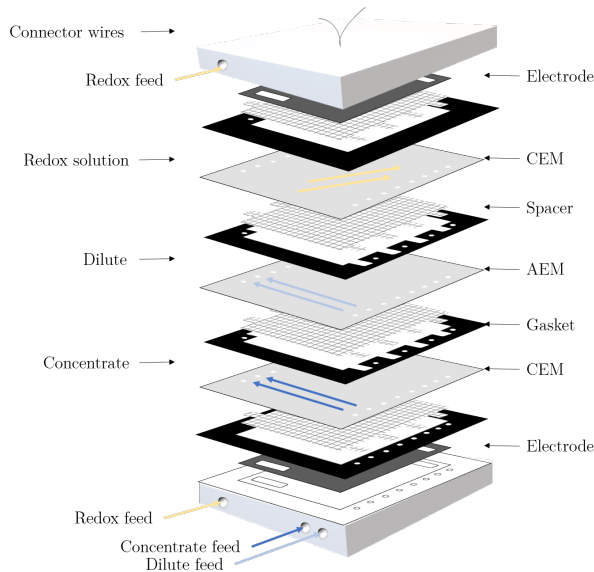
Figure 2.2: The opened RED-stack and all its components

2.3.1 Ion exchange membranes

A membrane is a selective barrier, allowing certain particles to pass through while blocking others. Ion exhange membranes (IEM) are the heart of the RED system and the reason why an electrical potential is present. Their properties are of major importance for the stack performance, and must be chosen carefully.

Like the name implies, ion exchange membranes only permits passage to electrically charged particles. The membranes may be tuned to be selective only to a certain group of ions, commonly ions with either negative or positive charges. This is done by fixing charged groups to the backbone structure of the membrane, giving the membrane itself a certain charge. Electric forces will block ions with the same polarity, allowing only oppositely charged ions that will neutralise the membrane. A membrane with positively charged ions in its structure is called an anion exchange membrane (AEM), and the opposite, where the fixed groups are negatively charged, are called cation exchange membranes (CEM). Both concepts are illustrated in Fig. 2.3. [28]

The kind of fixed charges in the membrane determines its classification. The charged groups of a strong acid membrane are sulfon groups, while weak acid membranes contain carboxylic acid. These are negative charges, making the membranes cation selective. Both
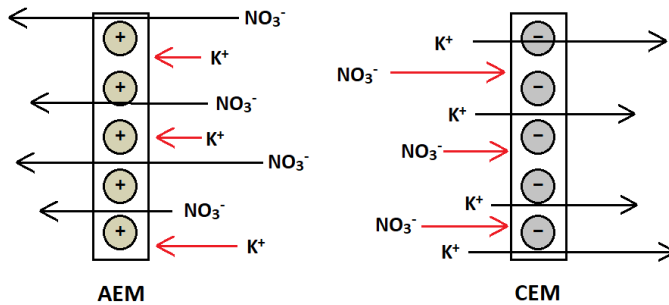
Figure 2.3: Illustration of anion and cation exchange membranes

strong and weak acid membranes contain amines, quaternary in the former case and tertiary in the latter. The membrane properties are influenced by the charge type present in the membrane. [29]

Depending on the way the fixed groups are attached to the structure, membranes are also sorted as homogeneous and heterogeneous. Homogeneous membranes have the charged groups chemically bonded to the bulk material in an evenly distributed fashion over the entire membrane surface. If the membrane is heterogeneous, the charged groups are instead a part of the membrane matrix itself. Most practical membranes are mostly homogeneous. This kind of IEM is generally thinner than the heterogeneous ones, allowing for a lower electrical resistance [29]. [28]

Important properties

The most important properties for ion exchange membranes used in RED are ion exchange capacity (IEC), fixed charge density, swelling degree, permselectivity and electrical resistance. The IEC describes the number of fixed charges per weight in milliequivalents per gram, and will affect most other properties of the membrane. It is therefore a parameter of great importance. [29]

If the number of fixed charges is expressed per volume of water rather than per weight, it is named the fixed charge density (meq./l). Together with the concentration difference of the electrolytes, the fixed charge density determines the ionic transport through the membrane. As the membrane swells, the distance between charges increases, making the fixed charge density strongly dependent on the swelling degree[1]. [29]

A membrane's ability to discriminate between desired counter-ions and unwanted co-ions is reported as its permselectivity. The permselectivity is measured by the transport number of the counter-ion and is related to the fixed charge concentration of the membrane. A

---

[1]The mass increase of the membrane in %, compared to its dry form

lowering of the charge density will also lower the permselectivity. Anion exchange membranes usually swell more than cation exchange membranes, and as a consequence are less selective. Permselectivity is also less ideal for increasing concentrations [30, 31]. [29]

The apparent permselectivity is the ratio between measured membrane potential and the membrane potential as it is theoretically calculated. In practice, this means that an ideally selective membrane has a selectivity of 1.0. The lower the apparent permselectivity, the more undesired ions are permitted through the membrane. This is typically counter-ions of the opposite charge, but can also be other co-ions if the membrane is tailored for one specific ionic species, such as K^+. Water transport may also be the cause of lower apparent permselectivity. [32]

Electrical resistance is crucial in RED applications, as every ohmic loss decreases the output potential and hence the available work. The membrane resistance describes how well the ions move through the structure, and both tortuous transport paths and low ion exchange capacity will increase the losses. Elevated temperatures does the opposite, and is beneficial for the system as long as the membrane material is not damaged.

Membrane resistivity ρ has the unit $\Omega \cdot m$ and is a material property, while membrane area resistance in $\Omega \cdot m^2$, r, is dependent on dimensions and is a membrane property. The two parameters are related through Eq. 2.1. δ is the membrane thickness. [33]

$$r = R \cdot A = \delta \cdot \rho \qquad [\Omega \cdot m^2] \qquad (2.1)$$

Ionic conductivity, κ, is the inverse of the resistivity. It relates to the area resistance as shown in Eq. 2.2. [34]

$$\kappa = \frac{\delta}{r} = \frac{1}{\rho} \qquad [S/m] \qquad \Rightarrow \qquad r = \frac{\delta}{\kappa} \qquad [\Omega \cdot m^2] \qquad (2.2)$$

The concentration of counter-ions within the membrane may be estimated from the IEC, along with the specific weight w and thickness of the membrane. This is shown in Eq. 2.3. Note that this is the concentration per volume membrane, not per volume water in the membrane.

$$c_{memb} = w \cdot \frac{IEC}{\delta} \qquad [mol/m^3] \qquad (2.3)$$

Membranes for RED

For a long time, the membranes used in RED research were not intended for the purpose. The membranes were rather produced for other and more established forms of salinity gradient power (SGP). This is not ideal, seeing as the purpose of the technologies are not the same. An example is the closest counterpart to RED, electrodialysis (ED), where the

stack uses energy to separate different substances rather than mixing substances to generate energy. The membranes used should reflect this difference. The focus of scientists working with RED has been directed towards stack design and the flow and composition of fluids. However, the topic has gained increased attention in the recent years, and several studies have been performed where membranes are benchmarked especially for reverse electrodialysis [30–32]. [29]

Długołęcki et al. (2008), did the first comprehensive study on ion exchange membranes for reverse electrodialysis. By identifying the parameters most dominant for RED power output, commercially available membranes were benchmarked and rated by performance. A model for predicted power density is also established. The membranes tested are chosen for their high selectivity and low electrical resistance, as concluded by Lacey (1980) [22]. The results show that the resistance should be as low as possible, while the permselectivity of the membranes is of lower significance. Hence, emphasis should be placed on resistance rather than the permselectivity when making the compromise in choosing membranes for reverse electrodialysis. [29]

The findings suggest that of the membranes available and tested at the time, the best AEMs for RED are Neosepta AFN from Tokuyama Co. (Japan) (Resistance 0.7 Ω/cm^2 from experiments, 0.4-1.5 Ω/cm^2 given from manufacturer), and Selemion APS from Asahi Glass Co., Ltd. (Japan) (Resistance 0.68 Ω/cm^2 from experiments, 0.5 Ω/cm^2 from manufacturer (measured with AC, where a lower resistance is expected). The best CEM in their experiments is Neosepta CM-1, also from Tokuyama Co. (Japan). Its resistance is found to be 1.67 Ω/cm^2 from experiments, and 1.2-2.0 Ω/cm^2 from manufacturer. [29]

Hong et al. (2015) [30] also did a thorough review of membranes used for RED . The work done by Vermaas et al. (2011) [35] stands out as most promising of the systems reviewed, with a high documented power density. The membranes used in this case were FKS (CEM) and FAS (AEM), both made by Fumatech GmbH(Germany) on demand, with a low thickness of only 33 µm (AEM) and 40 µm (CEM). These membranes are reported to have a resistance of 1.5 and 1.03 Ω/cm^2, respectively. Thinner membranes have a lower resistance, without a great loss of permselectivity [33]. [30]

In addition to good electrical properties, the mechanical properties of potential membranes should be considered. This is especially important in bench-scale research, as the handling of the membranes and the mounting of the stack will be performed manually. Previous experience [1] has shown that membranes as thin as 30 µm have a more significant risk of ruptures and curls, and tend to make the stack mounting process more challenging and time-demanding than what is the case with sturdier membranes. To ease membrane handling and reduce the risk of unforeseen errors, a slight increase in thickness may be favourable. This is however likely to lead to a somewhat higher ohmic resistance in the membrane, which may be of significance in larger stacks.

2.3.2   Spacers

RED -stacks usually contain spacers between the membranes. This is to provide mechanical support for the stack, as well as keeping the membranes sufficiently apart so that

electrolyte flow channels are established. Spacers also have an important purpose in mixing the solutions and deliver fresh supply of ions to the membrane surface to maintain the electric potential. Traditionally, such a spacer is a woven netting, often made from a non-conductive polymer material. [31]

The use of spacers will obstruct both through-plane ion flow and in-plane fluid flow. Obstruction of ion flow is the same as increased ionic resistance, and will cause ohmic electrical losses in the stack. A more complex fluid flow path will increase the pressure losses from pumping of the electrolytes, making the total net power output lower. This is further elaborated in Section 2.4. The growth of microorganisms ('fouling') on spacers in systems with organic material present may also inhibit stack performance, both mechanically and electrically. [31]

Spacer thickness is important for stack performance. In the experiments of Długołęcki et al. (2008), a spacer thickness of 600 μm made the resistance of the dilute compartment so high it dominated most other parameters. Only a low power density was obtainable in this case. With a spacer thickness of 150 μm however, the power density was much higher and the membrane properties, especially the resistance, are much more influential factors. Vermaas et al. (2011) further confirmed these findings, reporting much higher power densities for spacers of 100 μm than for 200 μm and higher. The electrical performance was found to improve with further reduction in spacer thickness, but as the thickness approach zero, the pressure drops and hence the pumping energy required will be unacceptably high. [29, 35]

An option to increase the stack performance is to make ion-conductive spacers out of membrane material. This was found to cut the stack resistance in half compared to geometrically similar spacers of a non-conducting polymer mesh. The pressure drop is still present however. In order to reduce the pressure losses, structured membranes may be an alternative to spacers. If the membrane is profiled, the flow channels and the structural integrity may be preserved without the spacer altogether. This would also improve the electrical performance, as no membrane area is covered by the spacer. [30]

2.3.3 Fluid properties

KNO$_3$ is intended as the electrolyte in the system. K$_2$SO$_4$ is added to the redox compartments, but it is the water itself, the solute, that will undergo reduction and oxidation. K$_2$SO$_4$ acts as supporting electrolyte, increasing conductivity (hence minimising ohmic losses in the electrode compartment) and diminishing the importance of migration as a contributor to transport overpotentials. The latter is elaborated further in Section 2.4.2.

Electrolytes

Accurate conductivity values are necessary knowledge if a good calculation model for the RED system is to be presented. Conductivity as a function of concentration and temperature is required to find the solution resistances r_{cons} and r_{dil}, and may also be used to find the concentration of the spent solutions.

Fig. 2.4 depicts the conductivity of KNO_3 at 25 [36] and 40 °C [1], along with the fitted curve. The conductivity values for 25 °C fit nicely to a second-order polynomial, given in Eq. 2.4. The conductivities for 40 °C are experimental values, and a polynomial of third degree gives the least deviations between fit and real value. This polynomial is given in Eq. 2.5. c is the molality of KNO_3 in g/100 g H_2O.
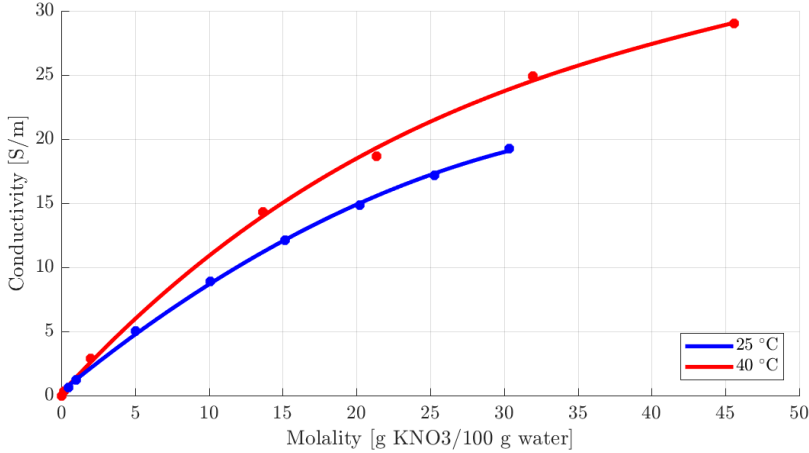
Figure 2.4: Conductivity curve for KNO_3 at 40 °C. [1]

$$\kappa_{KNO_3,25°C} = -0.01062 \cdot c^2 + 0.9414 \cdot c + 0.3086 \qquad [S/m] \qquad (2.4)$$

$$\kappa_{KNO_3,40°C} = 0.0001276 \cdot c^3 - 0.01936 \cdot c^2 + 1.251 \cdot c + 0.1799 \qquad [S/m] \quad (2.5)$$

Even prolonged exposure to air does not noticeably change the conductivity of KNO_3 [1]. A low sensitivity to air exposure is beneficial for laboratory scale experiments, as no special measures are required to ensure that measured results are in fact due to system properties, not air pollution.

Redox solution

The Donnan potential over the end membranes in the stack is positive on one end, and negative on the other. The net potential gain from the redox compartments due to concentration differences is thus zero, and is not necessary to account for. However, the electrode rinse solutions are associated with ohmic losses that should be prevented as much as possible.

To minimise ohmic losses, the solution needs to have as high conductivity as possible. Higher concentrations will increase the conductivity, and so the solution should be as con-

centrated as possible. Conductivity and solubility data for K_2SO_4 at 298 K are presented in Tables 2.1 and 2.2 [37].

Table 2.1: Conductivity of K_2SO_4, 298 K [37]

Concentration [g/100g]	0.50	1.00	2.00	5.00	10.00
Conductivity [mS/cm]	5.8	11.2	21	48	88.6

Table 2.2: Solubility of K_2SO_4, 298 K [37]

Temperature [°C]	0	10	20	25	30	40	60	80	100
Solubility [g/100 g]	7.18	9.3	11.1	12	13	14.8	18.2	21.4	24.1

2.4 Resistance in the stack

The internal resistance in a RED-stack determines the useful power output. It consists of the sum of all individual resistances present, regardless of origin and form. Simplified models only consider the ohmic resistance, while more comprehensive studies also include resistances of a different nature. [30]

In addition to the mathematically predicted resistances, a stack may experience losses from short-circuit currents in the feed channels of the stack, as they work as salt bridges between the compartments. This is prominent in the high salinity compartments, but less significant in the dilute compartments due to lowered conductivity. The short-circuit effect from the redox compartments may be eliminated either by making the solution circulate at each electrode separately, or by having sufficiently long tubes between the electrodes to increase the resistance enough to stop the ions from travelling that route. If the first option is used, where the circulation path is broken, measures must be taken to ensure that there is still fresh supply of both the oxidant and the reductant in the redox couple. [30]

2.4.1 Ohmic resistance

The ohmic resistance of a cell pair consists of the resistance in both membranes, as well as the resistance of the dilute and concentrate compartments. This is multiplied with the number of cell pairs to get the full stack resistance. The electrode resistance should also be taken into consideration, as shown in Eq. 2.6. The electrode resistance includes the resistance of one of the outer membranes, as there is one membrane that is not formally part of a membrane pair [33]. [22]

$$R_{stack} = \frac{N}{A}\left(r_{AEM} + r_{CEM} + r_{sol,dil} + r_{sol,cons} \right) + R_{elec} \qquad [\Omega] \qquad (2.6)$$

where

R_{stack}	Stack resistance [Ω]
N	The number of membrane pairs in the stack
A	Effective membrane area of the membrane pairs [m^2]
r	Area resistance [$\Omega \cdot$ m^2]
sol	Concentrated ($cons$) and diluted (dil) solutions
R_{elec}	Electrode resistance, including resistance of one outer membrane [Ω]

The ionic resistance of a solution in a bounded area is calculated from compartment geometry and conductivity of the electrolyte, similar to membrane resistance. The conductivity, and hence the resistance, is dependent on several factors, such as temperature, type of charge carrier and concentration. [38]

$$r_{sol} = \frac{\delta}{\kappa} \qquad [\Omega \cdot \text{m}^2] \qquad (2.7)$$

The resistance in the dilute compartment is expected to be higher than in the concentrated compartment, due to lower conductivity when fewer ions are present. r_{dil} is usually also dominant compared to the membrane resistance, and is a determining property in the RED stack [33]. Reduced solution resistance is achieved if the compartment thickness is decreased, but if both compartments in a cell are made thinner, the pumping energy required will increase due to larger pressure drops. Eventually, a high pump energy consumption may leave the energy efficiency unacceptably low. A better energetic performance is possible if only the dilute compartment is thinner, but the pressure difference could cause bulging and leakages in the stack. Another approach is to sacrifice some electrical potential by increasing the dilute concentration, this is a question of optimisation. [30]

When a spacer is present in the electrolyte compartments, the ionic resistance of the stack is significantly increased, as the spacer blocks part of the membrane area. Numerical quantification of the ohmic spacer losses is a complex task, without an established consensus on methodology. Usually, a factor is added to the resistance of either membranes or fluid compartments, increasing it. When applied to the membrane resistance, this is sometimes called the shadow factor [25, 30, 39], describing the portion of the membrane area covered by the spacer. When applied to the compartment resistance, both void factor [24, 26] and obstruction factor [33, 40] are used. The void factor is here the relative volume left for the solution, while the obstruction factor simply defines the extra resistance in the compartments that the spacer is creating. Compartment resistance corrected with the obstruction factor is shown in Eq. 2.8.

$$R_{comp} = f_{obs} \frac{\delta}{\kappa A_{cell}} \qquad [\Omega] \qquad (2.8)$$

One way of determining the spacer losses is to measure the experimental power density of a stack and compare with the theoretical output. The spacer influence may then be fitted to the experimental results. The accuracy of this method is higher the better known all the

parameters in the stack are, as everything not accounted for in the theoretical model will be bundled together in the correction factor. [39]

Mathematically, the obstruction factor may be calculated as full space divided by open space, or the inverse of the uncovered compartment in percent. This means that a spacer with an open area of e.g. 52 % will have an area based obstruction factor of $1/0.52 = 1.92$. Open area is usually given as a spacer property. Occupied space may be calculated both as covered area and covered volume. [41]

To calculate the non-covered volume, the spacer porosity ϵ is found. This property is the relation between the specific and apparent gravity g and g_{app} in $\mathrm{kg/m^3}$, which in turn is dependent on specific weight w and thickness δ of the fabric, as shown in Eq. 2.9 and 2.10. [39]

$$g_{app} = \frac{w}{\delta} \qquad [\mathrm{kg/m^3}] \qquad (2.9)$$

$$\epsilon = 1 - \frac{g_{app}}{g} \qquad (2.10)$$

Purely area based obstruction factors are usually too high, because the assumption is that current only follow straight lines. In reality, ionic current can also follow curved lines, making the blocked area smaller than the spacer area. If the obstruction factor is purely based on volume however, it tends to be too low because the ionic path is still tortuous. Hence, the average value of the two is usually closer to reality. The calculated obstruction factor then includes blocked ionic path as well as increased tortuosity, along with the decrease in available conducting solution. [41].

2.4.2 Non-ohmic resistance

Also non-ohmic resistances are found in an operational RED stack. Non-ohmic resistance is different from the ohmic resistance in the fact that it is time and current dependent [33]. When these phenomena are included, the total stack resistance is found through Eq. 2.11. Here, R_{ohmic} is the ohmic resistance as it is described in Eq. 2.6. The $R_{\Delta c}$-term is called the salinity gradient resistance, while R_{BL} is caused by diffusion boundary layers (DBL) in the stack. [30]

$$R_{stack} = N(R_{ohmic} + R_{\Delta c} + R_{BL}) \qquad (2.11)$$

As electrolytes flow through the cell, ions travel through the membrane, causing a slight increase in the dilute concentration and a corresponding decrease in the strong concentration. This concentration gradient causes the concentration difference at the outlet of the cell to be lower than it was at the inlet, with a resulting decrease in power production. This power loss is what $R_{\Delta c}$ represents. The salinity gradient resistance is calculated through

Eq. 2.12. The equation clearly shows that the total stack resistance is influenced by the fluid flow rate, in addition to current density and the more static ohmic resistances. [30]

$$R_{\Delta c} = \frac{\alpha RT}{zFjA} ln \left(\frac{1 + \frac{jL}{zFq_{dil}c_{dil}}}{1 - \frac{jL}{zFq_{cons}c_{cons}}} \right) \qquad [\Omega] \qquad (2.12)$$

where

α	Average membrane permselectivity
R	Universal gas constant, 8.314 J/(mol · K)
T	Temperature [K]
F	Faraday's constant, 96 485 C/mol
z	Charge number
j	Current density [A/m^2]
A	Effective membrane area [m^2]
L	Cell length [m]
q	Flow rate [m^3/s]
c	Concentration [mol/m^3]

As there is electrical interaction between the membranes and the solutions, some interface phenomena may be identified at the membrane surfaces. Closest to the membrane, an electric double layer (EDL) will form. This layer consists of counter-ions piling up near the surface of the membrane, caused by a very steep concentration gradient of counter-ions that arises at the interface. The sudden gradient is due to a much higher density of counter-ions relative to co-ions inside the membrane than in the bulk solution. The EDL is only a few tens of nanometers thick, and will usually not be of significance in a RED stack. Lower salt concentrations will increase the EDL thickness. [33]

Adjacent to the electric double layer, a diffusion boundary layer (DBL) will develop. This is a concentration gradient with a thickness on the scale of some hundred micrometers, caused by the ion transport through the membrane. The mobility of the ions is higher in the membrane than it is in solution, so transport both to and from the membrane is slower than transport through [30]. On the high salinity side, the ions closest to the membrane interface are quickly carried to the other compartment, leaving a lower ion concentration than in the bulk solution. [33]

The opposite is true on the dilute side, where the concentration of ions will be higher close to the membrane than in the bulk. Thin feed water compartments, higher salt concentrations (especially important for the dilute), better mixing and higher flow rates are all measures that may help improve convection and thus minimise the DBL. The term concentration polarisation (CP) refers to the combined effect of the diffusion boundary layers. The resistance from CP may be quite significant in RED systems [30]. [33]

Diffusion boundary layer resistances are often found through fitting of experimental data. Mathematical predictions exist, but they assume knowledge of the surface concentration, a parameter that is quite hard to measure. [30, 42]

2.5 Electrochemical potentials

The possibility to extract energy from salinity gradients is the motivation behind research on RED. This energy will manifest as an electrical potential, and it is of great importance to understand what is causing these potentials as well as being able to quantify the achievable magnitudes.

2.5.1 Liquid junction potentials

Whenever there is a concentration difference between two electrolytic solutions of the same composition, the solutions will also have a difference in chemical potential. This difference is a driving force for ion transport, where the most concentrated solution tends to diffuse into the weaker one. If the anions and the cations migrate at different rates, a potential difference will be established over the interface where the electrolytes meet. This potential is called a liquid junction potential. When expressed in terms of the reversible electrical potential, it is described by the Nernst equation as shown in Eq. 2.13. [27, 43]

$$E^{rev} = \frac{RT}{zF} ln \left\{ \frac{a_{cons}}{a_{dil}} \right\} \qquad [V] \qquad (2.13)$$

where

R	The universal gas constant (8.314 J/(mol $\cdot$ K))
T	Absolute temperature [K]
z	Charge number
F	The Faraday constant ($96\,485$ C/mol)
a	Activity of the concentrated ($cons$) and diluted (dil) solutions

The potential established depends on the migration speed of the ions relative to each other. If the negative anions cross the interface faster than the cations, a net positive potential will be established on the concentrated side (the side being vacated), and vice versa. When a barrier is put in place, preventing mixing of the solutions, the migration speed - and hence the potential - may be influenced and controlled. [43]

If the barrier between the solutions is non-selective, like a porous diaphragm, the mobility of the respective ions, divided by their charge number, will determine the rate. Larger differences in this ratio between the cations and the anions will establish higher potentials, and if the migration rates are identical, no liquid junction potential is expected. If a selective barrier is in place however, like the case is for an ion exchange membrane, the selectivity of the membrane will itself ensure that the ions migrating have a majority of one charge. [43]

Because of electroneutrality, the charge transported across a surface is always balanced. This means that the total charge passed equals the sum of negative and positive charges passed in the same time span. The transport number t of an ion is the ratio of the current it carries, or that ion's part of the current divided by the total current. In a solution of

monovalent ions such as KNO_3, the sum of the transport numbers must equal unity. In practice, the consequence is that when one negative charge is consumed, e.g. when an electron leaves the anode and enters the external circuit of the RED system, one positive charge migrates towards the cathode or a negative charge migrates towards the anode to replace the one consumed. A combination of the two is also possible, as long as balance is maintained. Eq. 2.14 for a species i is thus true. This in turn yields the correlation in Eq. 2.15. [27]

$$t_i^+ + t_i^- = 1 \qquad (2.14)$$

$$t^- - t^+ = (1 - t^+) - t^+ = 1 - 2t^+ = 2t^- - 1 \qquad (2.15)$$

Across a membrane, the liquid junction potential equals the contributions from anionic transport minus the cationic transport. This means that Eq. 2.13 takes the form of Eq. 2.16. The reversible potential E^{rev} is now called the open circuit potential E_{OCP}, because the irreversibilites from non-ideal ion transport are taken into account [42]. The liquid junction potential is also referred to as the membrane potential or the Donnan potential when the junction is across an ion exchange membrane. [27]

$$
\begin{aligned}
E_{memb}^{OCP} &= E_{memb}^{an} - E_{memb}^{cat} \\
&= t_{memb}^- \frac{RT}{zF} ln \left\{ \frac{a_{an,cons}}{a_{an,dil}} \right\} - t_{memb}^+ \frac{RT}{zF} ln \left\{ \frac{a_{cat,cons}}{a_{cat,dil}} \right\} \\
&= \left(t_{memb}^- - t_{memb}^+ \right) \frac{RT}{zF} ln \left\{ \frac{a_{sol,cons}^{1/2}}{a_{sol,dil}^{1/2}} \right\} \\
&= \left(t_{memb}^- - t_{memb}^+ \right) \frac{1}{2} \frac{RT}{zF} ln \left\{ \frac{a_{sol,cons}}{a_{sol,dil}} \right\}
\end{aligned}
\qquad (2.16)
$$

2.5.2 Activities

Activity is a quantity that describes how much the species interact with each other, or the "restlessness" of a substance compared to that in its standard state [43]. For very dilute or non-ionic solutions, the activity is assumed to be increasing linearly with concentration, i.e behaving in an ideal way. In practical application however, the opposite is true more often than not. Charged species affect each other, and an ion experiences coulombic forces from other ions even over relatively large distances. [43]

Substances with high activities are often associated with high Gibbs energy, making them prone to react with other species and to transfer towards lower energies, e.g. by diffusing into more dilute regions. Rates of reaction tend to be fast when the activity is high. [43]

Activity coefficients, γ, describe deviations from ideality. They are the link between concentrations and activities, in the sense that the chemical potential of real solutions depend on activity in the same way as the potential of an ideal solution is dependent on its concentration. In ideal solutions, as well as in pure liquids and solids, the activity coefficient is 1. Eq. 2.17 shows the relation between activity and concentration, with c° as an ideal solution of concentration 1.0 M. It is apparent that the activity coefficient describes how much the activity of an real solution deviates from that of an ideal solution. As the activity describes a ratio, it has no units. [43]

$$a_i = \frac{\gamma_i c_i}{c^\circ} \tag{2.17}$$

The mean activity coefficient for a salt, $\gamma_\pm$, is defined as equal for all species i, as electroneutrality demands that cations and anions always accompany each other. For salts that dissociate completely, for instance nitrates like KNO_3, the activity of the salt is the product of the activities of each of the species. When combining this, the relations in Eq. 2.18 and 2.19 for a salt $A_x B_y$ are found. [27]

$$a_{A_x B_y} = a_{A^{y+}}^x \cdot a_{B^{x-}}^y = a_\pm \tag{2.18}$$

$$a_\pm = \gamma_\pm^x c_{A^{y+}}^x \cdot \gamma_\pm^y c_{B^{x-}}^y = \gamma_\pm^{(x+y)} \cdot c_{A^{y+}}^x \cdot c_{B^{x-}}^y$$

$$= \gamma_\pm^{(x+y)} (x \cdot c_{salt})^x (y \cdot c_{salt})^y = x^x y^y \gamma_\pm^{(x+y)} c_{A_x B_y}^{(x+y)} \tag{2.19}$$

In the case of KNO_3, where both species have the same charge and so the salt dissolves into equally many moles of each type, both x and y are 1. Eq. 2.19 is then simplified to Eq. 2.20.

$$a_\pm = \gamma_\pm^2 c_{salt}^2 \tag{2.20}$$

Activity coefficients in low salinity compartments

The mean activity coefficients $\gamma_\pm$ for salt concentrations lower than about 1 M are found through the Debye-Hückel (DH) law. The law seeks to explain how much charged particles in a solution impacts each other, and hence also the ionic activity. It exists in two varieties; the limited and the extended law, where the extended law, given in Eq. 2.21, provides greater accuracy. However, the extended law contains the ionic radius R_c, a parameter associated with some controversy. It is not indisputably defined, and is seen by some as a mere experimental parameter, whilst in some cases a value close to the diameter of the

water molecule (300 pm) is used. Activity coefficients corresponding to the limited DH law are found for R_c equal to 0. [43]

$$\gamma_\pm = \exp\left\{\frac{z_+ z_- \sqrt{\mu/\mu_{DH}}}{1 + (R_c/\beta)}\right\} \qquad [-] \qquad (2.21)$$

The ionic strength of the electrolyte, μ, is found through Eq. 2.22, where c denotes the concentration of the electrolyte in mol/m^3. μ_{DH} is a property of the solvent, given in Eq. 2.23. The Debye length β for symmetric monovalent electrolytes is calculated through Eq. 2.24. Newly introduced parameters includes the Avogadro number N_a and ϵ, denoting the permittivity of the solvent (ϵ_{water} is 695.4 pF/m). [43]

$$\mu = \frac{1}{2}\sum_i z_i^2 c_i \qquad [\text{mol/m}^3] \qquad (2.22)$$

$$\mu_{DH} = (2\pi N_a)^2 (2RT\epsilon/F^2)^3 \qquad [\text{mol/m}^3] \qquad (2.23)$$

$$\beta = \sqrt{\frac{RT\epsilon}{2F^2\mu}} \qquad [\text{m}] \qquad (2.24)$$

Activity coefficients in high salinity compartments

Ions in solutions interact more and more with each other for increasing concentrations, enhancing the deviation from the ideal case. When the concentration of the dissolved salt exceeds a certain limit, the Debye-Hückel law loses its accuracy and is no longer representing reality. Some salts, like NaCl and KF, have minimums on their curves when γ is plotted versus high concentrations, features that are not revealed by the DH-equations [37]. [43]

Experimental values may be determined, for instance with ion selective electrodes [44]. Table 2.3 shows the mean activity coefficients for KNO$_3$ for concentrations ranging from 1 M to about 3.5 M. The temperature is 298 K.

Table 2.3: Mean activity coefficients for KNO$_3$ at concentrations over 1 M. 298 K. [44]

mol/kg	0.995	1.175	1.389	1.587	1.798	1.996	2.488	2.98	3.49
g/100 g	10.06	11.88	14.04	16.04	18.18	20.18	25.15	30.13	35.28
$\gamma_\pm$	0.523	0.483	0.455	0.439	0.431	0.427	0.404	0.398	0.382

Mean activity coefficients for the full range of KNO$_3$ concentrations possible at 298 K are presented in Fig. 2.5 [37, 44]. The two references give slightly differing values, but display a similar trend, especially for low concentrations.
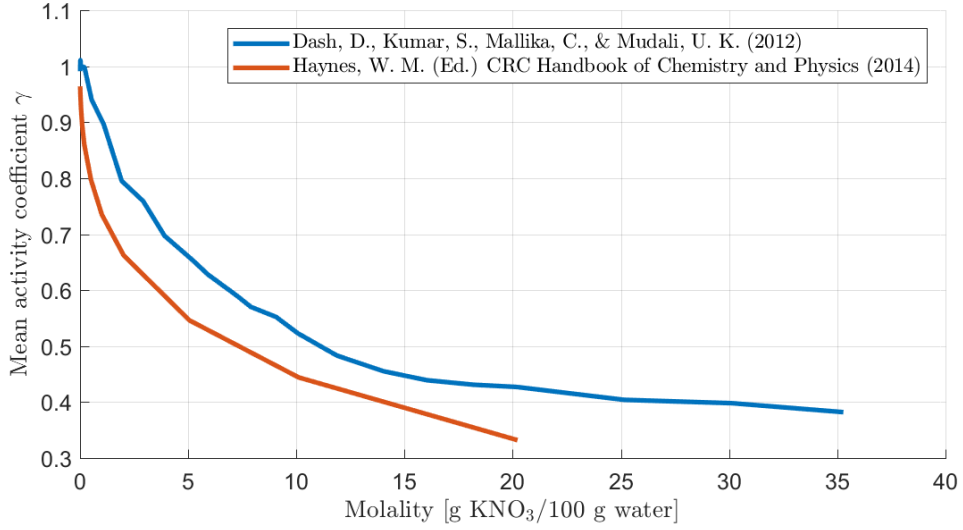
Figure 2.5: Mean activity coefficients for KNO_3 at 298 K [37, 44]

2.5.3 Unit cell and stack potential

When combined with streams of salt solutions, two membranes together make up a unit cell, and several unit cells make up a stack. Each membrane will contribute with a liquid junction potential as described in Eq. 2.16, establishing the unit cell potential in Eq. 2.25. Note that the signs of the transport numbers are shifted for the two membranes, and that both membrane contributions to the cell potential have the same polarity. [27]

$$E_{uc}^{OCP} = \frac{1}{2}\left[\left(t_{AEM}^{cat} - t_{AEM}^{an}\right) + \left(t_{CEM}^{an} - t_{CEM}^{cat}\right)\right]\frac{RT}{zF}ln\left\{\frac{a_{cons}}{a_{dil}}\right\} \quad (2.25)$$

The permselectivity α of the cation exchange membranes equals $(t^- - t^+)$. Conversely, the permselectivity of an anion exchange membrane is $(t^+ - t^-)$. When these simple relations are inserted into Eq. 2.25, the final OCP of the unit cell is as presented in Eq. 2.26. [27]

$$E_{uc}^{OCP} = \frac{1}{2}\left(\alpha_{AEM}^{an} + \alpha_{CEM}^{cat}\right)\frac{RT}{zF}ln\left\{\frac{a_{cons}}{a_{dil}}\right\} = \alpha_{avg}\frac{RT}{zF}ln\left\{\frac{a_{cons}}{a_{dil}}\right\} \quad (2.26)$$

When several unit cells are placed together in a stack, the theoretical potential is accumulated potential from each pair, shown in Eq. 2.27. N is the number of cell pairs. [33]

$$E = N \cdot E_{cell} = N \cdot \alpha_{avg}\frac{RT}{zF}ln\left(\frac{a_{cons}}{a_{dil}}\right) \qquad [V] \quad (2.27)$$

The total output voltage from the stack is the OCP subtracted the internal voltage drops across the stack.

$$E_{stack} = E_{OCP} - rj \qquad [V] \qquad (2.28)$$

2.5.4   Power density and area considerations

When current is drawn from the cell, the obtained power density is found from Ohm's law and Eq. 2.28, resulting in Eq. 2.30.

$$p = E_{cell}j \qquad [W/m^2] \qquad (2.29)$$

$$p = E_{OCP}j - rj^2 \qquad [W/m^2] \qquad (2.30)$$

The current in the stack is also found through Ohm's law, with the resistance being the sum of the internal resistance, r_{stack}, and the external load resistance r_{ext}.

$$j = \frac{E_{cell}}{r_{stack} + r_{ext}} \qquad [A/m^2] \qquad (2.31)$$

The maximum gross power output from the stack is obtained when the load resistance is equal to the stack resistance. This occurs when the current is half of the short circuit current, and the stack potential is approximately half of the open circuit potential [33].

$$p_{max} = \frac{E_{OCP}^2}{4r_{stack}} \qquad [W/m^2] \qquad (2.32)$$

When a current or current density is known, H_2-production rate may be calculated through Faraday's law of electrolysis, as shown in Eq. 2.33.

$$n = \frac{It}{zF} \qquad [mol]$$

$$\dot{n} = \frac{jM_m}{zF} \qquad [kg/(m^2 \cdot h)] \qquad (2.33)$$

All units in this section are given per area, so that system properties may be compared to previous and future research. To avoid confusion, it is of great importance to precisely define what area is used in the normalisation, as both membrane area and cross-sectional

area are meaningful parameters. The membrane area in a unit cell is twice as large as the cross-sectional area, as two membranes make up a cell. This means that power density per membrane area must be reduced with a factor two compared to power density per cross-sectional area. Membranes suited for RED come at a high cost, making them the limitation towards making RED economically viable [26]. It is thus reasonable to include the full membrane area required when evaluating systems. Power density per membrane area is also a common unit in prominent RED research [25, 26, 30, 31, 33].
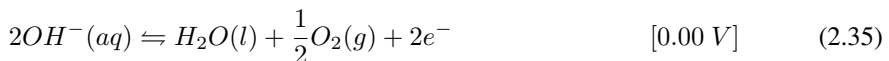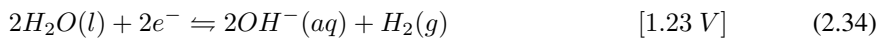
2.6   Electrodes

2.6.1   Redox reactions

The electrode rinse solution, or the redox solution, is circulating at the electrodes, with the purpose of converting the ionic potential to an electron surplus, enabling practical use of the stack. The redox name alludes to the reduction and oxidation reactions resulting from high potentials, releasing electrons. When an oxidation process takes place at the cathode, a reduction process happens simultaneously at the anode. In many cases, the redox couple is two oxidation states of the same ion, for instance Fe^{2+} and Fe^{3+}, where one is formed and one is removed on each electrode. [45]

When hydrogen evolution is the target, water is the redox solution. Oxygen gas is produced at the anode, while the reduction of H^+ at the cathode generates hydrogen gas.

In alkaline environments, the water splitting reactions are as presented in Eq. 2.34 and 2.35. The oxygen evolution reaction takes place at the cathode, and the cathode half cell potential is +1.23 V. The hydrogen evolution reaction has by definition a potential of 0 V, and so the total cell voltage for the reaction is $E_{cell}^\circ = E_{an}^\circ - E_{cath}^\circ = -1.23\ V$. [46]

$$2H_2O(l) + 2e^- \rightleftharpoons 2OH^-(aq) + H_2(g) \qquad [1.23\ V] \qquad (2.34)$$

$$2OH^-(aq) \rightleftharpoons H_2O(l) + \frac{1}{2}O_2(g) + 2e^- \qquad [0.00\ V] \qquad (2.35)$$

Anodic current at a working electrode is by convention positive. [43]

2.6.2   The use of Ni as electrode material

pH is defined as minus the logarithm of the activity of hydronium ions, as shown in Eq. 2.36. The concept of activity is elaborated in Section 2.5.2. For ideal solutions, the activity of a solution equals its concentration, and this is a simplification often made. [43]

$$pH = -log_{10}\left(a_{H_3O^+}\right) \approx -log_{10}\left[H_3O^+\right] \qquad (2.36)$$

Aqueous electrode reactions for many of the elements involve hydronium or hydroxide ions, H_3O^+ and OH^-. This means that the extent of the electrode reactions in many

cases depend on the pH of the solution. Pourbaix diagrams, also known as potential-pH diagrams, shows which species in an equilibrium are dominant for various potentials and pH-values, and are powerful tools to predict what reactions will take place in a system. Both corrosion and water splitting may be taken into account, and avoided if necessary. Horizontal lines in the diagrams represent purely electrical reactions, meaning simple redox reactions where only one electron is transferred. Vertical lines represent the opposite, namely purely chemical reactions without any electron transfer at all. The combination, where both electrons and protons are transferred in the same reaction, are represented as diagonal lines. [43]

The potential for a reaction is dependent on the Nernst reaction, as shown in Eq. 2.13. The hydrogen evolution reaction in Eq. 2.34 is combined with the equation for pH, Eq. 2.36. Together, they yield the pH-dependent potential for hydrogen evolution, as shown in Eq. 2.37. This results in a diagonal line in the Pourbaix-diagram for water. The activity of the solvent, water, is assumed equal to 1.0. [43]

$$E = E^\circ - \frac{RT}{zF} ln \left\{ \frac{a_{H_2}}{(a_{H^+})^2} \right\}$$

$$= 0 \ V - \frac{8.314 \cdot 298 \cdot \ln \ 10}{2 \cdot 96485}$$

$$= 0 \ V - \frac{0.059}{2} log \left\{ \frac{1}{(a_{H^+})^2} \right\}$$

$$= -\frac{0.059}{2} (log \ 1 - log \ (a_{H^+})^2)$$

$$= -\frac{0.059}{2} - log \ (a_{H^+})^2$$

$$= -0.059 \cdot -log \ (a_{H^+}) \ = \ -0.059 \ V \cdot pH \quad\quad (2.37)$$

The same logic is applied for the oxygen evolution reaction of Eq. 2.35, with the resulting pH-dependent potential shown in Eq. 2.38.

$$E = E^\circ - \frac{RT}{zF} ln \left\{ \frac{a_{O_2}(a_{H^+})^2}{(a_{H_2O})^2} \right\} \cdot \ln \ 10$$

$$= 1.23 \ V - \frac{0.059}{2} \cdot log \left\{ (a_{H^+})^2 \right\}$$

$$= 1.23 \ V + 0.059 \cdot -pH \ = \ 1.23 \ V - 0.059 \ V \cdot pH \quad\quad (2.38)$$

The Pourbaix diagram for nickel may be made very complex, depending on how many species, temperatures and concentrations of nickel ions one choose to include. A simplified version, relevant for the RED application in question, may include solid nickel, Ni^{2+} and NiO. The reduction of Ni^{2+} to solid nickel is a purely electrical reaction, given in Eq. 2.39. More negative potentials will drive the reaction in the cathodic direction, meaning
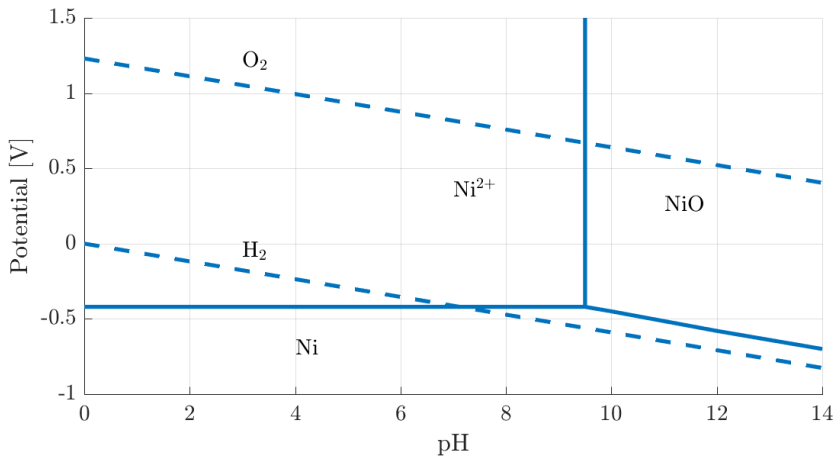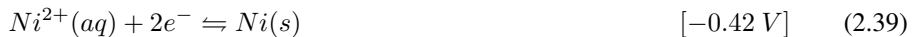
Figure 2.6: The Pourbaix diagram for the nickel-water system present at the electrodes

the reduced species is the dominant one. This means that solid Ni is dominating for lower potentials, and vice versa. [43]

$$Ni^{2+}(aq) + 2e^- \leftrightharpoons Ni(s) \qquad [-0.42\ V] \qquad (2.39)$$

The equlibrium between Ni^{2+} and NiO is purely chemical, and is represented by a straight line in the diagram. Both electrons and protons are transferred between solid nickel and NiO, resulting in a diagonal line in the plot. The total Pourbaix diagram for the nickel-water system is shown in Fig. 2.6. [47]

From the diagram, it is apparent that hydrogen evolution and oxidation of solid Ni to $Ni^{2}+$ competes for pH-values under 7. This means that the nickel electrodes may corrode, and the desired behaviour from the RED stack will not occur.

2.6.3 Kinetic overpotentials

If the forward and backwards reaction rates of an electrode reaction are not equal, meaning that the reaction move away from equilibrium, some potential is lost due to inherent reaction slowness. These electrode reaction overpotentials are denoted η.

The exchange current density j_0 is the current where chemical equilibrium occurs. This is where the products of a reaction are consumed as quickly as they are formed, also called the equilibrium current density. This is a parameter that differs between electrode materials as well as between reactions. [27]

The net current density j is obtained through Eq. 2.40. α is in this setting not related to permselectivity, but rather denotes the charge transfer coefficient for the electrode reac-

tions. For single-step reactions is this factor also called the symmetry factor, and always sums to 1 for the anodic and cathodic reaction direction. If the reaction is favoured more in one direction than the other, α have different values for each direction. If the opposite is true are both symmetry factors equal to 0.5. [27].

$$j = j_0 \left(exp \left[\frac{(1-\alpha)zF}{RT} \eta_{an} \right] - exp \left[\frac{\alpha zF}{RT} \eta_{cat} \right] \right) \qquad [\text{A/m}^2] \qquad (2.40)$$

where

α	Symmetry factor [-]
R	The universal gas constant (8.314 J/(mol $\cdot$ K))
T	Absolute temperature [K]
z	Charge number
F	The Faraday constant (96 485 C/mol)
eta	Overpotentials at the anode (an) and cathode (cat)

The cathode overpotential η_{cat} equal to the anode overpotential η_{an} is defined as the reaction overpotential η_{reac}, where sign convention indicates which reaction is involved. A positive reaction overpotential is an oxidation reaction, while a negative overpotential is a reduction reaction. Eq. 2.40 may then be written as in Eq. 2.41. [27]

$$j = j_0 \left(exp \left[\frac{(1-\alpha)zF}{RT} \eta_{reac} \right] - exp \left[-\frac{\alpha zF}{RT} \eta_{reac} \right] \right) \qquad [\text{A/m}^2] \qquad (2.41)$$

Product formation and reactant formation contribute with one part each to Eq. 2.41. For small overpotentials are both contributions important, but as the overpotentials increase, one side will dominate and the other is negligible. This allows the simplification in Eq. 2.42, valid for high positive overpotentials. This equation is known as the Tafel overpotential equation. The coefficient b is the slope of the potential vs. log j curve. [27]

$$j = j_0 exp \left[\frac{(1-\alpha)zF}{RT} \right]$$

$$\eta_{reac} = \frac{RT}{(1-\alpha)zF} ln \frac{j}{j_0}$$

$$\eta_{reac} = -\frac{2.303RT}{(1-\alpha)zF} log j_0 + \frac{2.303RT}{(1-\alpha)zF} log j$$

$$\eta_{reac} = b \, log \frac{j}{j_0} = -b \, log(j_0) + b \, log(j)$$

$$\eta_{reac} = a + b \, log \, j \qquad [V] \qquad (2.42)$$

The cell potential available for useful work is found when all internal losses as subtracted, as shown in Eq. 2.43

$$E_{cell} = E^{rev} - \eta - jr \qquad [V] \qquad\qquad (2.43)$$

2.7 Phase separation processes

The phase separation process is the key to a closed system, and the requirement to define the RED -system as a battery. If the spent electrolytes are recovered, heat may be used to restore them to their initial states. This ensures that heat is the only consumable in the system, preferably at a low temperature. Such heat is of low quality and is seldom put to use, often referred to as waste heat.

As the electrolytes flow through the stack, ions will move through the membranes from the concentrated to the dilute compartments. This causes the concentration of the stronger solution to decrease, while the dilute concentration increases. Eventually, this will degrade the electrical potential of the stack. To ensure continued and efficient operation, solution concentrations must be kept as constant as possible.

Two ways of utilising heat for phase separation are proposed. The first possibility is precipitation, where the saturation properties of the electrolyte are exploited to remove excess salt from the dilute. Alternatively, heat can be added to evaporate water from the concentrate, making it stronger.

The main question to be answered when evaluating separation techniques is efficiency, or how much energy input that is required compared to the electrical output expected from the stack. As the achievable concentration difference will differ between the techniques, the stack potential is likely to differ too. Simultaneously, the heat amount and temperature required to run the process is not the same in the two cases and this may affect the internal energy consumption.

The capital costs associated with the proposed RED system are dominated by expenses to membranes and heat exchangers. The heat exchanger area required to produce a certain amount of H_2 (i.e to restore a certain amount of electrolyte) is thus also of interest when evaluating the technologies.

2.7.1 Separation by precipitation

When precipitation is used for phase separation, saturated electrolyte is used in both compartments. For the concentrate, the objective is as before to use the concentration that yields the best electrical properties, usually as high concentration as possible. For the dilute however, it is now desired to choose a concentration so that it is saturated at a certain temperature. By cooling the pipe to the saturation temperature, excess salt will precipitate and may be transferred to the stronger reservoir. This is illustrated in Fig. 2.7.

To avoid high energy consumption for cooling, it is wise to choose the lower saturation temperature so that it corresponds to the temperature of any available cooling, e.g. seawa-
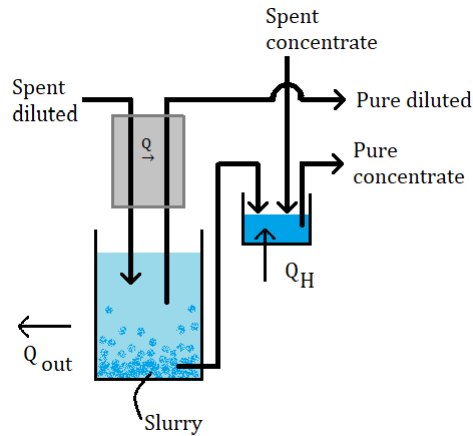
Figure 2.7: Process sketch of a separation system using precipitation

ter. The use of natural cooling will significantly reduce the energy consumption, and thus increase the potential for large scale operation. In Trondheim, the seawater temperature at 30 m below the surface is typically 7-12 °C [48].

For precipitation to be a reasonable separation alternative, the salt in question must have a solubility that is strongly dependent on temperature. Fig. 2.8 depicts the solubility curves for several common salts. It is apparent that KI and KNO_3 are examples of salt where a relatively large concentration difference is obtainable within a given temperature interval, while NaCl is less beneficial in a precipitation system.
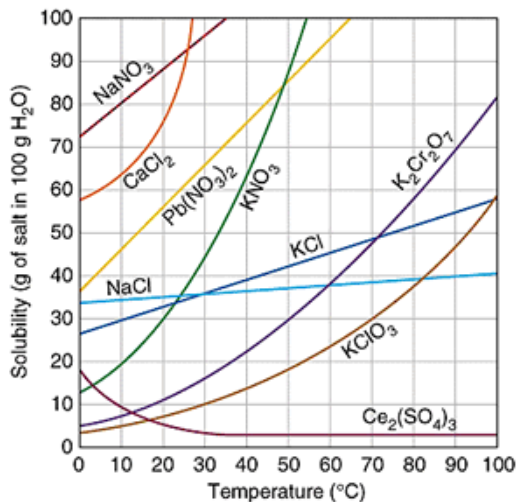

Figure 2.8: Solubility curves for a variety of common salts [49]

2.7.2 Separation by evaporation

A principle sketch of a separation system using evaporation is shown in Fig. 2.9. Here, external heat is added to the concentrate, making the water boil off. Eventually, the concentration will be strong enough for the original potential to be restored, while the removed water will ensure a low concentration in the dilute electrolyte. For improved energy efficiency, the condensation energy of the pure water should be used to maintain the temperature in the separation container.
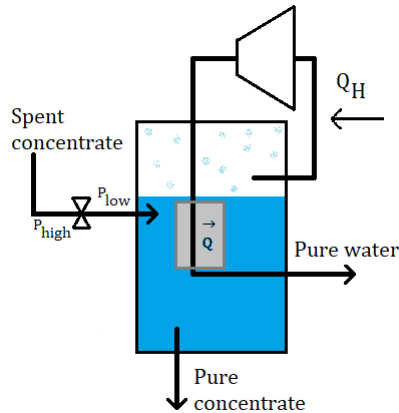

Figure 2.9: Process sketch of a separation system using evaporation

This separation system is presumably energetically disadvantageous, as large quantities of heat are required to make the water evaporate. The process will also be faster if the temperature is higher, thus creating a possible need for heat of higher quality. However, in this system the lower concentration limit is very low, making the possible Nernst's potential higher and allowing the use of electrically optimised solutions. The electrical gain must be weighted against the thermal loss in the evaluation. If the heat added is surplus, meaning that it would not have been put to any other use, the actual amount and temperature may be of less importance.

2.8 Measurement techniques

The sum of all the component resistances in the system is a good representation of the total stack resistance, with reservation that the individual resistances are measured in a satisfactory way. Membrane resistance is an important parameter, and erroneous assumptions in the calculation will impact the final output noticeably.

When the feed solution concentration differs from the concentration at which the measurements were performed, the resistance changes substantially, and so the apparent stack resistance is often quite different from the theoretically calculated resistance. An improved

representation of the stack must therefore contain updated models for the effect of concentration and temperature changes. [30]

2.8.1   Membrane resistance

Measured membrane resistance is dependent on numerous factors, such as temperature and type of solution used for membrane immersion. The measurement technique itself also impacts the result to a large extent, and it is therefore important to be aware of the features of the various methods.

A common way to measure the membrane resistance is through direct current (DC). Electrodes on each side of the membrane are used to apply an ionic current, while reference electrodes measures the voltage drop caused by the membrane. The DC-method measures ohmic resistance, as well as resistance due to double layers and diffusion boundary layers, and the obtained result is thus the sum of ohmic and CP resistance. [33]

When alternating current (AC) is used instead of DC, no net current is passed through the membrane. This allows for separate evaluations of the resistance of the polymer itself from that of the concentration polarisation effects. The resistance measured is generally lower when measured through AC than through DC. [33]

A third way of measuring the resistance, is through electrochemical impedance spectroscopy (EIS). AC current at a range of frequencies will be applied through the membrane. The results, in combination with knowledge of electrical components, are used to translate the cell response into physical circuit components. Each component will give information of the contribution of double layers, CP and ohmic resistance of a membrane or a cell, so the method is quite comprehensive. On the other hand it is also the most complex of the measurement techniques, and the double layers do not necessarily impact RED-applications to a large extent. [33, 38]

2.8.2   Electrochemical measurements with EIS

Impedance is, like resistance, describing to what extent a circuit inhibits the flow of electrical current. It differs from resistance in that it is not independent of frequency, and in the fact that an impedance in a circuit will impose a phase shift between the current and the voltage. An impedance contains both a real and an imaginary component. If the imaginary component is zero, the impedance equals the resistance value.

EIS is a measurement technique used to quantify and evaluate the properties of an electrochemical cell through its impedance. An AC-potential of a certain frequency is applied, and the resulting phase shift and amplitude of the current is analysed. Low frequencies, similar to when DC is used for analysis, will yield information about the total resistance of the system, composed of both the solution resistance, the resistance of the membrane and that of the concentration polarisation effects. When high frequencies are applied, the pure ohmic resistance of the membrane will be apparent. [30]

After an EIS has been performed for a wide range of frequencies, a resulting impedance spectrum is formed. This spectrum correspond to physical phenomena in predictable ways, and so the impedance may be used to construct a model of the examined system. This model may be either physical or empirical. A physical model takes care to match components to corresponding physical processes in the examined cell. The choice of model and model components must therefore build on knowledge of the specific system. In an empirical model, components are not assigned to specific physical processes, but rather tuned in order to match measured and modelled impedance. Physical models are generally preferable, as they provide a much stronger insight in the behaviour of the system. [38]

Chapter 3

Methodology

The practical part of the project consists of three steps. Firstly, the conductivity of the membranes used are measured. The effect of change in concentration (without current or flow applied) is investigated. The results are implemented in a calculation model, used to predict the behaviour of the RED system, as well as the impact of individual parameters. Finally, a bench scale RED-system is planned and realised, including the selection and purchase of all relevant components as well as the physical mounting and implementation of the stack and auxiliary hardware such as tubes, pumps and temperature control. The system has been tested in practice, and information about the practical performance is gathered.

3.1 Ionic conductivity of membranes

Membrane properties change with changing environments, such as temperature and type of surrounding electrolytes, meaning that the factory measured properties will be inaccurate in non-standardised surroundings. To investigate the membrane behaviour in the actual RED system, the membranes are prepared for use with the relevant electrolytes, and properties are measured at the relevant concentrations and temperatures. Measurements are performed on two thicknesses of the same anion membrane, with the intention of determining whether interface resistance will affect the total resistance when several membranes are stacked.

As investigated in Section 2.3.1, membranes used for RED should have good ionic conductivity, and preferably also high selectivity, although the latter is of somewhat less importance. Based on these criteria, two membranes from Fumatech GmbH (Germany) are chosen; FKE-50 is used as cation membrane, while FAS-50 is the anion membrane in the system. A thickness of 50 μm, rather than the less resistive 30 μm, is chosen for the stack

for improved mechanical resilience of the membranes. In addition, the conductivity experiments are also performed on thinner anion membranes of the same kind, FAS-30 (also from Fumatech), to investigate the significance of interface resistance. A thinner version was not available of the cation membrane.

Table 3.1 is an overview of the membranes as declared in their respective datasheets [50–52].

Table 3.1: Membrane properties as presented by Fumatech [50–52]

	FAS-30	**FAS-50**	**FKE-50**
Type	AEM	AEM	CEM
Counter ion	Br^-	Br^-	H^+
Thickness (dry) [µm]	27-33	47-53	45-55
IEC[*] [mmol/g]	1.6-2.0	1.6-2.0	1.4-1.5
Specific weight [mg/cm^2]	3.5-4.4	6.0-8.5	7.5-8.5
Dimensional swelling (comp. to dry form) [%]	0-2	0-1	0-2
Specific conductivity[*] [mS/cm]	> 5	> 5	2.5-3.5

* Given for membrane in Na^+-form for the CEM and Cl^- form for both AEMs

3.1.1 Membrane preparations

The membranes are shipped from the factory with mobile counter-ions embedded, not corresponding to the desired counter-ions in this system. The counter-ions must be exchanged before the membranes are suited for use, and failure to remove them will eventually lead to these ions entering the electrolytes during stack operation, potentially causing undesired behaviour. The factory embedded ions of the CEM and the AEMs are H^+ and Br^-, respectively. Especially excess H^+ have the potential to cause problems in this stack, as a lowering of pH may cause oxidation of the nickel electrodes, in accordance with the Pourbaix-diagram of Section 2.6.2. In the investigation of membrane characteristics for the specific purpose of RED with KNO_3, proper ion exchange is also required in order to find the true properties as found in the stack.

The desired counter-ions are K^+ in the cation exchange membrane and NO_3^- in the membrane exchanging anions. The ion-exchange itself is performed through soaking of the membranes in KNO_3 for 24-72 hours, in practice a soaking time close to 50 hours has proven to be sufficient. KNO_3 of 1 M is used, and the solution is changed at least three times. The completeness of the exchange in the CEM is verified by measuring the pH of the spent solutions, comparing the value with fresh KNO_3 before immersion. The pH sensor used is Knick SE555x/1-NMSN, connected to a Portavo 907 MultiCond meter. When the pH has stabilised, H^+ is no longer extruding from the membrane and the exchange is considered finished. Similar verification of the anion exchange process is possible by adding $AgNO_3$ to the spent solutions. As long as Br^- is still present, a solid AgBr precipitate will form. However, it is considered satisfactory to soak the membranes for a time

period well beyond what was needed for the CEMs, and to make sure the solutions are changed frequently. A minimum of 72 hours of soaking time is adopted.

After soaking, the ion-exchanged membrane samples are prepared as round discs with a diameter of 20 mm, cut out with a wad punch. It is important to cut samples after soaking is complete, as the membranes swell in solution and thus alter size. The swelling is often more prominent in one direction, making the sample prone to adopt an oval "egg-shape" if cut in the dry form.

The equilibrated membranes contain both counter-ions and co-ions from the solution. This means that in addition to the fixed cations in the membrane backbone, both NO_3^- and K^+ are present in both membranes, although in different quantities. This surplus of electrolyte is also naturally occurring in the RED stack. If the membranes are washed and soaked in DI-water after the KNO_3-equilibration, the co-ions, as well as the counter-ions superfluous to maintain electrical equilibrium, will be washed away. Conductivity measurements on these membranes are measuring the base conductivity of the membrane.

To compare and investigate how the membrane conductivity is impacted by electrolyte concentrations, the membranes are soaked in KNO_3 in addition to DI-water. Batches of five samples are placed in individual vessels containing concentrations of 0 g/100g (DI), 10.1 g/100g (~1 M) and 25.3 g/100g (~2.5 M) aqueous KNO_3 for at least 24 hours. In addition, five samples are also placed in a vessel containing 45.6 g/100g (~4.5 M). This concentration equals the saturation concentration of KNO_3 at 30 °C, and to avoid precipitation, this set of samples is kept at 40 °C at all times.
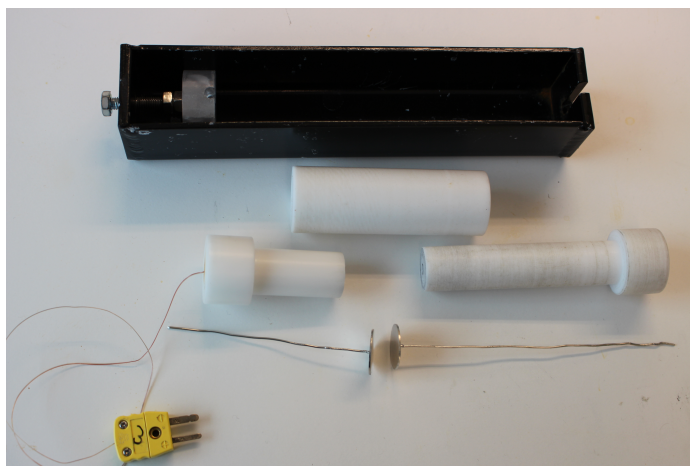
3.1.2 Conductivity measurements

The cell used to measure the conductivity contains two platinum electrodes with wire connectors, both with a surface area of 3.14 cm^2 and a thickness of 1.0 mm. They are mounted in a hard cylindrical shell, with the connectors protruding from the ends. A sliding tube is fitted closely to the cylinder, providing structural integrity while sealing the cell and keeping the membrane samples immobile. The full setup is shown in Fig. 3.1.

The membrane samples are placed between the electrodes of the conductivity cell. As the measurements are pressure sensitive, the cell is placed in a custom-made screw clamp, tightened with one bolt. A torque wrench is used to apply 2.0 Nm to the bolt, creating evenly distributed force due to the screw clamp. The electrodes of the conductivity cell are polished and fully polarised before use.

The conductivity experiments are performed at both 25 °C (the three lowest concentrations only) and 40 °C (all concentrations). In the latter case, both the cell and the samples are placed in a heating cabinet (Memmert UF 160 plus). To monitor the internal cell temperature, a K-type thermocouple is prepared and mounted in the measurement cell.

To make a reliable and resilient thermocouple, the two ends of a thermocouple wire are welded together. Initially, the two ends were twisted together and soldered, but this gave unreliable temperature measurements and fragile thermocouples. Instead, the welding is done by connecting the wire to the positive pole of a power supply. The negative pole is

(a) The physical conductivity cell, dismounted
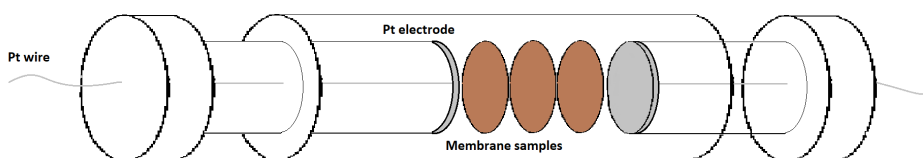
(b) Sketch of cell mounted with samples

Figure 3.1: The cell used for measurements of conductivity. The yellow bit is a thermocouple, while the black casing serves as a screw-clamp.

connected to the back of a graphite rod, creating an electrode. A potential of 50 volts is applied to the electrode, which in turn is used to fuse the twisted ends together.

The thermocouple is attached to the plastic shell directly behind and in contact with one of the platinum electrodes. As the electrode thickness is four times the membrane layer thickness even when five samples are tested at a time, the electrode temperature is assumed to be dominating and hence representative for the membrane temperature. The temperature is measured with a UNI-T UT58B multimeter.

Measurements are performed with a Gamry Interface 5000E potentiostat, in a two-electrode setup. The working electrode and the working sense are connected to one of the cell electrodes, while the counter electrode and the reference are connected to the other. The experiments are performed through Hybrid EIS, with the potentiostat settings shown in Table 3.2. Gamry Framework and Gamry Echem Analyst softwares are used to produce and analyse experimental data.

Table 3.2: Hybrid EIS settings for the potentiostat for conductivity experiments

AC voltage [mV rms]	**10**
DC voltage [mV rms]	**0**
Initial frequency [Hz]	**300 000**
Final frequency [Hz]	**1000**
Points/decade	**20**
Current convention	**Anodic**

Membrane thickness is crucial for accurate determination of resistance. The thickness of the membrane varies both from sheet to sheet, as well as from location to location on an individual sheet of membrane. The membranes also swell compared to their dry form, and thicknesses from the specification sheets are thus not accurate enough for this purpose.

The thickness of the sample stack is measured with a Mitutoya QuantuMike digital micrometer. The thickness at all stack heights, temperatures and concentrations are measured, in case conditions affect the swelling of the membrane.

The Pt-connector tip of one of the electrodes broke after a series of measurements. The electrode and the connector were still fully functional, but the tip was no longer protruding from the casing and could not be connected to the potentiostat. To remedy this, a copper cable was used as extension. Full connection between the various parts was ascertained with a voltmeter, and a test performed with the pure platinum connector was redone and compared with the results after the copper cable was put in place. No change in the obtained result was registered.

3.1.3 Data extraction and results

The conductivity cell hardware has its own impedance that should not be included when results are interpreted. This impedance contains both a real part, originating from the ohmic resistance in the electrodes and electric conductors, as well as an imaginary, inductive part due to the wiring and connectors of the potentiostat. To account for this inherent impedance, a blank experiment is run, where the cell is short-circuited. This is done for both relevant temperatures, as well as for variations such as dry electrodes, electrodes both slightly and thoroughly wetted in DI-water, as well as in the various concentrations of KNO_3. The purpose is to see whether double layers or other effects not directly related to the membrane parameters can be accounted for. Eventually, the impedance spectrum for the dry cell at the relevant temperature is subtracted from all measurements prior to any further analysis.

The ohmic resistance R of the membranes is found as the high frequency resistance, where no capacitive effects are present in the measurements. In the impedance spectrum, this is the point where the imaginary part of the impedance is zero, manifesting as the intersect with the real axis. This intersection point is found through a linear regression of the impedance curve, in the range from zero to four ohms imaginary. The regression curve is set equal to zero to find the accurate resistance value.

In the case where the impedance curve does not extend all the way to the real axis, an extrapolation of the curve is required. To minimise the impact of human errors, the extrapolation is performed three times for each curve, with three evenly spaced resistance values as the result. The calculation resistance used in the continuation is the average of the three values.

The area resistance r is the measured resistance multiplied by the membrane sample area. r is plotted against the corresponding sample thickness to show the correlation between the two parameters. As each set of experiments performed under the same conditions consists of three thicknesses, every r-d-plot will have three points, for 1, 3 and 5 membrane samples.

A linear regression is performed on each of the resulting plots. Every regression curve is describing the system for one kind of membrane, one concentration and one temperature, meaning that in total, 21 regression curves are produced in this step.

The slope of each regression curve is the membrane resistivity ρ, in $\Omega \cdot \mathrm{m}$. Every concentration yields one resistivity, meaning that four values are obtained for a given membrane and temperature. The inverse of the resistivity is the membrane conductivity κ, in $\mathrm{S/m}$. The conductivity values are then plotted against the concentrations. The average of the four concentration-dependent conductivities is the reported membrane conductivity. Double standard deviations are calculated through Gaussian error propagation.

3.2 Thermodynamical modelling

In order to construct a good theoretical model for the investigated system, important parameters are defined. The powerful mathematical software Matlab is used for the calculations.

3.2.1 Polarisation curves and power density

The open circuit potential of the stack is calculated according to Eq. 2.27. The charge number z is 1, as both ions are monovalent. As a first iteration are the permselectivities of both membranes equal to 1. This is likely to be too high, especially when high concentrations are involved, but good data for the behaviour of the membranes in KNO_3 and at 40 °C are not tabulated and must be experimentally obtained.

Temperatures used are 298 and 313 K, as these are the relevant operation temperatures for the stack in this setting. The membranes may decompose for temperatures higher than this. The activity coefficients are found from Dash et al, 2012 [44], as presented in Section 2.5.2. The coefficients from Dash are preferred over the data provided in CRC Handbook of Chemistry and Physics [37] because of the wider concentration range and presumed higher accuracy for higher concentrations. The CRC data extrapolates to zero for high salinities and will as such not give meaningful results in this case. A curve is fitted to the literature values through a second order exponential function, resulting in the expression of Eq. 3.1,

where c is the solution concentration. Both sets of literature report data exclusively for a temperature of 298 K, yet they are implemented for both temperatures as ΔT is relatively low. Activities for both high and low concentration solutions are finally calculated through Eq. 2.18.

$$\gamma_{KNO_3} = 0.5292 e^{-0.1979c} + 0.4738 e^{-0.00636c} \tag{3.1}$$

The total stack potential is calculated through Eq. 2.28. The total resistance consists of the elements presented in Eq. 2.6. The electrode resistance includes the resistance of the closing CEM membrane that is not part of a unit cell, but not a compartment resistance from the redox solution. The latter is because the modelled stack is intended to use a conducting nickel mesh as spacer, and this mesh is assumed to be in direct contact with both the membrane and the solid nickel electrode, thus circumventing the ohmic compartment contribution. The ohmic resistance of the nickel itself is assumed to be very low, and is neglected.

The membrane resistances are calculated through Eq. 2.7. Thickness values δ are the membrane thicknesses, 50 µm for FKE-50 and FAS-50, and 30 µm for FAS-30. Compartment thicknesses are 100 µm for both solutions, equal to the spacer thickness that will be used in the practical RED stack. Conductivity values κ are experimentally obtained for the membranes. For the solutions, resistance is calculated through Eq. 2.8 with an obstruction factor of 1.7, derived in Section 3.3.1. The functions of Eq. 2.4 and 2.5 are used to find the conductivity.

When the total stack potential is calculated for an array of current densities, a polarisation curve is established. The ohmic losses increase for increasing current densities, and as a consequence, the stack potential takes the form of a declining diagonal line. A power curve is found by multiplying the total stack potential with the current density array, as stated in Eq. 2.30. The power density is divided by 2 to normalise the value to membrane area rather than per cross-sectional area. The maximum power density is found as the maximum on the power curve, corresponding to Eq. 2.32.

Expected maximum hydrogen production is calculated through Faraday's law of electrolysis, Eq. 2.33. The current density input is the current density that yields the maximum power. The charge number z in this case is 2, as the hydrogen production is dependent on the number of electrons transferred in the water splitting reactions (Eq. 2.34 and 2.35).

To verify the model, a series of representative values are calculated manually and compared to the modelled numbers.

3.2.2   Potential profile in the stack

A potential profile for the stack is calculated to visualise the potential drops and gains over the stack. This is achieved by identifying the potential over specific stack components, and assigning a distance value to each one. If a potential contribution is non-ohmic, the distance assigned is 0.

The Donnan potential over each membrane is found through Nernst equation, Eq. 2.13. Permselectivity is still considered unity. As only one membrane at the time is investigated, activities for single ions must be used rather than for the full solution. The mean activity coefficients are the same, but the activity must be found through Eq. 2.17 instead of Eq. 2.18. For KNO_3, this is equivalent to taking the root of the previously modelled activity numbers for the salt.

The membrane concentration represent a junction potential of its own, and are important for accurate visualisation. Nernst equation is used also for this, with membrane concentration calculated with Eq. 2.3. Activity coefficients in the membranes are calculated as described in the previous section. To estimate the concentration per volume water rather than per volume membrane, experience [47] serves as guide. The share of polymer material in the membrane may be in the range of 80-90 % of the total membrane volume, leaving only a small fraction for water content. The number of ions is still dependent on the IEC, meaning there are a lot of charges present per water. The total membrane concentration is estimated as a factor (100 - 90) = 10 times higher than the result from Eq. 2.3.

The potential profiles are calculated for three different situations. This includes open circuit, where zero current is drawn, and maximum gross power output, in addition to the short circuited stack where the entire potential gain is dissipated in the internal resistances. The short circuit current is found as the current where the total stack potential is zero.

3.2.3 Concentration dependent potentials

One important use for a calculation model is optimisation of the system parameters. The concentration in the high salinity compartments is fixed to its practical maximum for a given operation condition, but the dilute concentration is not as straight-forwardly chosen.

The stack potential consists of both a gain from the Donnan potential across the membrane, and a resistance-dependent ohmic loss. The former increases with the natural logarithm of a concentration difference, while the latter increases directly with decreasing concentration due to lowered conductivity in the compartments.

When the stack is at open circuit conditions, the Donnan potential is the only contributor to the total stack potential, while for increasing current densities, the ohmic losses are increasingly significant, and dominates completely when the stack is short-circuited. The membrane resistance is constant, so the compartment resistance - in practice the low-salinity compartment resistance - is the only variable.

Because the potential loss increases faster than the gain for lower dilute concentrations, one may expect that a dilute concentration exists where the total stack potential reaches a maximum. More concentrated, and the decrease in Donnan potential will dominate, while less concentrated makes the ohmic losses too high.

To find this maximum, the power density from the stack is calculated for an array of dilute concentrations. The concentration range is 0 g to 45 g/100g water, the latter corresponding to the concentrated concentration, which is kept constant. The current density is constant,

corresponding to the current density that yields maximum power for an arbitrarily chosen dilute concentration of 1 g/100g. The effect of thicker dilute compartments is also investigated.

Also these results are manually calculated for representative values as a control of the findings and the methodology.

3.3   RED-stack performance

Leakages and elevated pressures have previously [1] proven to be a significant challenge for bench-scale RED experiments. A lot of attention and care has been put into elimination of this problem during the thesis work.

3.3.1   Preparation of components

Four unit cells are mounted in series, each consisting of one cation exchange membrane and one anion exchange membrane. An extra cation exchange membrane is closing the last cell, making the total number of membranes nine. A stack containing four unit cells is small enough to be considered ideal, as the cell performance will not be impacted by ionic short cut currents between the concentrate compartments [24].

The membranes used in the cells are ion exchanged as described in Section 3.1.1. The cation membranes are Fumasep FKE-50, and the anion membranes are FAS-50. The shape and the solution feed openings are cut out by hand, with the help of stencils. Sharp plugs are pushed through the stencil and then, with the help of a hammer, through the membrane. This method is chosen to minimise ruptures and jarred edges that may negatively impact the flow patterns. The active area of each membrane is 100 cm^2.

Between each ion exchange membrane, both a spacer and a gasket is present. The gaskets are designed to keep the stack from leaking, and to ensure that fluids flow only as intended. The gaskets chosen are 100 μm (0.005 inches) thick, and made of Teflon. Teflon will not compress under pressure, and is chemically inert. The material is also beneficial for stacking of the membranes, as it is not elastic and will thus stay in place and not unintentionally cover the feed holes. Gaskets were previously [1] cut with quite wide U-shaped openings where the feed solutions enter the compartments. This shape leaves critical points of the stack under less pressure than the rest, as the U-shapes overlap between layers, leaving space where only half as much gasket material as in the rest of the stack is present. This is a suspected source of leakages between compartments. To alleviate this, gaskets were cut with narrower openings, the width determined by the feed hole diameter.

Thin spacers are chosen, Sefar Nitex 03-160/53 with a thickness of 100 μm. Important spacer properties are presented in Table 3.3. [53]

Eq. 2.9 and 2.10 are used to calculate the volume occupied by the spacer. The spacer will occupy 30 % of the volume in its compartment and 47 % of the membrane area, making

Table 3.3: Important properties of Sefar Nitex 03-160/53 [53]

	Variable	Unit	Value
Material			PA 6.6
Thickness	δ	μm	100
Spec. gravity	g	kg/m^3	1140
Spec. weight	w	kg/m^2	0.034
Mesh opening		μm	160
Open area		%	53

the area and volume based obstruction factors 1.43 and 1.89, respectively. The average obstruction factor f_{obs} is 1.66. The outer spacer diameter corresponds to the inner gasket diameter, and the two materials will not overlap in the stack.

The electrodes are made of solid nickel (mechanical workshop, Faculty of Natural Sciences, NTNU), with platinum wire connectors protruding through the end plates. Gaskets limit the active surface to 10x10 cm^2. A nickel mesh of 300 μm is replacing the end plate spacer on both stack sides, for improved electrode kinetics. The mesh is originally the same size as the active electrode area, but it has been cut slightly smaller to ensure no overlap between mesh and gaskets that may cause leaking.

The thickness of the nickel mesh exceeds that of the Teflon gasket, making the Teflon unsuited as end gasket. Instead, two silicone rubber gaskets, each with a thickness of 254 μm when not compressed, are used to seal the electrode compartments. To avoid obstructing displacements and in the hope of non-leaking compartments, liquid gasket is used as an adhesive, fixing the end gasket to the end plate. The same is done between the two gasket layers. Fig. 3.2 depicts an end plate with one and two end gaskets put in place.
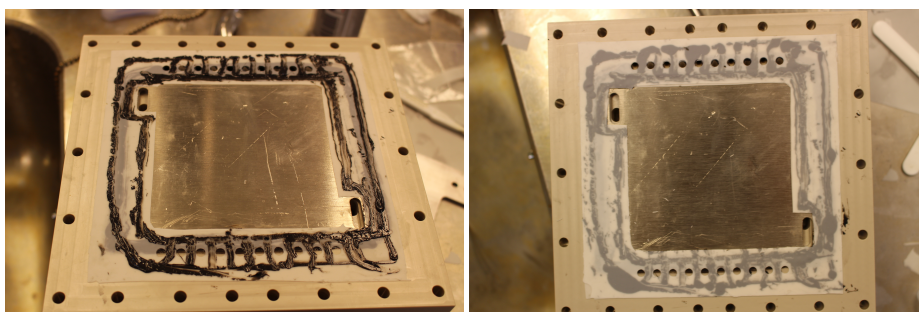
(a) End plate with one silicone gasket and extra liquid gasket

(b) End plate with double silicone gaskets

Figure 3.2: End plate and end gaskets of the RED stack. The gasket allows flow of one electrolyte and blocks the other. Redox solution enters and leaves through the rectangular openings.

The endplates of the cell are made of the very resilient material PEEK (PolyEther Ether Ketone, mechanical workshop, Faculty of Natural Sciences, NTNU), and have embedded electrode compartments. 12 stainless steel bolts are used to hold the stack together, tightened with a torque wrench. Initially, 2.5 Nm were applied to each bolt. This was later tightened to 3.5 Nm as leakages were observed. The flow inlets and outlets of the stack are also made of PEEK, 8 in total.

For accurate stacking, short rubber tubes were placed in the feed holes of the stack and used as placement "guides". This ensures that the holes have free passage all the way through. Table 3.4 contains a summary of all the stack layers, their make and their dimensions.

Table 3.4: Stack component details

Component	Quantity	Sold by	Make	Thickness [μm]
AEM	4	Fumatech	FAS-50	50
CEM	5	Fumatech	FKE-50	50
Gasket	4	Fuel Cell Store	HT6135, Silicon Rubber	254
Gasket	8	Fuel Cell Store	Teflon	100
Spacer	8	Sefar	03-160/53	100
Nickel mesh	2	Alfa Aesar	40 mesh woven from 0.13 mm dia wire	300

The connection between the connector wires and the electrodes are verified with an ohmmeter, ensuring that the platinum wires are intact and conducting. All wires are tested consecutively.

3.3.2 Electrolytes and redox flow

Electrolyte concentrations are chosen according to scenarios relevant for precipitation and evaporation. The membranes are not manufactured to operate at temperatures above 40 °C, thus setting the upper limit for the saturation temperature. To allow for heat losses in pipes and in the cell compartments, the saturation temperature used is 30 °C, corresponding to a molarity of 45.6 g KNO_3/100 g water if the system is kept at 40 °C, and 38.3 g/100g at room temperature. Both alternatives are tested.

The lower concentration limit in a precipitation system is given by the saturation concentration for KNO_3 at 10 °C, 21.3 g/100g. In an evaporation system, the lower concentration is only limited by the electrochemical properties. The results from Section 3.2.3 are used for this evaluation. It is decided that a good balance between electrochemical behaviour and lab practicalities such as maintaining purity without the influence of contamination is found for a concentration of 0.20 g/100g.

The redox solution is water mixed with K_2SO_4, which has a quite low solubility. A high enough concentration to ensure high conductivity is desirable, and the concentration of K_2SO_4 is set close to the solubility limit at 20 °C. The redox solution contains 10.5 g/100 g K_2SO_4, corresponding to 0.6 M. An operational pH of 10 is chosen, in accordance with the Pourbaix-diagram in Fig. 2.6. A slightly elevated pH will keep the nickel electrodes from corroding.

The pH of the pure K_2SO_4 redox solution is measured with the pH probe, and found to be 7.0 exact. A starting pH of 10 is obtained by introducing KOH into the redox solution. KOH dissolves completely, meaning that for every mole of KOH added to the solution, the concentration of OH^- also increases with one mole. The theoretical amount of KOH necessary to increase the pH from 7 to 9 is estimated according to equation 2.36. In practice, mixed solutions often have a certain buffer capacity, and the amount of KOH required is increased somewhat. The pH-probe is used to monitor the pH, while the K_2SO_4 is vigorously stirred and KOH added.

A small amount of KCl is added to all solutions. The reasoning behind was to ensure that the same anion is present in all compartments of the stack, as well as in reference electrodes made of Ag/AgCl. K^+ has this role as cation. In the end, reference electrodes were not used, but the practice of adding KCl was continued for consistency.

3.3.3 Experimental

The tubes used with the stack are made from marprene, by Watson Marlow. Both the inner diameter and the wall thickness are 1.6 mm. Short pieces of tubing with a larger inner diameter of 4.8 mm are used as joints with the flow inlets and outlets of the stack. This combination is made to decrease pulsing in the system, while still having large enough tubes to connect to the stack openings.

Two peristaltic variable speed pumps (Watson-Marlow 323D) are used, each with two 314D pump heads. The dilute electrolyte and the redox of the bottom plate are pumped on the same pump, while the two remaining solutions are pumped together on the other. This choice was made after cyclic pulsing in potential was observed when the electrolytes were pumped together. Pulsing was reduced, but not eliminated, after the change was made. To further alleviate the problem, the pump speed of the pump with the dilute solution was increased, making sure the flows were not in phase at all. This diminished the problem, and stable potential was established.

The pump speeds used are 20 rpm and 26 rpm. From the manual, the speed range 1.5 - 220 rpm corresponds to flow rates of 0.38-55 ml/min for the chosen tubes. The ratio of these ranges gives a conversion factor of 0.25. This means that the pump speeds in question correspond to flow rates of 5 ml/min and 6.5 ml/min, respectively.

Neither dilute or concentrated solution is recycled, meaning fresh electrolytes enter the stack continuously. The redox solution is recycled, but each electrode is in a separate loop, eliminating potential short circuiting between the electrodes.

The full operational RED stack in the heating cabinet is shown in Fig. 3.3. Fresh solutions are supplied on the right hand side of the stack, and leave the stack to the left. Pumps are situated right outside of the cabinet, and solutions leave and re-enter through the same wall openings. All tubing and glass ware are colour-coded to avoid confusion. Potentiostat wiring is passed through the cabinet wall on the left hand side.

(a) Close-up of the stack and the solutions   **(b)** Total setup with pumps and potentiostat

Figure 3.3: The operational RED stack in the heating cabinet. The potentiostat is attached to the connectors at the two endplates. A bucket with a drilled wire opening serves as stand for the stack.

Hybrid Electrochemical Impedance Spectroscopy

Hybrid EIS measurements are performed also on the stack as a whole, in order to analyse the internal resistance. The high frequency resistance is the ohmic resistance, as previously described.

Once stable stack conditions without pulsing was achieved, initial measurements on the stack were performed to define the proper frequency range as well as getting an overview of the total stack response. Initialisation was performed by running the EIS over a large frequency range, from 300 000 Hz to 0.01 Hz. These first results revealed that the high end of the frequency range was sufficient to evaluate ohmic resistance. In addition, it was clear from the measurements that frequencies lower than 10 Hz result in incoherent noise in the impedance spectra, and no patterns of interest were present for very low frequencies. The final potentiostat settings used are presented in Table 3.5.

Table 3.5: Hybrid EIS settings for the potentiostat for RED experiments

AC voltage [mV rms]	**10**
DC voltage [mV rms]	**0**
Initial frequency [Hz]	**300 000**
Final frequency [Hz]	**10**
Points/decade	**10**
Current convention	**Anodic**

Initial measurements are also used to investigate the time required for the stack to achieve steady state conditions and a stable OCP after an EIS is performed. Based on the observations, minimum 20 minutes of uninterrupted flow in the stack is implemented both before and after an experiment.

Impedance spectra are found for six operation conditions in the stack; three relevant for

precipitation and three relevant for evaporation. The operation conditions are presented in Table 3.6. All measurements are performed three times per scenario.

Table 3.6: The six RED operation scenarios used for EIS measurements

	Low conc. [g/100 g]	High conc. [g/100 g]	Temperature [°C]
Precipitation	21.3	38.3	25
	21.3	38.3	40
	21.3	45.6	40
Evaporation	0.2	38.3	25
	0.2	38.3	40
	0.2	45.6	40

Extraction of ohmic resistance values are performed as described in Section 3.1.3. Despite the initial investigations, the chosen initial frequency proved to be slightly too low for some scenarios. In cases where the plots do not fully extend to the real axis, extrapolation is used. Standard deviations are calculated using the "n-1" method, combined with Gaussian propagation of error in the transition from R to r.

Linear Sweep Voltammetry

Linear Sweep Voltammetry (LSV) was used to produce polarisation curves for the stack, crucial in the evaluation of the electrochemical stack performance. Initialisation was performed also for the LSV experiments, where the adequate voltage range and scan rate were investigated, along with the time required to achieve steady state conditions.

The experiments were performed for the most promising separation scenarios, meaning operation conditions with the highest achievable concentration difference and an elevated temperatures. This means that the temperature was kept at 40 °C, and the two concentration couples 21.3 g/100 g vs. 45.6 g/100 g and 0.20 g/100 g vs. 45.6 g/100 g were tested. Flow rates for all solutions are as before. Potentiostat settings for the LSV experiments are shown in Table 3.7.

Table 3.7: LSV settings for the potentiostat for RED experiments

Initial voltage [V]	**-4**
Final voltage [V]	**4**
Scan rate [mV/s]	**30**
Step size [mV]	**50**

LSV polarises the stack to an even larger extent than EIS does, and a stabilisation time of minimum 30 minutes with steady flow was implemented between experiments.

The stack performance both in ED and RED mode was investigated. To compare the two cases, the polarity of the stack was shifted, and LSV performed. All experiments were done twice, to have a basis for comparison.

Tafel curves for the stack are obtained by subtracting the ohmic jr-losses from the potential data. The r-values are experimental values from the EIS results. The Tafel coefficients b are found as the slopes of the curves where they are stable, and the exchange current densities j_0 are the intersects between the slopes and the OCP. Finally, the coefficient a is found form the Tafel equation in Eq. 2.42 when b and j_0 are known, as $a = -b \, log j_0$.

3.3.4 Membrane transport numbers/permselectivity

The apparent permselectivity of the membranes are found by a comparison between the measured and the theoretical Donnan potential. The theoretical potential is found from the calculation model, corresponding to the reversible potential presented in Eq. 2.13. The practical Donnan potential is the difference between the water splitting potential and the potential at zero current, the latter manifesting as a straight line in polarisation plots.

The resulting apparent permselectivity is implemented back into the theoretical model, to find current density and expected hydrogen production at the maximum gross power output. The current density is in turn used to analyse the Tafel overpotentials from the experimental results.

4

Results

This chapter highlights trends and important results from the experiments and calculations performed. All obtained experimental results from the membrane conductivity measurements are presented in Appendix A, and all results from the practical RED operation are shown in Appendix B. Potentials are in this setting defined as positive if they contribute to work out of the system, while negative potentials equal potential drops.

4.1 Ionic conductivity of membranes

Initialisation measurements are performed to map the frequency range required to see the features of interest in the membrane impedance plots. The initialisation reveals that a range from 300 000 to 1000 Hz should be sufficient. The plots are dominated by noise for frequencies lower than about 100 Hz.

Figure 4.1 shows the unadjusted impedance spectra for 1, 3 and 5 samples of FKE-50, soaked in 2.5 M KNO_3 and measured at 25 °C. The shape of the curve and the spacing between the intersects with the real axis are similar for all measurements on the membranes FKE-50 and FAS-30. Corresponding frequencies are added to selected datapoints in the plot.

The displayed results have a capacitive linear shape, with an angle away from the y-axis at about 70°. The intersect points with the x-axis are quite evenly spaced, meaning that the measured resistance increases linearly with thickness. Some plots display minor deviations, but not in any identifiable pattern.

The FAS-50 membrane behaves differently from the other two types of membrane. These EIS-plots take the shape of a semicircle in the high frequency range, especially for higher concentrations. The resistance values are also significantly higher than for FKE-50 and FAS-30. Yet, the intersects with the real axes are still evenly spaced, and the standard
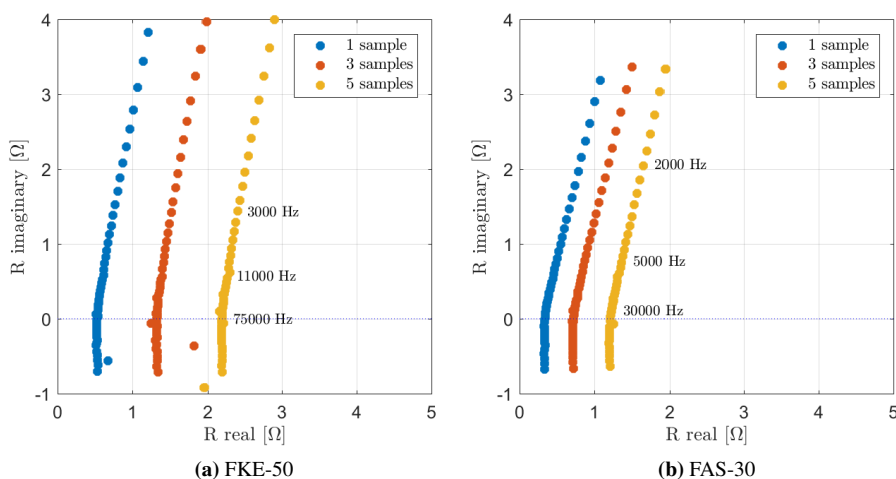
Figure 4.1: Hybrid EIS impedance spectra for FKE-50 and FAS-50 in 2.5 M at 25 °C, before impedance subtraction. The shape of the curves is representative for all FKE-50 and FAS-30 results

deviations of the conductivity are low. The shape of the spectra for samples soaked in DI-water is more like expected, but still with very high resistance values. The resistance values are consistent over the full range of concentrations.

Figure 4.2 shows how subtraction of hardware impedance affects the measured data. The ohmic resistance is slightly reduced, and the inductive (negative in this plot) region is no longer present. Instead, the beginning of a high-frequency semicircle is visible. Ideally, the change of direction should occur exactly at the real axis if the correct hardware impedance is subtracted.

Figure 4.3 presents all the measured impedance spectra for five samples of FKE-50, put together for comparison. Several trends are apparent from the plot. The resistances show no signs of concentration dependency. Furthermore, the results obtained at 40 °C have consistently lower resistances than the room temperature results, but also spread over a larger range. The results for 25 °C have no significant variation.

The same trends are observed when area resistance is plotted against thickness, illustrated in Fig. 4.4. This figure also illustrates the use of slopes to determine resistivity values, examplified through the FAS-30 membrane at 40 °C.

The final conductivity plots for the three membranes are shown in Appendix A.2. The numerical results are summarised in Tab. 4.1, along with a comparison with the tabulated properties reported by the manufacturer at 25 °C. For 40 °C, there is no basis for comparison. All measured conductivities appear to be higher at 40 °C than at 25 °C. Furthermore, the membranes seem to have different responses to the exchange from NaCl to KNO_3. The cation membrane, FKE-50, seems to have better conductivity in K^+ than in Na^+, at least for 25 °C. The FAS-50 anion membrane has very large deviations from the
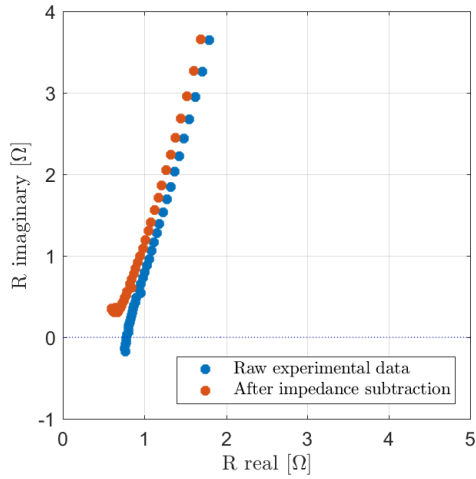
Figure 4.2: Impedance spectra for one sample of FKE-50 in DI water, before and after impedance correction

expected values, confirming the trend observed in the preliminary results. The thinnest anion membrane, FAS-50, has no significant response to the ion exchange. The conductivity may seem to be somewhat decreased when the membrane is in NO_3^--form compared to its Cl^--form, but the difference is not statistically significant.

Table 4.1: Experimental conductivity results for all membranes, compared with tabulated values

Membrane	d [μm]	T [°C]	r [Ω cm^2]		κ [mS/cm]	
			Fumatech*	Measured	Fumatech*	Measured
FKE-50	50	25	1.5-2.3	1.1 ± 0.11	2.5-3.5	4.5 ± 0.5
		40	-	0.77 ± 0.15	-	6.6 ± 1.3
FAS-50	50	25	< 1.8	4.7 ± 0.19	> 5	1.1 ± 0.04
		40	-	3.5 ± 0.9	-	1.5 ± 0.4
FAS-30	30	25	< 2.0	0.70 ± 0.18	> 5	4.3 ± 1.2
		40	-	0.47 ± 0.17	-	6.5 ± 2

* Given for membrane in Na^+-form for the CEM and Cl^- form for both AEMs
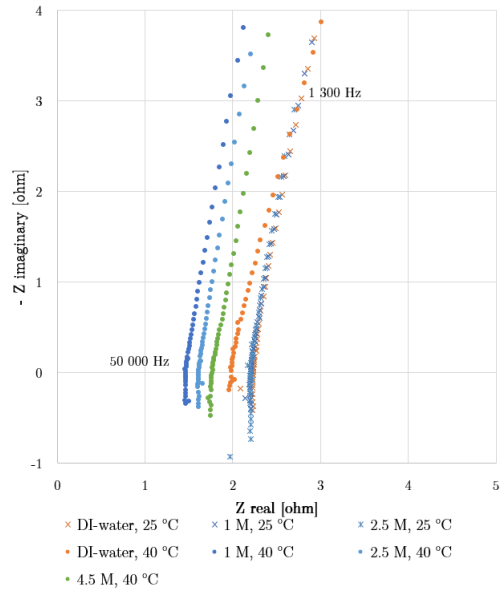
Figure 4.3: All Hybrid EIS impedance spectra for five samples of FKE-50 before impedance subtraction
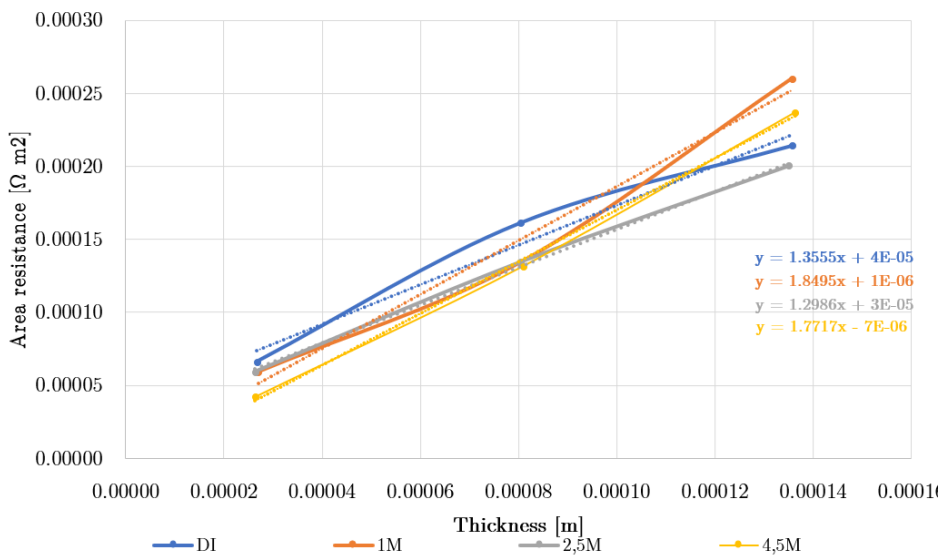
Figure 4.4: Area resistance versus thickness of membrane for FAS-30, with linear trend lines. The slope of the linear curves is the membrane resistivity for each concentration.

4.2 Thermodynamical modelling

A thermodynamical model is constructed to increase the knowledge about the stack behaviour. This model is used to predict stack potential and power density for a number of scenarios, in addition to determination of the possible hydrogen production.

One important benchmark for the stack is the power and hydrogen production per active membrane area. Fig. 4.5 displays the power and polarisation curves for one unit cell at 40 °C. The FAS-50 membrane is the intended AEM for use in the stack, but because the conductivity results show deviating behaviour for this membrane, the thinner FAS-30 is modelled instead. The obstruction factor is 1.7, and permselectivity is 1. Electrodes and electrode overpotentials are not included in this figure, to give a true impression of the stack potential comparable to other research.
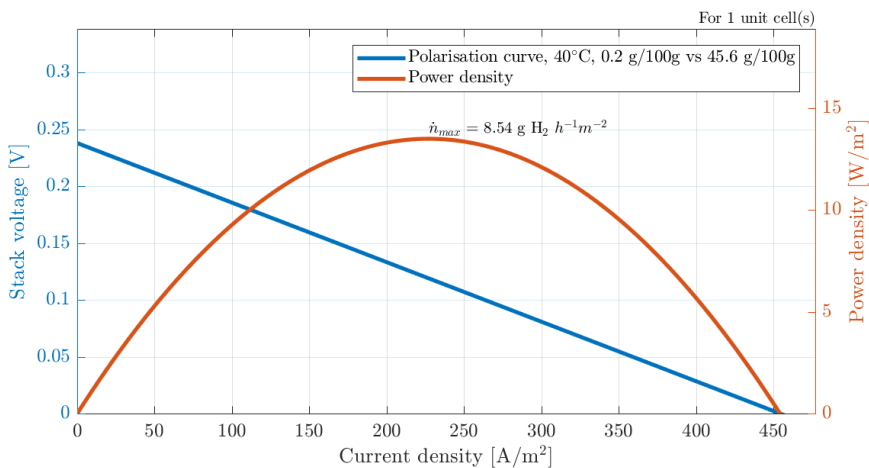
Figure 4.5: Modelled power- and polarisation curve for one unit cell for the largest concentration difference possible at 40 °C

The expected potential per unit cell is 0.24 V/m^2, meaning that for this idealised case, 6 unit cells are required to achieve the water splitting potential of 1.23 V. In practice, higher voltage is required because of the presence of overpotentials. Expected power density is 13.5 W/m^2, a high value relative to previously reported numbers for RED. The expected hydrogen production is 8.5 g H$_2$/h m^2, occurring for a current density of 227 A/m^2.

Table 4.2 shows the manually calculated values for representative current densities, along with references to the equations used. The table has good correlation with Fig. 4.5.

To investigate how different concentrations and temperatures affect the power output, all the operation scenarios from Table 3.6 were modelled. Figure 4.6 shows how the power density changes in the evaporation system. The yellow curve depicts the same situation as Fig. 4.5. The maximum power densities for the three evaporation scenarios in decreasing order are 13.5, 12.7 and 11.4 W/m^2, with corresponding optimal current densities of 227,

Table 4.2: Verification of the model results for selected current densities

Eq. $j\ [\frac{A}{m^2}]$	3.1 γ_{con}	2.20 a_{con}	3.1 γ_{dil}	2.20 a_{dil}	2.26 $E_{ocp}\ [V]$	2.6 (2.2, 2.8) $r_{tot}\ [\Omega\ m^2]$	2.28 $E_{cell}\ [V]$	2.30 $p\ [\frac{W}{m^2}]$
10	0.36	261	0.98	0.039	0.24	5.24E-04	0.23	1.2
20	0.36	261	0.98	0.039	0.24	5.24E-04	0.23	2.3
40	0.36	261	0.98	0.039	0.24	5.24E-04	0.22	4.3
80	0.36	261	0.98	0.039	0.24	5.24E-04	0.20	7.8
160	0.36	261	0.98	0.039	0.24	5.24E-04	0.15	12
320	0.36	261	0.98	0.039	0.24	5.24E-04	0.07	11

221 and 207 A/m^2, respectively.
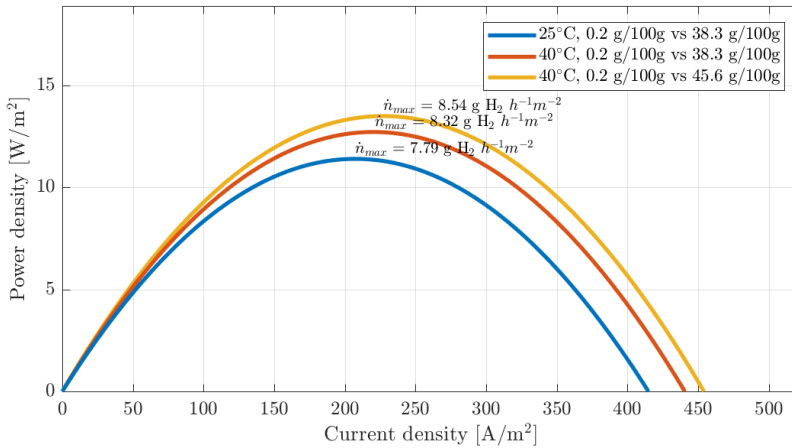
Figure 4.6: Temperature dependent power curves for the RED stack as a function of current density

It is apparent from the evaporation curves that increased temperature definitely is a driver for higher power densities, and the power increase from increased temperature is larger than the power increase from increased high salinity concentration. For a temperature increase of 5 %, the stack experiences a power density increase of 11 %, while for an increase in high salinity concentration of 19 %, the stack power increases by 6 %.

Fig. 4.7 shows the impact on power density and hydrogen production in the separation system using precipitation. The concentrations suitable in this kind of system allow for considerably less power densities, 0.35, 0.56 and 0.92 W/m^2 in the three cases. This is more than one order of magnitude lower than what is seen for the evaporation system. Corresponding current densities are 59, 91 and 115 A/m^2. The three curves are quite evenly spaced in this case, making the absolute impacts from temperature and concentration change comparably large. Both changes are also far more significant. The temperature increase yields 64 % higher power density, while the high salinity concentration increase

gives a 60 % larger gross power output. This means that the power density increases 13 times faster than the temperature, and with a factor close to 3 for increased concentration difference.
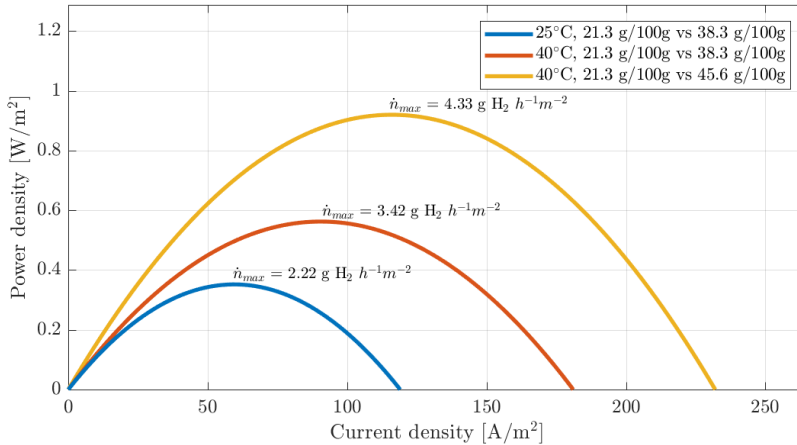
Figure 4.7: Temperature dependent power curves for the RED stack as a function of current density

The shifts in optimum current density (and thus hydrogen production) between the curves are not the same in both systems. Evaporation scenarios display a relatively small shift between the curves, with 3 % increase for elevated temperature and 7 % increase for higher concentration. In the precipitation system, the temperature increase increases the current density by 26 %, while increase in high salinity concentration increases the current density by 54 %. In general, while the evaporation system has a power density that is more than one order of magnitude larger than the precipitation system, the current density is only between doubled and tripled.

The potential profile in one unit cell has been modelled. The calculated membrane concentrations are 2.3 M for the FKE-50 membrane, 2.4 M for the FAS-30 and 2.6 M for FAS-50. The resulting profile for operation conditions as in Fig 4.5 is shown in Fig. 4.8. The potential difference between the dilute solution and the membranes are quite large, because of a large difference in concentration between membrane and solution phases. Conversely, the potential difference between AEM and concentrate is quite small, as the concentration difference is comparably a lot smaller.

When current is applied to the stack, ohmic voltage drops are present and visible in the figure. The largest potential drops originates in the dilute compartment, as expected. In the case where the stack operates at maximum power, the stack potential is half of the open circuit potential, and the current is half of the short circuit current. Larger currents cause larger potential drops, clearly visible as the difference between the maximum power and the short circuit graphs. The short circuit current is 545 A/m^2, and the potential over the stack is zero.

The stack power density as a function of dilute concentration is plotted for four different
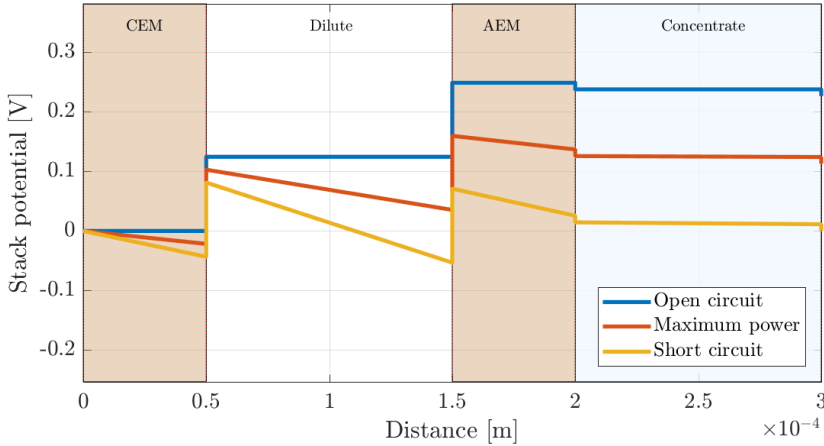
Figure 4.8: Modelled potential profiles for open circuit, maximum power density and short circuited stack in one unit cell at 25 °C.

compartment thicknesses, shown in Fig. 4.9. The high salinity concentration is kept constant at 45.6 g/100 g. The temperature is 40 °C, and a constant current density of 141 A/m^2 is applied, corresponding to the optimal current density (for maximum power production) when dilute concentration is 1 g/100 g. This figure also implements the measured resistance of the FAS-50 membrane rather than the FAS-30 AEM, as the intention is to clarify real operation behaviour. FAS-50 is the membrane used for practical experiments on the stack.

A maximum on the power curve is expected as the ohmic losses start to dominate the stack potential for low dilute concentrations. This maximum is visible for compartment thicknesses of 200 and 400 μm, appearing at 0.4 and 2 g/100 g respectively. However, for thinner compartments, an exponentially growing curve is apparent instead, indicating that the resistance in the dilute compartment is never large enough to dominate the potential gain from higher concentration differences. Another interesting feature of the figure is the fact that power production goes below zero for sufficiently high dilute concentrations, in this case close to 10 g/100 g for all compartment thicknesses. For a given current density will the stack seize to produce power, even though the membranes still provide a certain Donnan potential. All of this potential is dissipated as ohmic losses. The figure is verified with manual calculations, shown in Table 4.3 for a compartment thickness of 100 μm.

4.3 RED-stack performance

The operational RED stack has been tested for both resistance, through hybrid EIS, and for performance parameters through LSV. All potentials are measured over the entire stack rather than over one electrode, meaning that both cathodic and anodic reactions are present
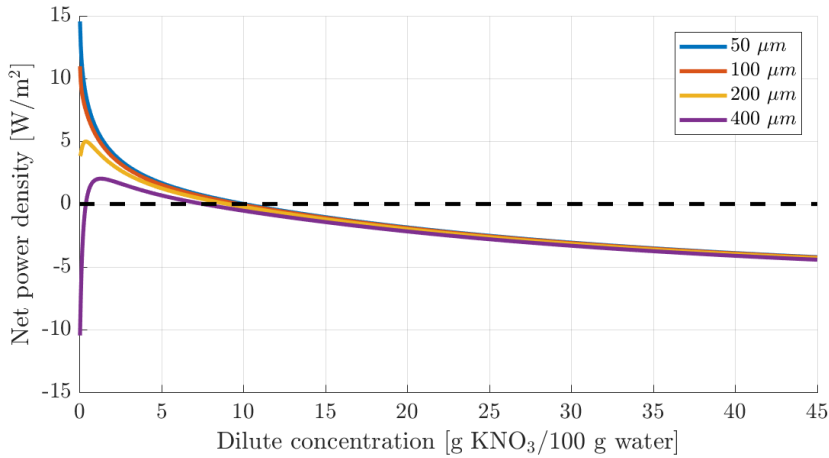
Figure 4.9: Potential for one unit cell for varying dilute concentration at a current density of 141 A/m^2.

Table 4.3: Verification of model results for selected dilute concentrations. Compartment thickness is 100 μm and the current density applied is constant at 141 A/m^2.

Eq.	3.1	2.20	2.26	2.8	2.6	2.28	2.30
Dil cons	γ_{dil}	a_{dil}	E_{ocp} [V]	r_{dil} [$\Omega\,m^2$]	r_{tot} [$\Omega\,m^2$]	E_{cell} [V]	$p\left[\frac{W}{m^2}\right]$
1 g/100 g	0.91	0.819	0.16	1.20E-04	5.48E-04	0.078	11
2.5 g/100 g	0.79	3.89	0.11	5.33E-05	4.80E-04	0.046	6.5
5 g/100 g	0.66	10.7	0.086	2.85E-05	4.56E-04	0.022	3.1
10 g/100 g	0.52	26.8	0.061	1.56E-05	4.43E-04	-0.001	-0.14
20 g/100 g	0.43	73.0	0.034	9.20E-06	4.36E-04	-0.027	-3.8
40 g/100 g	0.37	216	0.005	6.20E-06	4.33E-04	-0.056	-7.9

in the curves.

Figure 4.10 shows the obtained EIS-results for one of the six investigated scenarios. The molarities used are 0.20 g/100 g together with 38.3 g/100 g, for a temperature of 25 °C. All the obtained EIS results for the stack are gathered in Appendix B. The ohmic stack resistance is read from the high-frequency intersect with the real axis. For these operating conditions is the ohmic resistance 0.80 ± 0.19 Ω, equal to a specific resistance of $8.0 \cdot 10^{-3} \pm 4 \cdot 10^{-3}$ $\Omega \cdot m^2$ when the cross sectional area is taken into account. The modelled resistance value for the same temperature and concentrations is $1.4 \cdot 10^{-3}$ $\Omega \cdot m^2$, a value that is considerably lower even when compared to the lower confidence interval bound. All ohmic resistances from the EIS-experiments are shown in Table 4.4.

Table 4.4 displays quite stable resistance values, although higher than modelled. However, especially r-values have quite high standard deviations, in many cases around half of the
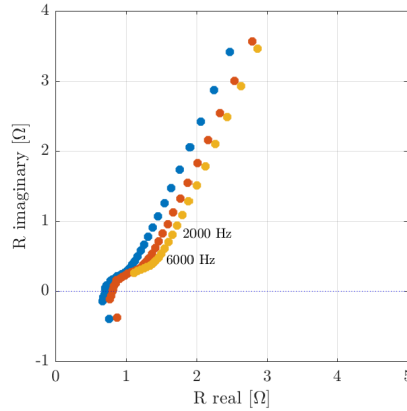
Figure 4.10: Example of EIS-result for the operational RED stack

Table 4.4: Experimental values for total R and r in the stack, with double standard deviations σ

	$c\,[\frac{g}{100g}]$	$T\,°[C]$	$R\,[\Omega]$	$2\sigma_R\,[\Omega]$	$r\,[\Omega\cdot m^2]$	$2\sigma_r\,[\Omega\cdot m^2]$
Precipitation	21.3, 38.3	25	0.47	0.03	4.7E-03	5E-04
	21.3, 38.3	40	0.45	0.3	4.5E-03	5E-03
	21.3, 45.6	40	0.44	0.11	4.4E-03	2E-03
Evaporation	0.20, 38.3	25	0.80	0.20	8.0E-03	4E-03
	0.20, 38.3	40	0.79	0.19	7.9E-03	4E-03
	0.20, 45.6	40	0.91	0.18	9.1E-03	4E-03

measured value. This in turn makes it hard to read clear trends from the results. For instance, there is no clear decrease in resistance for neither increased concentration nor temperature.

Expected impedance spectra for the RED stack include a semicircle, containing information about the non-ohmic resistances present for lower frequencies. There are no clear shapes of this kind in the obtained spectra. All the spectra do however contain a "bulge" on the curve around 1-2 Ω on the real axis, most prominent on the results from 0.20 g vs. 38.3 g for 25 °C, previously shown in Fig. 4.10. It is possible that this is the onset of a semicircle, but it is not an obvious conclusion.

Fig. 4.11 shows a polarisation curve for the stack, where the measured voltage is plotted against the logarithm of the current. This figure shows the full voltage range used for obtaining the results. The anodic (positive) part of the voltage range is due to back-reactions and corrosion effects on the electrode, and is not relevant for the further analyses.

The horisontal part of the potential curve is the region where the electrodes are totally polarised, where the applied current leads to no change in potential. The net current at the electrodes is zero, and the potential value is read as the open circuit potential.
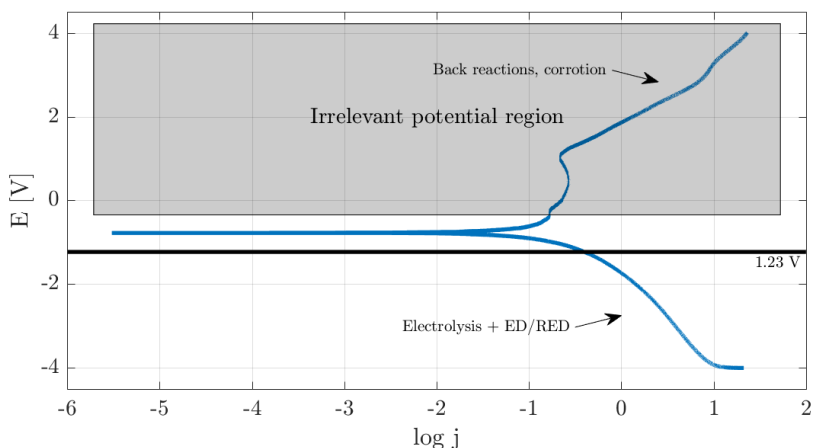
Figure 4.11: Example of E vs. log j polarisation curve for the stack in RED-mode

1.23 V is the water splitting potential, emphasised in the figure as a solid black line. The differential between the water splitting potential and the OCP is the Donnan contribution from the membranes. The Donnan contribution makes the reaction happen for a lower applied potential when the stack is in RED operation mode. The target in full-scale operation is to have the stack produce sufficiently high Donnan potential to split water without any applied power.

Fig. 4.12 depicts the obtained polarisation curve for the stack operating under optimal temperature and concentration conditions for separation by evaporation. The molalities used are 0.20 and 45.6 g/100 g, and the stack is heated to 40 °C. The OCP values obtained from the stack are -0.77 V when the stack is in RED-mode, and -1.60 V when the polarity is switched to ED operation. The Donnan contributions are 0.45 V and -0.37 V, respectively. The signs of these numbers reflect that the Donnan contribution is a gain for the RED-process, potentially constituting the entire driving force, while it is potential that must be "paid" to get the ED process to go.

Fig. 4.13 depicts the polarisation curves for the optimal separation scenario when precipitation is the intention; 21.3 g/100g and 45.6 g/100 g at 40 °C . The potentials are smaller in this case, as expected for low concentration differences. Perhaps more unexpected, is the fact that the curves are actually inverted. The polarity where positive membrane contribution was recorded for the lower dilute concentration in Fig. 4.12 gives negative contributions in this case. This behaviour is consistent over all four LSV tests for this concentration combination. OCP values with corresponding Donnan contributions are -1.26 V and -0.0291 V for the blue curve, and -1.21 V and 0.0135 V for the red curve.
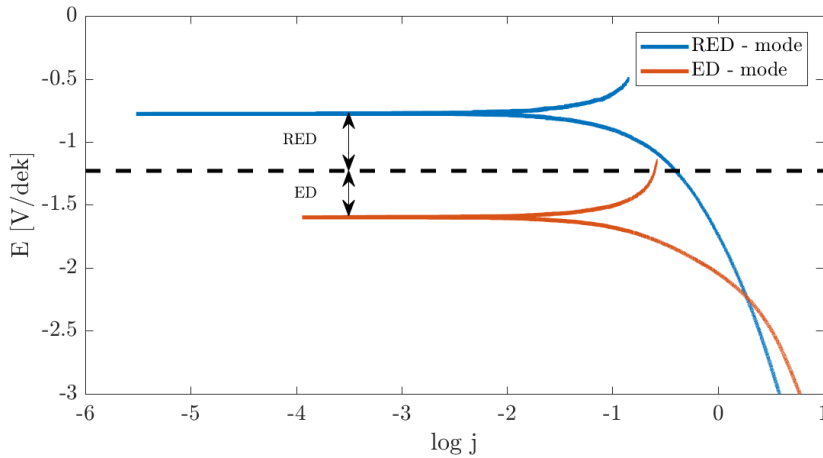
Figure 4.12: Polarisation curves for the RED stack operating with 0.20 and 45.6 g/100g KNO_3, T = 40 °C
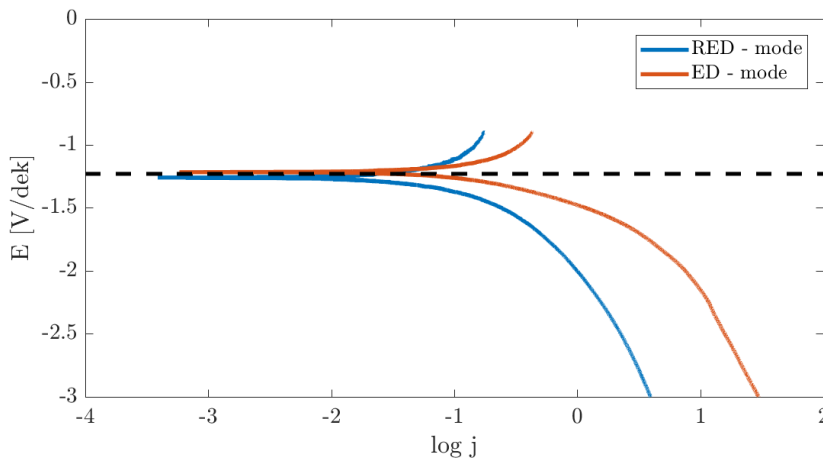
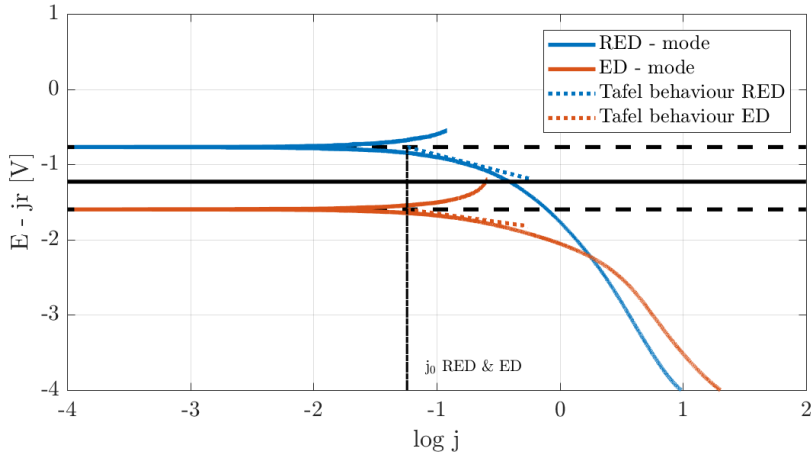**Figure 4.13:** Tafel-curves for the stack operating with 21.3 and 45.6 g/100g KNO_3, T = 40 °C

All the obtained values for the OCP and the Donnan contributions are gathered in Table 4.5, along with the modelled values for comparison. The apparent permselectivities α_{app} are also included. These values are low, significantly lower than the permselectivities in the membrane data sheets.

Fig. 4.14 shows the Tafel curves for the evaporation system, obtained by subtracting the ohmic jr-losses from the polarisation curves in Fig. 4.12. Fig. 4.15 shows a zoomed version of the same figure, emphasising on the Tafel slopes.

Table 4.5: Summary of potentials and apparent permselectivities found from LSV experiments

Molarity [g/100 g]	E_{OCP} [V]	E_{Donnan} [V]	$E_{Donnan,theo}$ [V]	α_{app}
0.20 vs. 45.6	-0.77	0.46	0.95	0.48
0.20 vs. 45.6	-1.6	-0.37	-0.95	0.39
21.3 vs. 45.6	-1.3	-0.029	-0.13	0.22
0.20 vs. 45.6	-1.2	0.014	0.13	0.10

Figure 4.14: Tafel-curves for the operational stack after subtraction of jr - losses

The Tafel responses of the two curves are very similar. The Tafel slopes b are found as the slope of the curves where they have linear behaviour, marked in the figure with dashed coloured lines. The slopes are -0.420 mV/dek and -0.230 mV/dek for the RED and ED curves. The logarithms of the exchange current densities j_0 are marked as vertical lines in the figure, from the intersect of the slope and the measured OCP. It is apparent that $\log(j_0)$ is -1.24 for both curves, corresponding to a j_0 of 57 mV. The total expressions for the Tafel overpotentials are shown in Eq. 4.1 and 4.2.

$$\eta_{RED} = a \ + \ b \, log \, j = -0.50 \ - \ 0.42 \, log \, j \qquad [V] \qquad (4.1)$$

$$\eta_{ED} = a \ + \ b \, log \, j = -0.21 \ - \ 0.23 \, log \, j \qquad [V] \qquad (4.2)$$

Several pieces of information are read from the Tafel diagram, in addition to the Tafel features already mentioned. Firstly, both graphs have a very steep dive for high current densities. The slopes are far too steep to be Tafel features, and they occur for higher current densities than where kinetics usually are important.
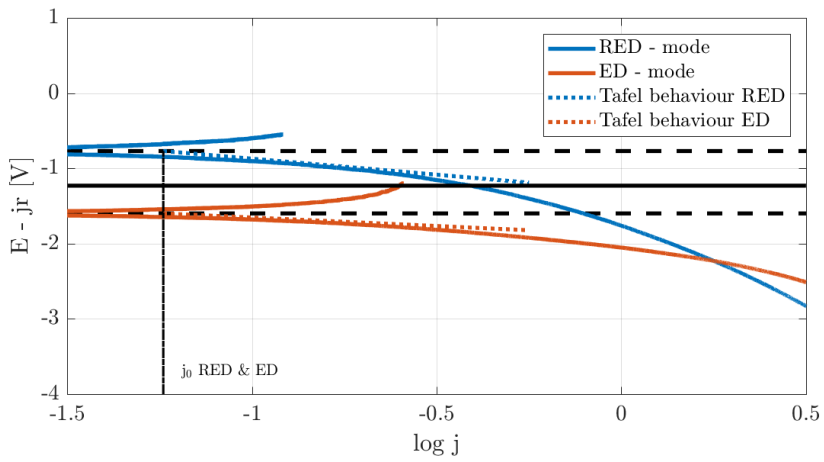
Figure 4.15: Closer view of the Tafel slopes of the RED stack

Chapter 5

Discussion

Due to difficulties with obtaining precise molarities when temperatures are above 25 °C, all solutions were prepared as molalities to improve accuracy. Here it is doubly difficult, because the solving of KNO_3 is an endothermic process, making the fresh solution quite cold, at the same time as saturated solutions are required, making it impossible to have accurate volume measurements at 25 degrees, where the lab equipment is calibrated. Concentrations are still reported as approximate molarities on some occasions, this is to provide the reader with more recognisable numbers which are easier to compare with known thermodynamical properties. For the purpose of reproduction of results, however, one should be careful to use the molalities stated.

Several identical potentiostats are available in the lab, sometimes used simultaneously. In case of faulty or wrongly calibrated devices, care has been taken to use the same potentiostats for all experiements of the same kind, meaning that all conductivity measurements are done with one unit and so forth. This will contain potential systematic errors in the results to one set of measurements, making the individual results comparable with each other.

The membrane samples are handled by hand quite substantially during the measurements of conductivity. This places high demands on lab hygiene, in the sense that gloves must be changed often, and that attention must be given to avoid contaminating the membranes with change in concentration of KNO_3 or other sources of pollution.

5.1 Ionic conductivity

In general, the experimental resistance values for the membrane samples are quite evenly spaced on a distance axis. The correlation between thickness and resistance is overall quite good, a feature that instils confidence in both the measurement method and the obtained

results. The results show no dependency on concentration. Two of the membranes display quite linear impedance spectra, while one tested membrane have large and unexpected features present, especially for higher concentrations.

The linear impedance response of the FKE-50 and FAS-30 membranes are likely to indicate a double layer. Double layers building up between the membrane and the electrodes, or between several samples of membrane, will show as straight lines angled away from the ordinate at 70 - 80°. Ohmic resistance and capacitance of the membrane itself shows in impedance spectra as a *high frequency* semicircle, of which the start is visible when hardware impedance spectra are subtracted. Measurements at very high frequencies, higher than the frequencies obtainable from laboratory equipment, are required to see the full semicircle.

The resistance values for five samples of FKE-50 displayed in Fig. 4.3 are very stable at 25 °C, and less so at 40 °C. Variations in temperature itself may be a contributing factor to this behaviour. A stable temperature of 40 °C is hard to achieve, due to the high thermal inertia of the test cell. As a consequence, the experiments may have been performed for transient temperatures rather than stationary, thus less accurate than desirable. In addition, the time required to reach the desired temperature between mounting and start of the EIS tests varies quite significantly, meaning that some membrane samples may be exposed to more potential water evaporation or drying than others.

The accuracy of the thermocouple used to control the temperature is in itself not very high. This may contribute further to the observed variations in conductivity. Ideally, this should be specifically investigated through error propagation analysis.

The interface resistance possibly present between the membrane samples in the conductivity test cell is not verified or accounted for, as the thicker version of the FAS-50 membrane had deviating behaviour. The resistivity results clearly show that the tested samples are from two different membranes, that may not be compared to each other. The number of interfaces in the sample stack also increases linearly with thickness, and the interface is undetectable unless two membranes of equal make and different thickness are tested together. This is a weakness in the results. However, the conductivity found is in the high range of comparable values, at least for the FKE-50 membrane. If interface resistance is present, it is not likely to dominate. For the purpose of modelling the RED stack behaviour, the potential impact from too high membrane resistance is negligible.

The frequency range reveals that the bends and semicircle-like features displayed for the FAS-50 membrane are in fact not the semicircles caused by the membrane material itself. The observed circles appear in the range between 200 000 Hz and 3 000 Hz. The circles are never approaching origo, and membrane bulk impedance has to pass through origo in order for readings of the resistance as the circle diameter to be meaningful.

It is verified that similar features do not appear for the FKE-50 and FAS-30 membranes even for very low frequencies, enhancing the impression that the behaviour exclusively occurs for the one kind of membrane.

Several possible explanations are proposed. One possibility is drying. If the estimated membrane concentration is wrong, and the concentration of ions per volume water is lower

than the concentration in the liquid, water may diffuse out of the membrane instead of ions diffusing into it. This in turn leads to lower conductivity. According to the assumptions in the calculation model should the membrane concentration be well above any solution concentration. If these assumptions are invalid and the membrane concentration is greatly overestimated, should the result show in all the investigated membrane, not just one.

If the concentration is altered for structural reasons instead, where some kind of manufacture flaw leads to a lower membrane concentration, this may explain the deviating behaviour. The membrane flaw may be in the charged groups, leading to a lower IEC than assumed. It may also be porosities in the membrane structure, leading to a high water content.

The FAS-50 membranes are behaving as the other two membranes and displaying the expected linear behaviour when soaked in DI-water, but the conductivity is consistent with the values found for higher concentrations. Conductivity should not be lower due to water diffusion when the water has no driving force to diffuse. This means that if drying occurs, it is not the only explanation.

Another proposed explanation is degrading of the membranes due to the strongly oxidising behaviour of NO_3^-. Arguments against are that the other membrane types should be affected too, at least the anion exchange membrane. This is not the case.

Due to the large size of the NO_3^- ions, the pores of the membrane could be too small to conduct the anions properly. Only the largest pore sizes would effectively be conducting ions in this case. The same counter argument as for degrading is valid also here, as this is also a condition that should affect both anion membranes. If a manufacture flaw has occurred however, where the pores are smaller than normal for the material, this may be the reason. This could possibly also explain the parallel capacitance that appears to be present. If the IEC is unaltered and there is a strong positive charge in the membrane structure, but ions can not enter the membranes in sufficient amounts to establish electroneutrality, negative ions will pile up at the membrane surface, creating a strong double layer. This effect would be more pronounced for higher concentrations, well in line with the observations from the EIS plots. Double layers would effectively block the counter-ions from entering the membrane, possibly lowering the apparent permselectivity.

Faulty membrane porosity is a flaw that may pass through control procedures at the manufacturer without detection, as the membrane in its dry state is not affected. It could also be that the membrane in its H^+ form does not show the same features, due to the small size of the protons.

The hardware spectra obtained and used for impedance correction may be inaccurate. Several reasons for this are imaginable. One is the corrosive effect of KNO_3, potentially leading to deterioration of equipment. The blank tests are not performed after each membrane test, but rather on occasion either before or after a batch of measurements at a given temperature. Variations in wire or electrode conductivity will thus not be captured, as the same impedance spectrum is subtracted from all measurements at that temperature. Other reasons for the observed variation may be inaccurate temperature values, instrument artifacts or changes in the surface of the electrode, leading to variations in the contact surface.

The frequency range used for the EIS is calibrated through the initialisation tests. It is well suited for the linear impedance spectra, but for the FAS-50 membrane it appears to be somewhat short. Not all measurements have an actual intersect with the real axis, and manual extrapolation is performed. This leads to much larger uncertainties in the results than an automated process, especially because some extent of human decisions are inevitably involved. Interestingly, the standard deviations for the faulty membrane is a significantly smaller than for the membranes with normal behaviour. In either case, a larger frequency range would be beneficial, also for confirmation of the presence of a high-frequency semicircle.

The final conductivity results are gathered from the measured resistances after impedance subtraction rather than from the raw data material. As the subtracted spectra display signs of deviations from the expected behaviour, errors or inaccuracies may be passed on to the end results. All the raw data material are still available, and could be re-analysed in the future as a control procedure.

The measurements of membrane thickness is performed with a micrometer. Conductivity results are very dependent on the thickness, and even small errors will have considerable impact. The micrometer, despite being a high-precision tool, is not always reliable. The threads of the instrument are somewhat worn, and sometimes one or more threads are skipped as the clamps are tightened on a sample. All thicknesses are measured three times, on varying parts of the sample surface, to account for this. Yet, one can not be absolutely certain that the measurement is accurate. A compilation of all the gathered thickness data shows that the thickness is not dependent of neither temperature nor concentration. In fact, the differentials in thickness within one sample or stack are larger than the variations between different samples, meaning that standard deviations are completely due to material variations.

It is possible that poor contact between the electrode and membrane surfaces lead to inaccurate estimations of the membrane bulk impedance. One cause of impaired contact may be a thin layer of electrolyte at the interface, especially at low concentrations. The membrane samples are immersed in KNO_3 or deionised water until the point of contact, and are for that reason covered in electrolyte. For very high concentrations, the conductivity of the electrolyte should well surpass that of the membrane, leading to a low offset in the measured impedance. There are no trends of lower resistance for higher concentrations however, so if a liquid layer is present, its effect is not pronounced. Increased pressure in the cell may improve the surface contact.

KNO_3 is a strong oxidiser, and has a pronounced corrosive effect on non-precious metals. The last conductivity measurement performed (5 samples of FAS30 in 2.5M KNO_3) deviated greatly from previous experiments, and upon investigation the copper cable showed clear signs of corrosion. The affected section of the cable was removed and the experiment redone, but as corrosion is a gradual process, it is not clear whether other results may have been affected, and if so, to what extent. However, all other measurements immediately preceding the discovery of the corroded cable have results that match the predictions well, and are deemed reliable.

The membranes are not wiped before the experiments, meaning that the amount of elec-

trolyte residue may vary. The reason for this is the very concentrated solutions they are soaked in - the risk of crystals forming on the membrane surface was considered a more significant source of error than then potential variations in surrounding electrolyte volume. The membranes are, however, handled individually, and each membrane is shaken, counted and stacked before mounting in the cell. All of these steps will remove some of the surplus electrolyte, meaning that in the end, the experimental conditions are believed to be quite identical from experiment to experiment. It could still be that variations may influence the results, both in terms of ionic resistance and as one or several double layers building up as the electrolyte is polarised.

The possible polarisation of the electrolyte could be avoided by washing the membranes briefly in DI-water before stacking. This would also allow wiping with lint-free paper, creating overall more controlled test environments. The argument against is that it is desirable to investigate the membranes in conditions as close to the ones encountered in the RED stack as possible, including surplus electrolyte in the membranes. It could be interesting to do the DI-variation of the experiment in the future, allowing for a comparison between the results and a better understanding of how the membranes could be affected.

The individual experiments are at this point only performed once, a necessary consequence of a time-limited project. For reproducibility, and to clarify if the results really are representable for the investigated membranes, repetition is required. However, as each reported conductivity is not a direct measurement but rather the calculated result from a series of twelve experiments (three stack thicknesses for four concentrations), the obtained results are considered to have a high credibility. The observed trends in the results are also consistent for the various membranes across thicknesses, temperatures and concentrations. It is reasonable to assume that the deviating behaviour from the linear relationship between resistance and thickness would change or disappear if the measurements were repeated.

The manual handling of the samples mechanical strain on the fragile membranes, which then may be subject to ruptures or cracks. The latter is also a risk due to drying, especially when experiments are performed at temperatures higher than room temperature the threshold for drying is quite low. Ruptures in the membrane may cause ionic short-circuits, which may influence the results. This is particularly a factor to consider when only one membrane is subject to the EIS-test, as a rupture would allow direct contact between the electrodes.

5.2 Calculation model and separation system

The theoretical power output of 13.5 W/m^2 from the stack is very high compared to literature values, but correspond to the manually calculated power densities for the same conditions. The reason why the power densities are so high as they are is most likely the low system resistance. The model implements several optimisation measures at the same time, while it is more common among scientist to concentrate on one focus area at the time. In this case, both thin flow channels and low resistance membranes are implemented together, along with very high concentration ratio between the compartments. As the elec-

trolytes are intended for circulation, limitations such as the use of concentrations naturally occurring in nature do not apply. The model values are not experimentally confirmed, and a lot of work probably remains before practical numbers of this magnitude are achieved. However, the model shows that the possibility for high power output with simple measures is present, and should be strived for in practice.

The evaporation system displays significantly higher output values than the precipitation system when several scenarios are compared. The theoretical values for the precipitation system is much more in line with results achieved by others. A loop is used to calculate the scenarios, meaning that the calculations are exactly equal in all cases. This is good for the credibility of the higher values.

When the scenarios from the two separation systems are compared to each other, it is apparent that the evaporation based separation system displays a much higher maximum power density than the precipitation based, with more than ten times higher values. Yet, the increase in current density is relatively lower, where only a factor 2 or 3 differentiates between the systems. This means that the evaluation of the two systems depends on the intended usage. If the stack is used for power production, as most RED systems traditionally have been designed for, the evaporation system must be more than ten times more expensive over its lifetime than the precipitation system before it is no longer the most viable choice. However, when hydrogen evolution is the target, the evaporation system only has to be between two and three times as expensive as the precipitation system before it is out-conquered. Energy prices for the thermal heat are very influential in this case.

The stack potential and power density are negative for dilute concentrations too close to the high salinity concentration in this stack. Other setups may yield other results, but it is likely that a certain limit exists in most comparable systems. This may cause trouble for the precipitation system, as even the minimum dilute concentration in this case is too high to produce useful work.

When evaluating separation by evaporation, thermal energy need should be weighted against electrical gain to find the overall situation. If the external heat comes from a surplus, meaning it is added for free, the calculations may be more advantageous for the evaporation system. However, if heat of higher quality is used (close to 100 °C), one should also include the Gibbs free energy in the consideration, meaning that the fact that electricity *could* have been produced from the same heat through an Organic Rankine Cycle or similar should be taken into account. The use of district heating may also be an option, although if there is a network close by the heat may never have been classified as waste in the first place.

For the precipitation system is the required heat input temperature quite low, which is advantageous. Heat of such low quality is difficult to put to use anywhere else. Tomato production, domestic heating applications and deicing of roads may be examples of applications, but all of these are geographically bounded. The heat resource is also very abundant. It is important to make use of all available energy resources if we are to reach the climate goals. The use of the RED-stack converts thermal energy of very low quality to high quality electricity, and is arguably a better way to utilise the thermal energy than heat purposes are.

5.3   RED-stack

The obtained resistances from the EIS experiments are quite stable, without clear trends. The precipitation system displays a slight decrease in resistance both for higher molarity and for higher temperatures, this is as expected. However,while the double standard deviation for the first experiment in Table 4.4 is quite small, are the other two very high. In fact, the high temperature experiment for molalities of 21.3 and 38.3 g/100 g have a standard deviation that is larger than the result itself, making it insignificant. However, one of the experimental results included in this standard deviation is an outlayer. If this result is not included, is the standard deviation reduced to $4.6 \cdot 10^{-4}$ Ωm^2, a number that is more in line with the previous results. Still, this also reduces the resistance r itself to $3.8 \cdot 10^{-3}$ Ωm^2, which in turn is noticeably lower than the remaining precipitation experiments. It is not clear from this whether inclusion or exclusion of the outlayer reflects reality the best.

The evaporation system has a similar trend as what is seen for the precipitation system. The obtained resistance values are relatively stable, but the standard deviations are too high to establish whether the results are systematic or if they have similar values by chance. In either case, it is clear that several measured values reveal a lot more information than single standing experiments would. The values for resistance in the stack are significantly higher than the modelled values even when standard deviations are implemented in the most beneficial way possible.

The presence of a semicircle in the EIS spectra for the stack could provide valuable information about non-ohmic resistances. It is hard to draw conclusions based on the slight trend that is apparent. One way of determining this could be to extrapolate a semicircle with an outer diameter fitting to the bend on the curves. The bend occurs in the same resistance and frequency regions in all the results, and it could seem likely that the patterns are consistent. In that case, the non-ohmic resistance could be read as the second intersect with the real axis. The first intersect of the semicircle should be compared with the obtained values for ohmic resistance. A correlation would be expected. It may be possible that the use of the semicircle could yield more consistent results than the linear extrapolations performed did.

It appears from the plots that the frequency range is too short in the upper region, despite the initial testing. It is unclear what is causing this, as only the range was changed. Stabilisation time was carefully maintained for all experiments, and was the same as during initialisation. Fig. B.1 contains both data taken in the preparations and after (represented as the yellow curve), and the difference is clear to see in this case. It appears as the experimental resistance is unaltered, which is a good sign for the value of the results. Still, extrapolation brings larger uncertainties, and the risk of errors is absolutely larger. The high standard deviations for the resistance values could maybe be smaller if the actual intersects were known, but it does not appear to be the case for the figure in question.

The possible onset of a semicircle in the plots would be clearer to evaluate if the frequency range was higher. As much of the circumference as possible is of course beneficial. Semicircles are increasingly visible for frequencies higher than the characteristic peak frequency of the system, and no semicircle is expected if the applied frequency is too

low.

The linear sweep voltammetries of the RED stack reveal a shift in the stack polarity observed for the highest dilute concentration. This seems to indicate that the stack enters ED mode by itself. This is actually corresponding quite well with the concentration dependent potentials modelled in Fig. 4.9 and Table 4.3, where the cell potential is negative for higher dilute concentrations. Ohmic losses are present as long as a current is applied, and for small enough Donnan potentials are the potential drops completely dominating the net output.

It could be a possibility that the polarities are not swapped in the polarity curves, but rather, the experiments are labelled erroneously. However, due to the order the experiments are performed in, this would require the polarity to be shifted two times over a set of eight measurements without registration. The polarity change is physically conducted, and the process is both challenging due to all the tubing and the constricted space, and delicate as the platinum wires are fragile and must be treated carefully. It is considered highly unlikely that two full shifting procedures like this are simply forgotten.

The apparent permselectivities found from the experimental results are very low. In part, this could be explained by the very high concentrations used, as high salinities usually lower the permselectivity. This is supported by the comparably higher permselectivity when the dilute concentration is lower.

Another reason may be leakages between compartments, causing altered concentrations than what is modelled. If this is the case, the net leakages between two or several compartments must be quite close to zero, as no significant deviations in flow rate out of the stack were observed. This could be verified with measurements of conductivity of the spent solutions. Added colorant to the solutions would be an efficient tool to trace mixing, provided that the colorant itself is not detrimental to the membranes or other components.

An important factor to remember when analysing the obtained results, is that the membranes used in the stack are subject to a not clearly identified error. The conductivity is measured with EIS, but as long as the reason for the observed behaviour is not known, other symptoms than increased resistance can not be excluded. It is possible that some of the features of the results are not reproducible with functioning membranes, and are thus not meaningful to analyse.

The Tafel slopes in the plot are steeper than what is expected, even for several reactions together. One possible explanation for this is that the lines are not exclusively Tafel features, but rather combinations of Tafel and ohmic overpotentials for instance. Ohmic losses are supposedly subtracted at this point, but there may still be losses that are not accounted for.

The even steeper slopes occuring in the Tafel plot for high current densities, could be indicators of concentration polarisation. Ions can not be supplied fast enough to maintain the reaction rate, and potential drops are the result as the current density is approaching the limiting current. A possible catalyst for this behaviour is the flow rate of the electrolytes. A higher flow rate will both supply and remove ions faster, avoiding depletion or pile-ups of ionic species. The draw back is mechanical stability, as increased flow rates increases the risk of leaking. Pump power cost is also a factor.

A too low flow rate could possibly also contribute to low apparent permselectivity. If the supply of ions is insufficient in the electrolytes, meaning that there are no more ions to transport, the perceived concentration difference will be lower than expected. However, ions move mainly when current is applied, and the impact on OCP is not considerer very important.

The experiments could be redone for a higher flow rate, to see if the performance is improved. The flow rate of both compartments should ideally be calculated, corresponding to the optimum concentration difference between inlet and outlet. Economical considerations should take into account the increased pump power consumption for higher flow rates.

From the calculation model, it can be found that the performance of the stack is expected to be about 6% better with the FAS-30 membranes than what is expected for the FAS-50 membranes. This is provided that the FAS-50 membrane is without damage and behaves as expected. The conductivity of the FAS-30 membrane is assumed for both thicknesses in this case, in lack of reliable data. This project is proof of concept, and mechanical strength was prioritised over optimal electrical properties. In larger implementations of the system however, the difference in potential should be taken into account when selecting components.

In a larger scale is it imaginable that the temperature of solutions and hardware may be kept much more constant than laboratory work allows. If so, the high salinity molality may be increased so that it is closer to the solubility limit at 40 °C than 30 °C as it is now. This could lead to a significant potential gain from increased concentration difference. If the temperature could be increased too, for instance because of the development of membranes with a higher tolerance, would even rather slight temperature increases be very beneficial for the power production. The combined effect of increased concentration and temperature would then drive the production higher. Membranes are thus still a very important area of research, both in terms of properties and in terms of cost.

The experimental stack performance is poor enough to imply that whatever happened to the FAS-50 membrane, it is not contained to the one sheet that supplied the samples for the conductivity experiments. It could even be worse for the rest of the sheets in the batch.

All values for power production, both experimental and practical, are reported as the gross power output. For real applications should the auxiliary power consumption, in practice pump power, also be taken into account. This is especially relevant when thin compartments are used, such as in this research, as thinner flow channels increase the pressure drops over the stack.

Chapter 6

Conclusions

The measured membrane conductivities of FAS-30 and FKE-50 membranes are unaltered and higher in KNO_3 compared to in NaCl, respectively. Obtained values are FAS-30 and FKE-50 have respective conductivities of 4.3 ± 1.2 mS/cm and 4.5 ± 0.5 mS/cm at 25 °C, and 6.5 ± 2 ms/cm and 6.6 ± 1.3 mS/cm at 40 °C. The batch of FAS-50 received from the manufacturer is likely damaged or faultily produced, possibly with pore dimension errors. The measured conductivities are not likely to be representative for this kind of membrane.

The maximum power output from the stack for the modelled operation conditions is 13.5 W/m^2, occurring for a current density of 227 $A/^2$. This corresponds to 8.5 g H_2/h m^2.

According to modelled results are separation systems with evaporation ten times more efficient than precipitation systems for power production, and three times as efficient for hydrogen production. Benefits of the precipitation system in terms of economy, available temperature and other considerations must be correspondingly much larger, depending on application.

Experimentally obtained values for resistance in the stack yield about $0.0045 \ \Omega m^2$ for precipitation conditions and $0.0084 \ \Omega m^2$ for evaporation conditions, but the standard deviations are quite large.

Practically obtained OCP values are lower than expected, and apparent permselectivities are between 0.1 and 0.5 for all measurements. Faulty membranes may be a contributor to this.

Precipitation is not viable for this stack, as the available concentration range is too short. The Donnan potential is not sufficient to compensate for the internal losses, and the total stack potential is negative relative to useful work.

Chapter 7

Further work

The conductivity values for the membranes could be further confirmed with variations in the test parameters. An example is washing (and wiping) of the membranes in DI-water before the EIS experments, to investigate potential side effects of surplus electrolyte. Also, a general repetition of the experiments should be done to increase the reproducibility. If the standard deviations are not lowered for a larger populations, the test method itself should be evaluated.

A recalculation of conductivity results based on raw data rather than impedance-corrected data could verify whether or not inconsistencies in the hardware spectra have a great impact, and also to what extent the subtraction has impacted the ohmic values.

Membrane resistance should be measured in a way where the concentration difference on each side of the membrane, as encountered in RED, is accounted for. The measurements performed through this project analyses how the membranes are influenced by higher concentrations, but not the impact of concentration gradients.

The calculation model should be further expanded, and more details about complex stack process should be implemented.

Both modelled and experimental values for the RED stack performance would have increased confidence if the experiments are repeated for membranes without known irregularities in behaviour. This is relevant both for EIS tests of resitance values and LSV experiments for electrochemical performance. Both experiments also have room for improvement; the EIS experiments should be performed for higher frequencies, to cover the entire relevant range. The fitting of a semicircle should also be performed, to evaluate the non-ohmic resistances. The LSV experiments should be performed with reference electrodes on the inside of the stack electrodes, to differentiate much more clearly between the various present processes. All stack experiments should be done at an optimised flow rate.

Several LSV experiments, for a larger number of concentration combinations and tem-

peratures, are recommended. This would both increase the confidence in the results, and confirm or disprove the observations regarding shifted polarities. A Faraday cage should be fitted to the stack to eliminate external disturbances.

Pump energy should be taken into consideration, to find the real and expected net power output from the stack. This is very important to evaluate the technology for real applications.

Bibliography

[1] Ida Johanne Haga. Heat to H2. Specialisation project, Technical University of Norway (NTNU), 2017.

[2] The World Bank. Fossil fuel energy consumption, November 2017.

[3] Paris agreement. *United Nations Treaty Collection*, CHAPTER XXVII: ENVIRONMENT 7.d, 12 December 2015.

[4] National Research Council et al. *The National Academies Summit on America's Energy Future: Summary of a Meeting*. National Academies Press, 2008.

[5] Moran, Shapiro, Boettner, and Bailey. *Principles of Engineering Thermodynamics*. Jon Wiley & Sons, 7th edition, 2012.

[6] Jan W Post, Joost Veerman, Hubertus VM Hamelers, Gerrit JW Euverink, Sybrand J Metz, Kitty Nymeijer, and Cees JN Buisman. Salinity-gradient power: Evaluation of pressure-retarded osmosis and reverse electrodialysis. *Journal of membrane science*, 288(1):218–230, 2007.

[7] Marta C Hatzell, Ivan Ivanov, Roland D Cusick, Xiuping Zhu, and Bruce E Logan. Comparison of hydrogen production and electrical power generation for energy capture in closed-loop ammonium bicarbonate reverse electrodialysis systems. *Physical Chemistry Chemical Physics*, 16(4):1632–1638, 2014.

[8] Ramato Ashu Tufa, Elisabetta Rugiero, Debabrata Chanda, Jaromir Hnàt, Willem van Baak, Joost Veerman, Enrica Fontananova, Gianluca Di Profio, Enrico Drioli, Karel Bouzek, et al. Salinity gradient power-reverse electrodialysis and alkaline polymer electrolyte water electrolysis for hydrogen production. *Journal of Membrane Science*, 514:155–164, 2016.

[9] Enova SF. Potensial for energieffektivisering i norsk landbasert industri. Technical Report 2009:5, Enova, 2009.

[10] O Burheim. Red-ed-enabling-technology reverse electrodialysis and electrodialysis for renewed resources. Research proposal Heat to H2, 2017.

[11] Adam Z. Weber, Matthew M. Mench, Jeremy P. Meyers, Philip N. Ross, Jeffrey T. Gostick, and Qinghua Liu. Redox flow batteries: a review. *Journal of Applied Electrochemistry*, 41(10):1137, Sep 2011.

[12] RE Pattle. Production of electric power by mixing fresh and salt water in the hydro-electric pile. *Nature*, 174(4431):660–660, 1954.

[13] John D Isaacs and Richard J Seymour. The ocean as a power resource. *International Journal of Environmental Studies*, 4(1-4):201–205, 1973.

[14] Richard S Norman. Water salination: a source of energy. *Science*, 186(4161):350–352, 1974.

[15] Gerald L Wick. Power from salinity gradients. *Energy*, 3(1):95–100, 1978.

[16] O Kedem, G Tanny, and Y Maoz. A simple electrodialysis stack. *Desalination*, 24(1-3):313–319, 1977.

[17] John N Weinstein and Frank B Leitz. Electric power from differences in salinity: the dialytic battery. *Science*, 191(4227):557–559, 1976.

[18] Martin Alexander Mason. *Saline Water Conversion: Proceedings of a Symposium, 4-6 November 1957*, volume 568. National Academies, 1958.

[19] RE Lacey. Office of saline water research and development report 135. *US Government Printing Office, Washington, DC*, 1965.

[20] Georges Belfort and GA Guter. An electrical analogue for electrodialysis. *Desalination*, 5(3):267–291, 1968.

[21] C Forgacs. *Generation of electricity by reverse electrodialysis (RED)*. Ben-Gurion University of the Negev, 1978.

[22] RE Lacey. Energy by reverse electrodialysis. *Ocean engineering*, 7(1):1–47, 1980.

[23] Joost Veerman, Michel Saakes, Sybrand J Metz, and GJ Harmsen. Reverse electrodialysis: evaluation of suitable electrode systems. *Journal of Applied Electrochemistry*, 40(8):1461–1474, 2010.

[24] J Veerman, JW Post, M Saakes, SJ Metz, and GJ Harmsen. Reducing power losses caused by ionic shortcut currents in reverse electrodialysis stacks by a validated model. *Journal of Membrane Science*, 310(1):418–430, 2008.

[25] Ryan S. Kingsbury, Kevin Chu, and Orlando Coronell. Energy storage by reversible electrodialysis: The concentration battery. *Journal of Membrane Science*, 495(Supplement C):502 – 516, 2015.

[26] Ramato Ashu Tufa, Sylwin Pawlowski, Joost Veerman, Karel Bouzek, Enrica Fontananova, Gianluca di Profio, Svetlozar Velizarov, João Goulão Crespo, Kitty Nijmeijer, and Efrem Curcio. Progress and prospects in reverse electrodialysis for salinity gradient energy conversion and storage. *Applied Energy*, 225:290–331, 2018.

[27] Odne Stokke Burheim. *Engineering Energy Storage*. Academic Press, 1st edition, 2017.

[28] Tongwen Xu. Ion exchange membranes: State of their development and perspective. *Journal of Membrane Science*, 263(1):1 – 29, 2005.

[29] Piotr Długołęcki, Kitty Nymeijer, Sybrand Metz, and Matthias Wessling. Current status of ion exchange membranes for power generation from salinity gradients. *Journal of Membrane Science*, 319(1):214 – 222, 2008.

[30] Jin Gi Hong, Bopeng Zhang, Shira Glabman, Nigmet Uzal, Xiaomin Dou, Hongguo Zhang, Xiuzhen Wei, and Yongsheng Chen. Potential ion exchange membranes and system performance in reverse electrodialysis for power generation: a review. *Journal of Membrane Science*, 486:71–88, 2015.

[31] Ying Mei and Chuyang Y. Tang. Recent developments and future perspectives of reverse electrodialysis technology: A review. *Desalination*, 425:156 – 174, 2018.

[32] A. Zlotorowicz, R.V. Strand, O.S. Burheim, Ø. Wilhelmsen, and S. Kjelstrup. The permselectivity and water transference number of ion exchange membranes in reverse electrodialysis. *Journal of Membrane Science*, 523:402 – 408, 2017.

[33] J Veerman and DA Vermaas. Reverse electrodialysis: fundamentals. In *Sustainable Energy from Salinity Gradients*, pages 77–133. Elsevier, 2016.

[34] Franciélli Müller, Carlos A Ferreira, Denise S Azambuja, Carlos Alemán, and Elaine Armelin. Measuring the proton conductivity of ion-exchange membranes using electrochemical impedance spectroscopy and through-plane cell. *The Journal of Physical Chemistry B*, 118(4):1102–1112, 2014.

[35] David A. Vermaas, Michel Saakes, and Kitty Nijmeijer. Doubled power density from salinity gradients at reduced intermembrane distance. *Environmental Science & Technology*, 45(16):7089–7095, 2011. PMID: 21736348.

[36] Toshiaki Isono. Density, viscosity, and electrolytic conductivity of concentrated aqueous electrolyte solutions at several temperatures. *Journal of chemical and engineering data*, 29(1):45–52, 1984.

[37] William M Haynes. *CRC Handbook of Chemistry and Physics*. CRC press, 2014.

[38] Gamry. Application note - basics of electrochemical impedance spectroscopy, August 2004.

[39] Jan W. Post, Hubertus V. M. Hamelers, and Cees J. N. Buisman. Energy recovery from controlled mixing salt and fresh water with a reverse electrodialysis system. *Environmental Science & Technology*, 42(15):5785–5790, 2008. PMID: 18754509.

[40] Joost Veerman, M Saakes, SJ Metz, and GJ Harmsen. Reverse electrodialysis: A validated process model for design and optimization. *Chemical Engineering Journal*, 166(1):256–268, 2011.

[41] J. Veerman, M. Saakes, S.J. Metz, and G.J. Harmsen. Reverse electrodialysis: Performance of a stack with 50 cells on the mixing of sea and river water. *Journal of Membrane Science*, 327(1):136 – 144, 2009.

[42] Odne S Burheim, Jon G Pharoah, David Vermaas, Bruno B Sales, Kitty Nijmeijer, and Hubertus VM Hamelers. Reverse electrodialysis. *Encyclopedia of Membrane Science and Technology*, 2013.

[43] Keith Oldham, Jan Myland, and Alan Bond. *Electrochemical science and technology: fundamentals and applications*. John Wiley & Sons, 2011.

[44] Debasmita Dash, Shekhar Kumar, C Mallika, and U Kamachi Mudali. New data on activity coefficients of potassium, nitrate, and chloride ions in aqueous solutions of KNO_3 and KCl by ion selective electrodes. *ISRN Chemical Engineering*, 2012, 2012.

[45] Odne S Burheim, Frode Seland, Jon G Pharoah, and Signe Kjelstrup. Improved electrode systems for reverse electro-dialysis and electro-dialysis. *Desalination*, 285:147–152, 2012.

[46] Gordon H Aylward and Triston John Victor Findlay. *SI Chemical Data*. New York, Wiley, 1973.

[47] Odne Burheim, Professor, Department of Energy and Process Engineering, NTNU . Personal communication.

[48] Jørn Stene, Associate Professor, Department of Energy and Process Engineering, NTNU. Personal communication.

[49] Dynamic Science. Solubility curves, February 2018.

[50] Fuel Cell Store. Technical Data Sheet - Fumasep FAS-30.

[51] Fuel Cell Store. Technical Data Sheet - Fumasep FAS-50.

[52] Fuel Cell Store. Technical Data Sheet - Fumasep FKE-50.

[53] Sefar AG. Technical Data Sheet - Sefar Nitex 03-160/53.

Appendices

Appendix A
Membrane conductivity

This appendix contains all experimental results from the measurements of membrane conductivity.

A.1 Electrochemical impedance spectroscopy

EIS-experiments were performed for 1, 3 and 5 samples of membranes for various temperatures and concentrations. The obtained results are presented in Fig. A.1 to A.7 for FKE-50 membranes, Fig. A.8 to A.14 for the FAS-50 membranes and in Fig. A.15 to A.21 for the FAS-30 membranes from Fumatech.

FKE-50
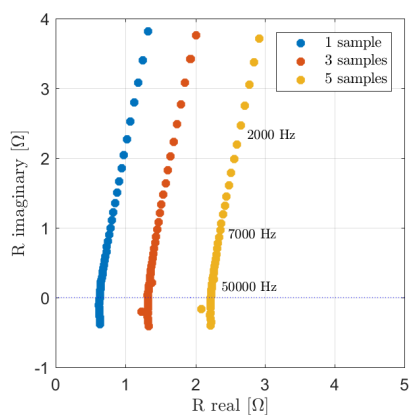
Figure A.1: FKE-50, 25 °C, DI-water
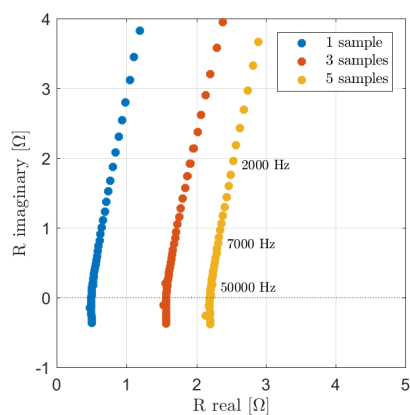
Figure A.2: FKE-50, 25 °C, 1M
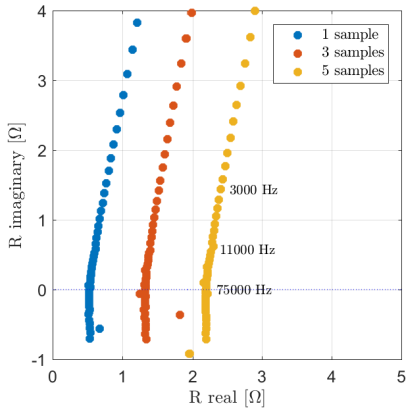
Figure A.3: FKE-50, 25 °C, 25M
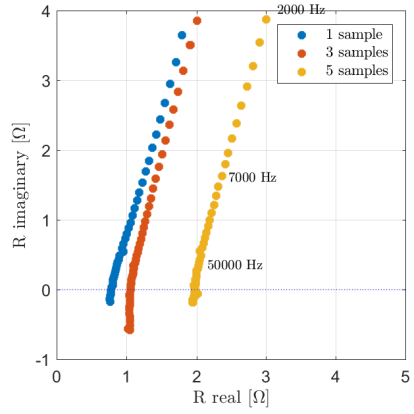
Figure A.4: FKE-50, 40 °C, DI-water
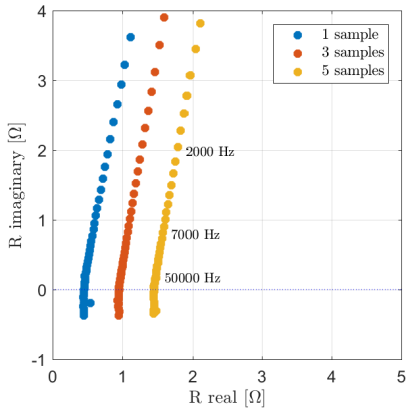
Figure A.5: FKE-50, 40 °C, 1M
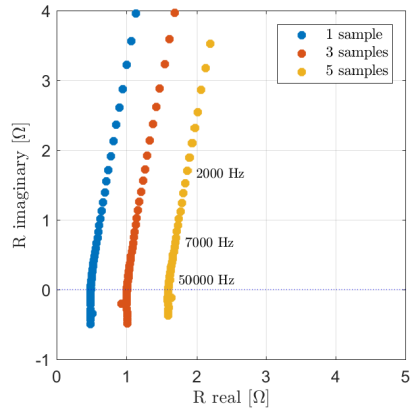
Figure A.6: FKE-50, 40 °C, 2.5M
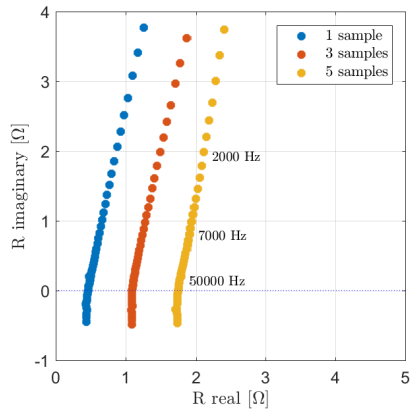
Figure A.7: FKE-50, 40 °C, 4.5M

FAS-50
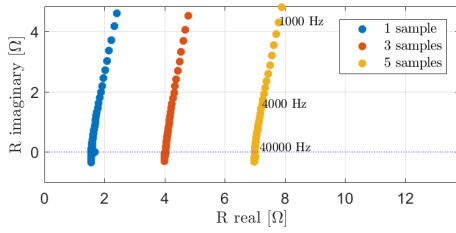
Figure A.8: FAS-50, 25 °C, DI-water
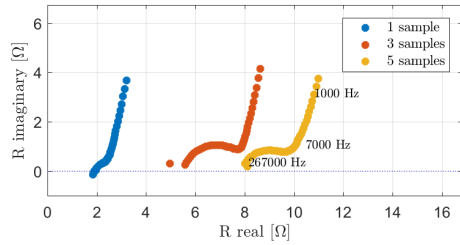
Figure A.9: FAS-50, 25 °C, 1M
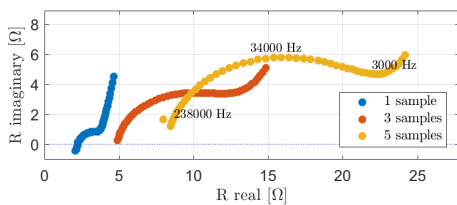
Figure A.10: FAS-50, 25 °C, 25M
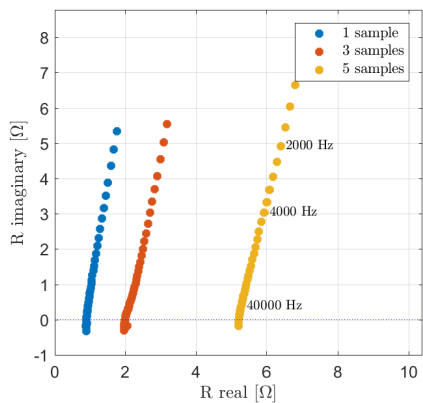
Figure A.11: FAS-50, 40 °C, DI-water
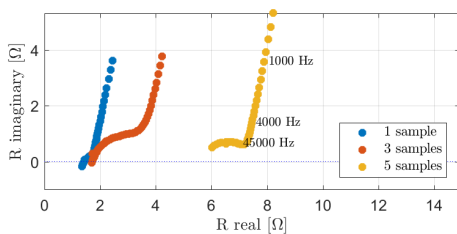
Figure A.12: FAS-50, 40 °C, 1M
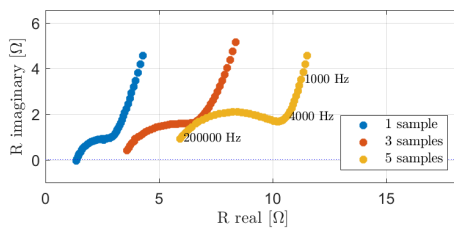
Figure A.13: FAS-50, 40 °C, 2.5M
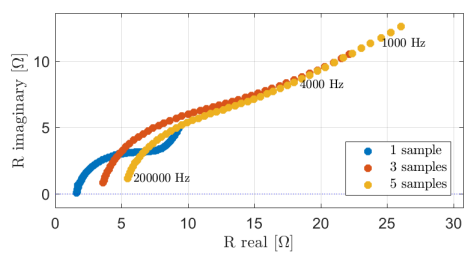
Figure A.14: FAS-50, 40 °C, 4.5M

FAS-30
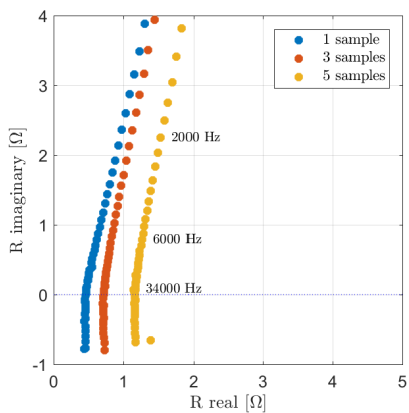
Figure A.15: FAS-30, 25 °C, DI-water
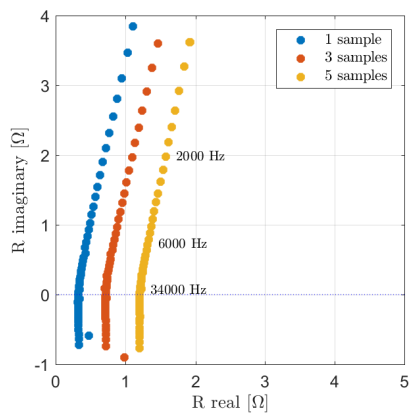
Figure A.16: FAS-30, 25 °C, 1M
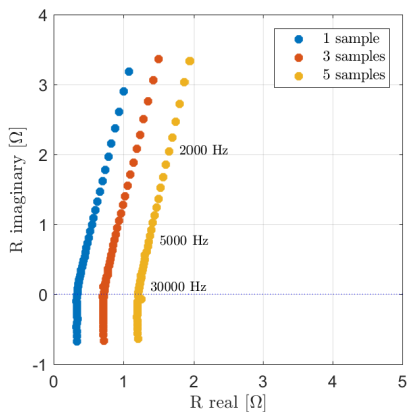
Figure A.17: FAS-30, 25 °C, 25M
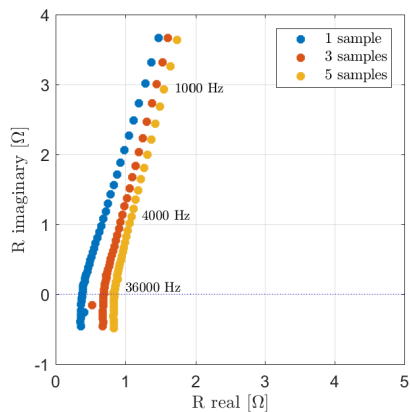
Figure A.18: FAS-30, 40 °C, DI-water
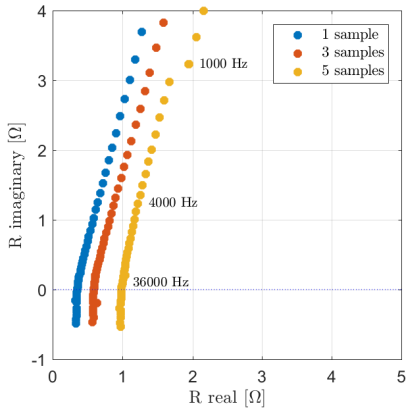
Figure A.19: FAS-30, 40 °C, 1M
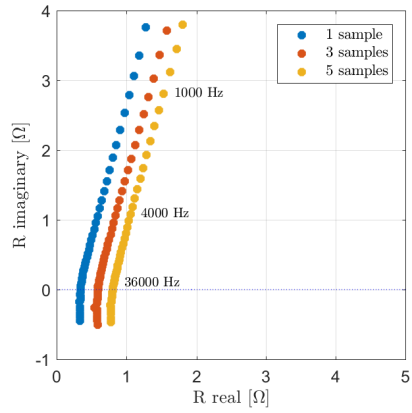
Figure A.20: FAS-30, 40 °C, 2.5M
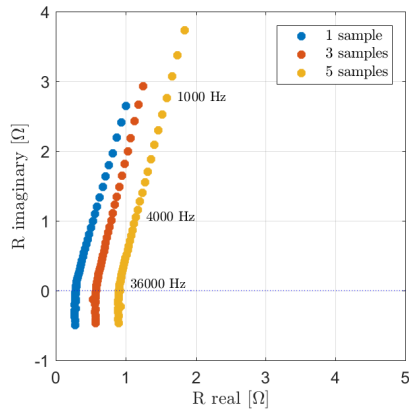
Figure A.21: FAS-30, 40 °C, 4.5M

A.2   Conductivity versus concentration

Figures A.22 to A.24 present the final conductivity results for all three membranes.
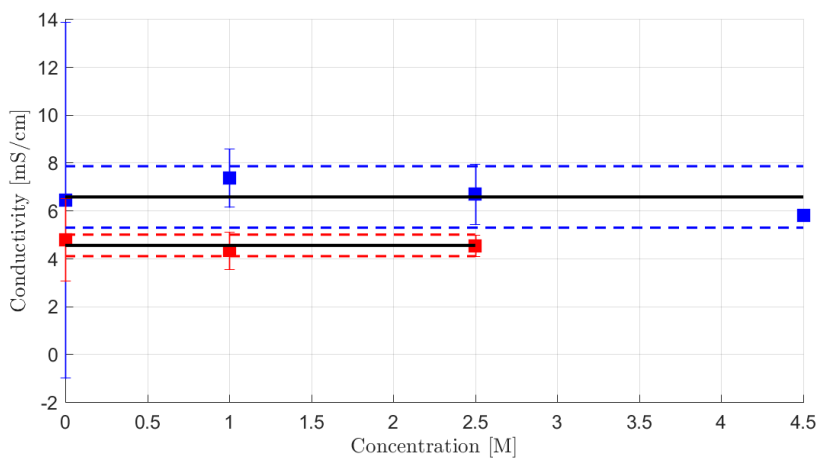
Figure A.22: Conductivity of FKE-50 with standard deviations
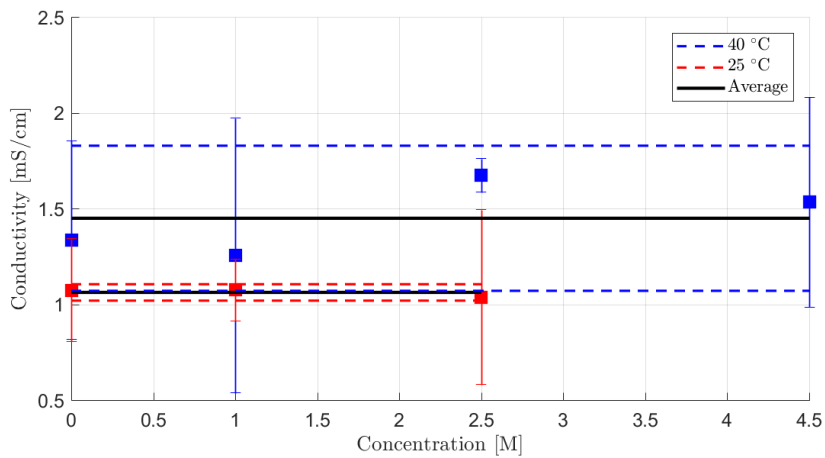
Figure A.23: Conductivity of FAS-50 with standard deviations
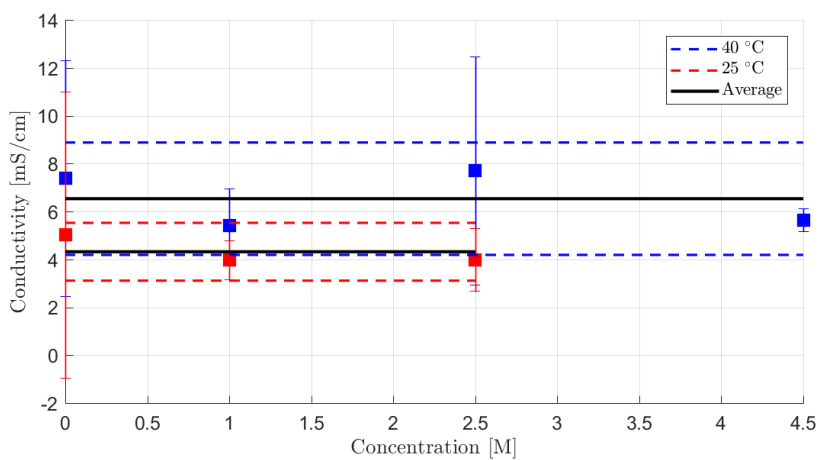
Figure A.24: Conductivity of FAS-30 with standard deviations

Appendix B
Practical RED operation

Linear sweep voltammetries are performed for six scenarios of RED operation. All experiments are conducted three times, and the plots belonging to the same operation scenario are in the same figure. Fig. B.1, B.2 and B.3 display stack resistances in an evaporation based system, while Fig. B.4, B.5 and B.6 show the results for a precipitation system.
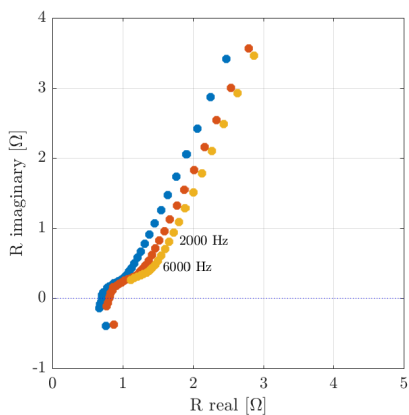

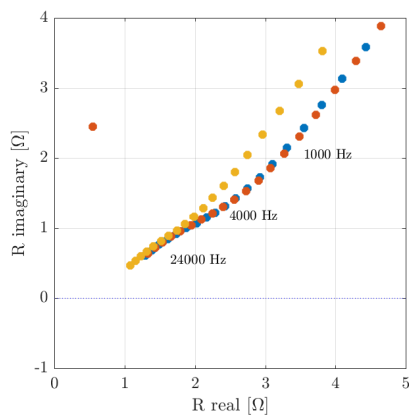**Figure B.1:** 0.2 g/100 g vs. 38.3 g/100g, 25 ° C
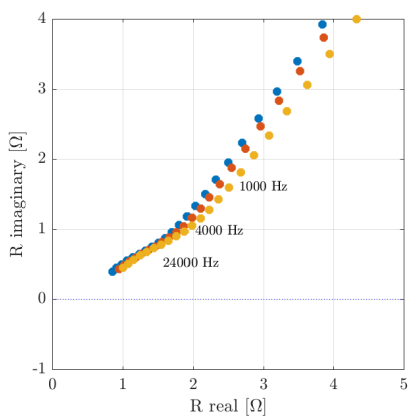

Figure B.2: 0.2 g/100 g vs. 38.3 g/100g, 40 °C

Figure B.3: 0.2 g/100 g vs. 45.6 g/100g, 40 °C
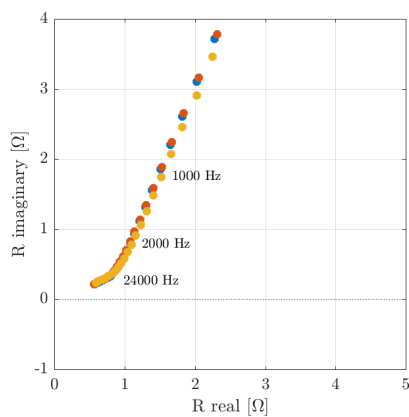

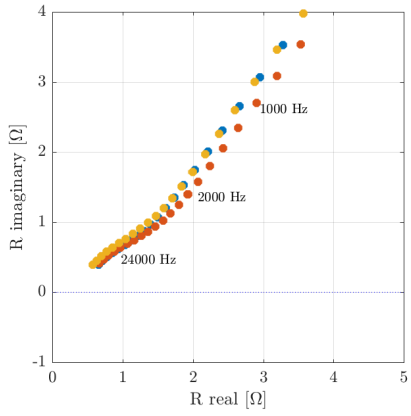**Figure B.4:** 21.3 g/100 g vs. 38.3 g/100g, 25 °C

Figure B.5: 21.3 g/100 g vs. 38.3 g/100g, 40 °C
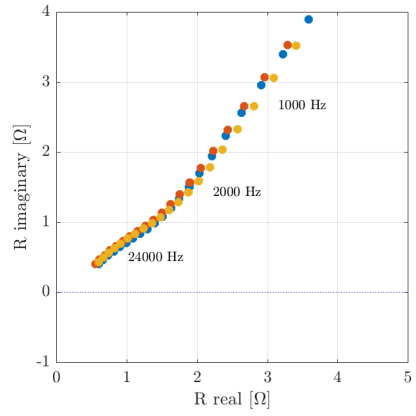

Figure B.6: 21.3 g/100 g vs. 38.3 g/100g, 40 °C

Appendix C
Risk Assessment

The following document is the risk assessment performed for experimental work in the laboratories at NTNU.

Kartlegging av risikofylt aktivitet

Enhet: _____ **EPT** **Dato:** 01.02.2018

Linjeleder: Anita Yttersian

Deltakere ved kartleggingen (m/ funksjon): Kjersti Krakhella, ansvarlig veileder. Ida Johanne Haga, student.
(Ansv. veileder, student, evt. medveiledere, evt. andre m. kompetanse)

Kort beskrivelse av hovedaktivitet/hovedprosess: Masteroppgave Ida Johanne Haga. Heat to H2.

Er oppgaven er rent teoretisk? *(JA/NEI)* NEI *"JA" betyr at veileder innestår for at oppgaven ikke innholder noen aktiviteter som krever risikovurdering*

Dersom "JA": Beskriv kort aktiviteten i kartleggingsskjemaet under. Risikovurdering trenger ikke å fylles ut.

Signaturer: *Ansvarlig veileder:* _Kjersti Krakhella_ *Student:* _Ida J Haga_

ID nr.	Aktivitet/prosess	Ansvarlig	Eksisterende dokumentasjon	Eksisterende sikringstiltak	Lov, forskrift o.l.	Kommentar
1	Blande KNO3	Kjersti Krakhella	EcoOnline, safety data sheet	Labfrakk, vernebriller, hansker	Arbeidsmiljøloven, med tilhørende forskrifter	
3	Håndtering av varmeskap og varmebad	Kjersti Krakhella	Medfølgende dokumentasjon varmeskap, Memmert UF 160plus	Labfrakk, vernebriller, hansker	Arbeidsmiljøloven, med tilhørende forskrifter	
4	Manuell tilskjæring av materiell	Kjersti Krakhella		Labfrakk, vernebriller, hansker	Arbeidsmiljøloven, med tilhørende forskrifter	
5	Stansemaskin	Kjersti Krakhella	Atom S/MF Series	Instruks om klemfare	Arbeidsmiljøloven, med tilhørende forskrifter	
7	Elektrokjemiske målinger med potensiostat	Kjersti Krakhella	Gamry Interface 5000 E	Labfrakk, vernebriller, hansker	Arbeidsmiljøloven, med tilhørende forskrifter	
8	Motstandscelle	Bjørn Volseth		Labfrakk, vernebriller, hansker	Arbeidsmiljøloven, med tilhørende forskrifter	

9	Konduktivitetsmåler		Kjersti Krakhella	Knick SE680 sensor, Portavo 907 MultiCond bordapparat	Labfrakk, vernebriller, hansker	Arbeidsmiljøloven, med tilhørende forskrifter	

Risikovurdering

		Utarbeidet av	Nummer	Dato
		HMS-avd.	HMSRV2603	04.02.2011
		Godkjent av	Side	Erstatter
		Rektor		09.02.2010

Enhet: EPT **Dato:** 01.02.2018

Linjeleder:

Deltakere ved risikovurderingen (m/ funksjon):
(Ansv. veileder, student, evt. medveiledere, evt. andre m. kompetanse) Kjersti Krakhella, ansvarlig veileder, Ida Johanne Haga, student.

Risikovurderingen gjelder hovedaktivitet: Masteroppgave Ida Johanne Haga. Heat to H2.

Signaturer: **Ansvarlig veileder:** *Kjersti Krakhella* **Student:** *Ida J Haga*

ID nr.	Aktivitet/prosess fra kartleggingsskjemaet	Mulig uønsket hendelse	Vurdering av sann- synlighet (1-5)	Vurdering av konsekvens				Risiko- verdi (menn- eske)	Kommentarer/ status Forslag til tiltak
				Menneske (A-E)	Ytre miljø (A-E)	Øk./ materiell (A-E)	Om- dømme (A-E)		
1	Blande KNO3	Søl på hud, kontakt med øyne, irriterende. Oksidering av avløp og metaller.	2	A	A	A	A	A2	Fortsatt forsiktighet ved håndtering
3	Håndtering av varmeskap og varmebad	Brannskade	3	A	A	A	A	A3	Unngå langvarig arbeid med åpen dør til varmeskap, unngå sterk PID-reaksjon fra varmeelement. Utvis forsiktighet ved høye temperaturer.
4	Manuell tilskjæring av materiell	Kuttskade	2	A	A	A	A	A2	Utvis normal forsiktighet
5	Stansemaskin	Klemskade	1	D	A	A	B	D1	Følg håndteringsinstruks.
5	Elektrokjemiske målinger med potensiostat	Ødelegging av utstyr	2	A	A	C	A	A2	Utvis forsiktighet.

| 8 | Motstandscelle | 3 | A | A | B | A | A3 | Utvis forsiktighet. |
| 9 | Konduktivitetsmåler | 2 | A | A | C | A | A2 | Utvis forsiktighet. |

Ødelegging av utstyr

Ødelegging av utstyr

Appendix D
Heat to H_2 - ECS Transactions

Appendix D contains the scientific paper submitted to ESC Transactions (ECTS), titled "Heat to H_2 - Using Waste Heat to Set Up Concentration Differences for Reverse Electrodialysis Hydrogen Production". ECTS is the official conference proceedings publication of The Electrochemical Society.

Heat to H$_2$

Using Waste Heat to Set Up Concentration Differences for Reverse Electrodialysis Hydrogen Production

Ellen S. Skilbred*[a], Kjersti W. Krakhella*[a], Ida J. Haga*[a], Jon G. Pharoah[b], Magne Hillestad[c], Gonzalo d. A. Serrano[d] and Odne S. Burheim[a]

*Shared first authorship
[a]Dep. of Energy and Process Engineering, NTNU, Norway

[b]Dep. of Mechanical and Materials Engineering, Queen's University, Canada
[c]Dep. of Chemical Engineering, NTNU, Norway

[d]SINTEF Energy Research AS, Norway

Abstract

The present work suggests two concepts for producing hydrogen by reverse electrodialysis. Reverse electrodialysis is a technology that uses concentration differences to create electrical energy. In this work, the energy is utilised as direct hydrogen production within a closed-loop system. For both system alternatives, waste heat is used to set up the mentioned concentration differences. The first concept is evaporation, where heat is added to boil off excess water from a concentrated solution and thereby increase its concentration. The second concept removes heat to precipitate excess salt. For the precipitation concept to work, a salt where the solubility is highly dependent on temperature must be used. KNO$_3$ fulfils this requirement. As part of a proof of concept, the conductivity of membranes soaked in KNO$_3$ was investigated. The conductivity of the salt in two commercialised membranes, Fumatech FKE-50 and FAS-30, was measured and compared to NaCl in the same membranes. The conductivity of K$^+$ in FKE-50 was found to be 4.5 and 6.6 mS cm^{-1} at 25 °C and 40 °C respectively. The conductivity of NO$_3^-$ in FAS-30 was found to be 4.3 mS cm^{-1} and 6.5 mS cm^{-1} at 25 °C and 40 °C respectively. Neither of the membranes change conductivity with soaking concentrations. The conductivity at 40 °C compared to 25 °C is significantly better in the FKE membrane, and seemingly better in the FAS membrane. Potential peak power densities

for a RED unit cell is 1.29 W m^{-2} with the precipitation system, and 28.1 W m^{-2} when evaporation is used.

Introduction

The increased global energy demand and undesired climate changes motivates studies of new renewable energy sources. Energy for the future needs to be rapidly provided, dependable and have as low negative impact as possible. The most commercial renewable energy technologies, like wind and photovoltaics, delivers energy intermittently and electrically. Supply and consumption fluctuations do not necessarily match, making energy storage important to provide energy where and when it is needed. Storing renewable energy in hydrogen is one alternative to handle the potential mismatch of energy supply and consumption. This article suggests two methods for converting waste heat to hydrogen through reverse electrodialysis (RED).

RED is a technology that converts the energy of mixing two solutions of different salinity to electrical energy while driving a red-ox reaction (20, 26). Ionic solutions of different concentrations are supplied on each side of an ion exchange membrane. Ions will then seek to even out concentration differences and travel through the membrane. This, in turn, establishes an electrical potential, which increases when several membranes are combined in a stack. Similar attempts using membranes to drive ions through membranes with different temperature solutions have been attempted briefly before, but in different solutions and only with electric energy as a potential output (21). When the potential established by the reverse electrodialysis is higher than the potential required for water splitting, hydrogen evolution is possible (13, 22). Anion and cation exchange membranes (AEM and CEM) control the transport of ions from the concentrated to the dilute solutions. A RED stack is illustrated in Fig. 1.
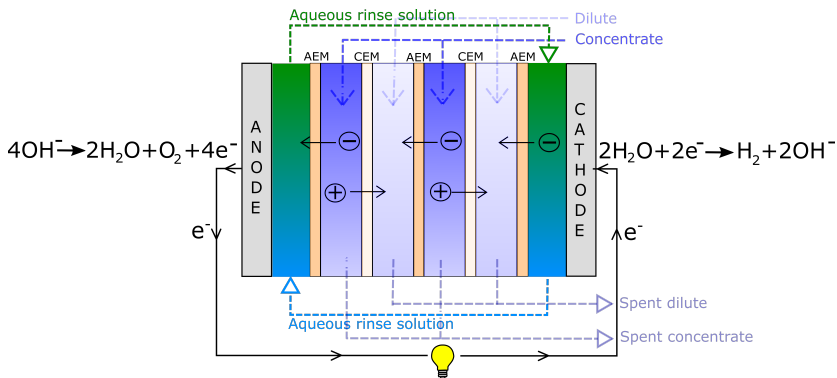

Figure 1. Illustration of a RED-cell. Hydrogen is produced by the cathode and oxygen at the anode.

The open circuit potential, E_{ocp} [V], over a RED unit cell is given by

$$E_{OCP} = \alpha \frac{RT}{zF} \ln \left(\frac{a_c}{a_d} \right) \qquad [1]$$

where α is the apparent permselectivity of the membrane defined as $E_{OCP}^{measured}/E_{OCP}^{theoretical}$, R is the gas constant, T [K] is the temperature, z is the valence number of the ions transported, F is Faraday's constant, and a is the activity of the transported salt in the concentrated, c, and dilute, d, solutions (3).

The total potential in a unit cell is given in Eq. 2. Non-ohmic losses are not considered in this paper.

$$E = E_{OCP} - rj \qquad [2]$$

where j is the current density in A m^{-2}. Area resistance r [Ω m^2] is given in Eq. [3].

$$r = r_d + r_c + r_{CEM} + r_{AEM} \qquad [3]$$

The resistance of the solutions, r_d and r_c is the solution resistivity, ρ [Ω m], multiplied with the compartment thickness, and r_{CEM} and r_{AEM} are the resistance of the membranes. The power density is the cell potential multiplied with the current density.

$$P = E_{OCP}j - rj^2 \qquad [4]$$

The first focus of RED was to exploit the energy of mixing when natural seawater mix with less saline water (14, 20, 25, 26). In the later years, attention has been given to closed-loop RED stacks, where heat is utilised for reversing the salt solutions back to their original concentrations (11, 15, 16, 18, 27). The recycling of solutions increase the economical feasibility of using other salts than NaCl and allows for a freer choice of concentrations than those found in nature, in addition to preventing fouling mechanisms. From Eq. [1] we see that it is beneficial with a large concentration gradient over the membrane and a high temperature. The latter was tested experimentally by Długołęcki et al. and Van Egmond et al. (4, 23), among others.

The cell potential will be lower than the theoretical for a number of reasons, including concentration polarisation and ohmic losses. When compartment thicknesses and solution concentrations are optimised, ionic resistance in the membranes is the main contributor to ohmic losses (10, 14).

We suggest reversing the concentrations used in RED by a thermal separation unit shown in Fig. 2, that is either evaporating water from the used concentrate or precipitating a slurry from the used dilute. An ideal salt solution would have a pronounced change in ts solubility in response to temperature changes. NaCl, which is the salt most used in RED experiments, do not have a steep solubility curve slope, and will thus not give significant
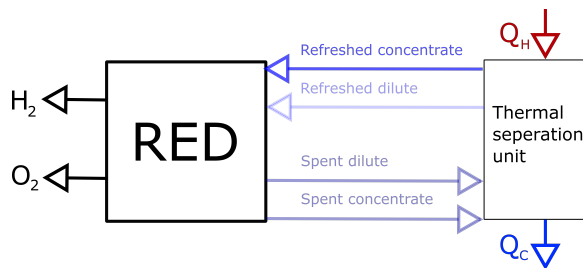
Figure 2. Reversing the spend concentrations from RED using a thermal separation unit.

potential in the precipitation system. An alternative is KNO_3, where a higher potential is achievable given that membrane conductivity is not a limiting factor. To investigate this, conductivity measurements of AEMs and CEMs soaked in KNO_3 at 25 °C and 40 °C are performed for concentrations up to the saturation point.

Concept

The phase separation process is the key to regenerate spent solutions in the closed-loop RED-systems that are presented. If the spent electrolytes are recovered, heat may be used to restore them to their initial states. This ensures that heat is the only consumable in the system, preferably at as low temperature as possible. Such heat is of low quality and is seldom put to use, often referred to as low grade waste heat (5). As mentioned, two methods for separation are presented; evaporation and precipitation.

As the achievable concentration difference will differ between the techniques, the stack potential is likely to differ too. Simultaneously, the heat and temperatures required to run the process are not the same in the two cases and this may affect the internal energy consumption. This will be elaborated in the next two sections.

Evaporation

A principle sketch of a separation system using evaporation is shown in Fig. 3a. Here, external heat is added to the concentrate, making the water boil off at low pressure. Eventually, the concentration will be high enough for the original potential to be restored, while the removed water will ensure a low concentration in the dilute electrolyte. For improved energy efficiency, the condensation energy of the pure water should be used to maintain the temperature in the separation container.

This separation system is presumably energetically disadvantageous, as large quantities of heat are required to make the water evaporate and because of the need for compressor power. Heat exchange capacity is also associated with large capital costs. However, this system allows for lower concentrations in the dilute compartment, as the precipitation
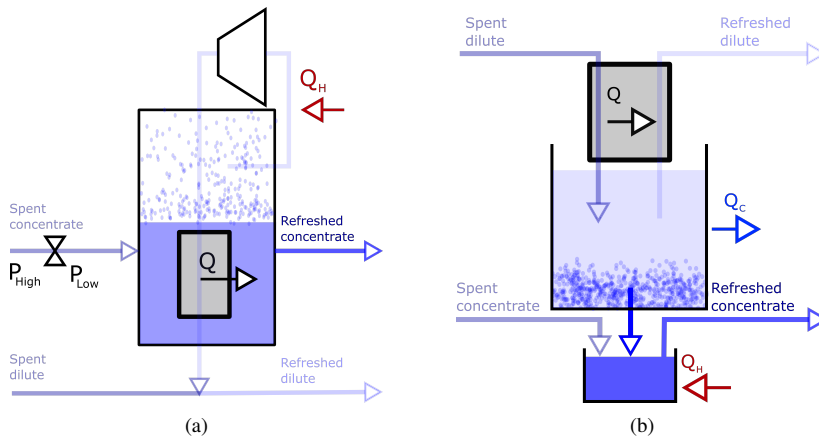
Figure 3. Sketch of principle of (a) separation by evaporation and (b) separation by precipitation

temperature is no longer a limitation. This increases the possible Nernst potential. This electrical gain must be weighted against the disadvantages when the system is evaluated. If the heat added is surplus, meaning that it would not have been put to any other use, the actual heat quantity and temperature may be of less importance.

Precipitation

As previously mentioned, the salt used in this concept needs to have solubility that change substantially with temperature. The dilute concentration in the RED stack is at the solubility limit at a low temperature while the concentrated concentration equals the saturation concentration at a higher temperature. The stack will be operated under conditions where neither solution will spontaneously precipitate, ensuring that all separation happens in the intended components.

Spent dilute is cooled until it precipitates. The excess salt is transported to the used concentrate where it dissolves. The transportation is envisioned to take place in an Archimedes pump based transport unit where a slurry of the precipitate is continuously in motion to avoid accumulation and solid precipitation of salt. Both electrolytes are now reset and may be fed back into the stack. This is illustrated in Fig. 3b.

To avoid high energy consumption for cooling, it is wise to choose a lower saturation temperature that corresponds to the temperature of any available cooling, e.g. seawater. The use of natural cooling will significantly reduce the energy consumption, and thus increase the potential for large scale operation.

Experimental

To investigate the membrane behaviour in the actual RED-system, the membranes are prepared in the relevant electrolytes and conductivities are measured at the relevant concentrations and temperatures. The membrane conductivities are included in a simple model of the RED power density for the two separation systems.

In precipitation, the dilute solution should be 21.3 g KNO_3 / 100 g H_2O, which is the solubility limit at 10 °C. For evaporation, the dilute solution is restricted by the ohmic losses in the dilute compartment; therefore, the concentration is chosen to be 0.2 g KNO_3 / 100 g H_2O. The concentrated solutions for both techniques are 38.3 g KNO_3 / 100 g H_2O and 45.6 g KNO_3 / 100 g H_2O, which is the solubilities at 25 °C and 40 °C respectively.

Two membranes from Fumatech GmbH (Germany) were tested; FKE-50 (CEM) and FAS-30 (AEM) (see (8) and (6) for datasheets). The material datasheets for the membranes provide the conductivity of the membrane in NaCl form. Since this conductivity has been found through a different test procedure, we wanted to verify that our method gives similar results. The verification was successful and the results are given in Appendix A.

Membrane Preparations

The ion-exchange is performed through soaking of the membranes in KNO_3 for more than 52 hours. KNO_3 of 1 M is used, and the solution is changed at least three times. The completeness of the exchange in the CEM is verified by measuring the pH of the spent solutions, comparing the value with fresh KNO_3 before immersion. It is considered satisfactory to soak the AEMs for more than three nights, well beyond what was needed for the CEM, with solutions changed frequently. After soaking, the ion-exchanged membrane samples are prepared as round discs with a diameter of 20 mm, cut out with a wad punch.

In addition to the counter-ions that are present in the membrane due to the fixed charges, the membranes are believed to contain a small amount of solution with both anions and cations due to microcavities in the membrane structure (9). When the membranes are washed and soaked in deionized water (DI) after the KNO_3-equilibration, the co-ions, as well as the counter-ions superfluous to maintain electrical equilibrium, will be washed away. Conductivity measurements on these membranes are measuring the base conductivity of the membrane.

To compare and investigate how the membrane conductivity is impacted by electrolyte concentrations, the membranes are soaked in KNO_3 in addition to DI after the initial soaking and cutting. Batches of five samples are placed in individual vessels containing concentrations of 0 g/100 g (DI), 10.1 g/100 g (~1 M) and 25.3 g/100 g (~2.5 M) aqueous KNO_3 for at least 24 hours. In addition, five samples are also placed in a vessel containing 45.6 g/100 g (~4.5 M). This concentration equals the saturation concentration of KNO_3 at 30 °C.

Conductivity Measurements

A series of measurements are performed to establish the membrane conductivity and its relation to concentration. The cell used to measure the conductivity is shown in Fig. 4. It consists of two electrodes with wire connectors, both made from platinum with a surface area of 3.14 cm^2 and a thickness of 1 mm. They are mounted in a hard cylindrical shell, with the connectors protruding from the ends. A sliding tube is fitted closely to the cylinder, providing structural integrity while sealing the cell and keeping the membrane samples immobile. This cylindrical cell shape is common when EIS is used for experiments of this kind (2, 17).
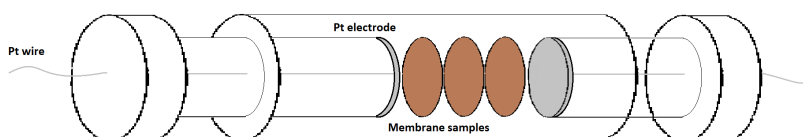

Figure 4. The cell used for measurements of conductivity

The membrane samples are placed between the electrodes of the conductivity cell. As the measurements are pressure sensitive, the cell is placed in a custom-made screw clamp, tightened with one bolt (M6, hexagonal head). A torque wrench is used to apply 2 Nm to the bolt, creating evenly distributed force due to the screw clamp. The electrodes of the conductivity cell are polished and fully polarised before use.

The membranes are taken out of solution immediately before measurements, to avoid precipitation of salt on the membrane surface, and are therefore wet during measurements. When pressure is applied on the stack of membranes, excess solution may escape to the plastic shell, which is not completely tight. Doing so, the membranes are ensured to have approximately the same solution content for each measurement.

The conductivity experiments are performed at both 25 °C and 40 °C. In the latter case, both the cell and the samples are placed in a heating cabinet, long enough prior to measurements to establish stationary temperature conditions. Temperature is measured by a K-type thermo-couple attached to the plastic shell directly behind, and in contact with, one of the platinum electrodes.

Measurements are performed with a Gamry Interface 5000E potentiostat, in a two-electrode setup. The experiments are performed through Hybrid EIS, with the potentiostat settings shown in Table I. Gamry Instruments Framework and Gamry Echem Analyst software are used to produce and analyse experimental data.

TABLE I. Hybrid EIS settings for the potentiostat

Variable	Value
AC voltage [mV rms]	**10**
DC voltage [mV rms]	**0**
Initial frequency [Hz]	**300 000**
Final frequency [Hz]	**1000**
Points/decade	**20**

Data Extraction and Obtaining Results

To account for inherent impedance from hardware, a blank experiment is run, where the electrodes are in contact. Eventually, the impedance spectrum for the dry cell at the relevant temperature is subtracted from all measurements prior to any further analysis.

The ohmic resistance, R [Ω], of the membranes is found as the high frequency resistance, where no capacitive effects are present in the measurements. In the impedance spectrum, this is the point where the imaginary part of the impedance is zero, manifesting as the intersect with the real axis. This intersection point is found through a linear regression of the impedance curve, in the range from 0 Ω to 4 Ω for the imaginary impedance.

The area resistance r [Ω m^2] is the measured resistance multiplied by the membrane sample area. r is plotted against the corresponding sample thickness. A linear regression is performed on each of the resulting plots, where the slope of each regression curve is the membrane resistivity, ρ [Ω m]. Every concentration yields one resistivity. The inverse of the resistivity is the membrane conductivity κ [S m^{-1}]. The conductivity values are then plotted against the concentrations, where the average of the four concentration-dependent conductivities is the reported membrane conductivity.

Modelling Power Density and Hydrogen Production

The unit cell power density is calculated from Eq. [4], with permselectivity at 0.9 and activity coefficients set to unity. The thicknesses of the compartments is set to 100 μm, since RED stacks have better performance with thinner spacers (24). The resistances measured for the AEM and CEM are used in the calculation of the unit cell power density. The parameters are summarised in Table II in Appendix B.

The power density is plotted versus current density, where the hydrogen production is calculated from the peak power current density and Faraday's law of electrolysis.

Results and Discussion

To achieve an open circuit potential higher than the reversible potential for the water splitting reaction, 1.23 V, the RED stack needs 66 membranes (67 in a real RED-system, since an odd number is required) using concentrations relevant for precipitation, activity

coefficients set to unity and permselectivity equal to 0.9. Using concentrations relevant for evaporation at 40 °C, the number of membranes needed is reduced to 9. To run the cell at maximum power density, twice as many membranes are needed.

The conductivity, as function of concentration and temperature, are given in Fig. 5 and 6. The conductivity of K^+ in FKE-50 is found to be 4.5 ± 0.4 mS cm^{-1} at 25 °C and 6.6 ± 1.3 mS cm^{-1} at 40 °C. These values are higher than the reported values for Na^+ from Fuel Cell Store (7). The conductivity increase significantly from 25 °C to 40 °C, but the resistance of the membrane does not change considerably with concentration. This is in agreement with previous research (19).
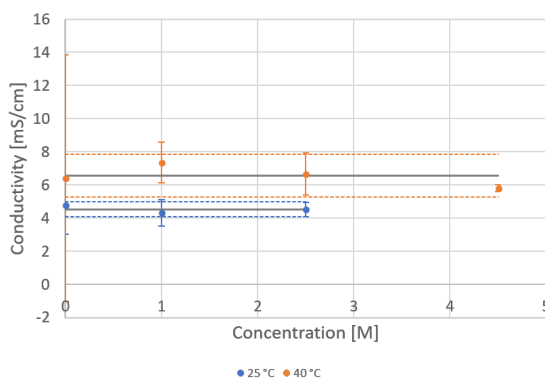

Figure 5. Conductivity of FKE-50 at 25 °C and 40 °C, with mean value and double standard deviation.

The conductivity of NO_3^- in FAS-30 was measured to 4.3 ± 1.2 mS cm^{-1} at 25 °C and 6.5 ± 2.3 mS cm^{-1} at 40 °C. These values are comparable to the reported values for Cl^- from Fuel Cell Store (6). The dependency of concentration is as negligible for FAS-30 as it is for FKE-50.

The standard deviations of the conductivity measurements are generally high, but the measurements do confirm that the conductivity of the membranes is independent of concentration. With this established, there is no need for testing membranes soaked in solutions close to the saturation point. In the future, we suggest removing more of the excess solution when testing membrane conductivity in a set-up similar to ours. This was not possible in the present work due to the risk of salt precipitation on the membrane surface when measuring membranes soaked in saturated solution.

Given these resistances, the power density of one RED unit cell has been calculated and plotted versus current in Fig. 7. The maximum power per membrane area using 21.2 and 38.3 g KNO_3/ 100 g H_2O is 0.476 W m^{-2} at 25 °C and 0.768 W m^{-2} at 40 °C. For maximum solubility at 40 °C, 45.6 g KNO_3/ 100 g H_2O, the power density is 1.29 W m^{-2}.

Using solutions of 21.2 g and 38.3 g KNO_3/ 100 g H_2O, the hydrogen production at
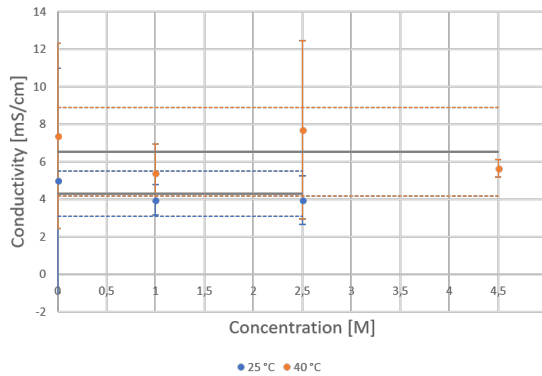
Figure 6. Conductivity of FAS-30 at 25 °C and 40 °C, with mean value and double standard deviation.
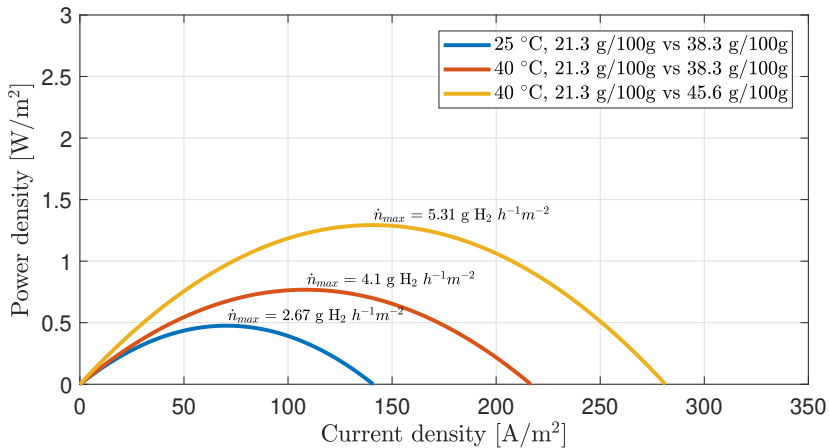

Figure 7. Power density per membrane area from a RED unit cell. Concentrations are suited for use in the precipitation separation technique with KNO_3.

peak power is 2.97 and 4.55 g m^{-2} h^{-1} at 25 °C and 40 °C, respectively. When changing to 45.6 g KNO_3/ 100 g H_2O for the concentrated solution at 40 °C, the hydrogen production is 5.91 g m^{-2} h^{-1}.

If evaporation is to be used as separation technique, the dilute concentration can be lower. The maximum power per membrane area using 0.02 and 38.3 g KNO_3/ 100 g H_2O is 20.9 W m^{-2} at 25 °C and 26.3 W m^{-2} at 40 °C. Increasing the concentrated solution to maximum solubility at 40 °C, 45.6 g KNO_3, gives 28.1 W m^{-2} power density. Power density versus current density is shown in Fig. 8.
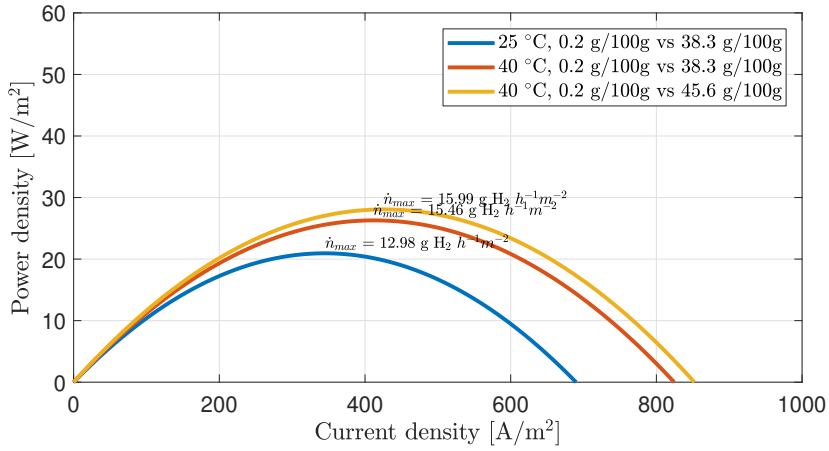
Figure 8. Power density per membrane area from a RED unit cell. Concentrations are suited for use in the evaporation separation technique with KNO_3.

The hydrogen production at peak power is 14.4 and 17.2 g m^{-2} h^{-1} at 21.2 and 38.3 g KNO_3/ 100 g H_2O at 25 °C and 40 °C, respectively. At 45.6 g KNO_3 and 40 °C, the hydrogen production is 17.8 g m^{-2} h^{-1}.

The power density in the precipitation system is more dependent on concentration difference than change in temperature. For the evaporation system, however, the power density depends more on temperature than concentration difference.

The power densities predicted in this work are not large compared to the power densities available from polymer electrolyte water electrolysers (PEMWE), which can reach power densities in the order of 50 kW m^{-2} and current densities around 20 kA m^{-2} (1). The nature of the two systems are rather different, as a PEMWE is a device meant to adsorb electric power for hydrogen production and the present system is intended to adsorb low quality heat for hydrogen production. Moreover, the material selection is very different of the two, as the RED HeatToH2 system has its min cost driver in hydrocarbon based membranes and the PEMWE has its cost driver in perfournated membranes (Nafion), Pt-group catalyst (Ru, Rh, and Ir) in addition to corrosion treated titanium porous support and bipolar plates. To assess the viability of the RED systems presented, one must consider that the electricity cost will be lower than for electrolysers. A detailed cost analysis, along with potential measurements for RED stacks with the relevant salt, concentration and temperature, is necessary for addressing the viability of the two concepts.

Conclusion

Two concepts for producing hydrogen from waste heat using RED were presented; one where salt is precipitated from spent dilute and one where water is evaporated from spent concentrate. As part of proof of concept for the precipitation method, the conductivity of a CEM and an AEM in KNO_3-form has been tested.

The results show that at 25 °C, FKE-50 has higher conductivity in K^+-form than in Na^+-form at 25 °C, while the average conductivity of FAS-30 in NO3$^-$-form is similar to its conductivity in Cl^--form. Neither of the membranes change conductivity with concentration of solution in the membrane.

The conductivity of K^+ in FKE-50 is significantly better at 40 °C than 25 °C. For FAS-30 the conductivity of NO_3^- is seemingly better at 40 °C than 25 °C, but the standard deviation is too high to confidently conclude. Based on these observations, KNO_3 is suitable for use in a RED system where solutions are regenerated by waste heat, and higher conductivities are expected at 40 °C than 25 °C.

The peak power hydrogen production per membrane area at maximum concentration difference is 4.25 g m^{-2} h^{-1} at 40 °C, and 2.97 g m^{-2} h^{-1} at 25 °C, for using precipitation. When using evaporation as separation technique, however, the peak power hydrogen production is 27.7 g m^{-2} h^{-1} at 40 °C and 14.4 g m^{-2} h^{-1} at 25 °C. The maximum peak power density available using evaporation is over 20 times higher than the available maximum peak power density using precipitation at 20 °C, and over 30 times better at 40 °C. The precipitation as separation needs to be equally less expensive to match the evaporation system.

References

1. U. Babic, M. Suermann, F. N. Büchi, L. Gubler, and T. J. Schmidta. *Journal of the Electrochemical Society*, 164:F387 – F399, 2017.

2. E. Barsoukov and J. R. Macdonald. *Impedance spectroscopy: theory, experiment, and applications*. John Wiley & Sons, 2005.

3. O. S. Burheim. *Engineering Energy Storage*. Academic Press 2018, 2017.

4. P. Długołęcki, A. Gambier, K. Nijmeijer, and M. Wessling. *Environmental Science and Technology*, 43(17):6888–6894, 2009.

5. Enova SF. Annual Report 2009 - Enova. Technical report, Enova, 06 2010.

6. Fuel Cell Store. *Technical Data Sheet - fumasep®FAS-30*, 2018.

7. Fuel Cell Store. *Technical Data Sheet - fumasep®FKE-50*, 2018.

8. Fuel Cell Store. *Technical Data Sheet - fumasep®FKS-50*, 2018.

9. A. Galama, D. Vermaas, J. Veerman, M. Saakes, H. Rijnaarts, J. Post, and K. Nijmeijer. *Journal of Membrane Science*, 467:279 – 291, 2014.

10. E. Güler, R. Elizen, D. A. Vermaas, M. Saakes, and K. Nijmeijer. *Journal of Membrane Science*, 446:266 – 276, 2013.

11. M. C. Hatzell, I. Ivanov, R. D. Cusick, X. Zhu, and B. E. Logan. *Phys. Chem. Chem. Phys.*, 16:1632–1638, 2014.

12. T. Isono. *Journal of chemical and engineering data*, 29(1):45–52, 1984.

13. Y. Kim and B. E. Logan. *Proceedings of the National Academy of Sciences*, 108(39):16176–16181, 2011.

14. R. Lacey. *Ocean Engineering*, 7(1):1–47, 1980.

15. X. Luo, X. Cao, Y. Mo, K. Xiao, X. Zhang, P. Liang, and X. Huang. *Electrochemistry Communications*, 19:25 – 28, 2012.

16. X. Luo, J.-Y. Nam, F. Zhang, X. Zhang, P. Liang, X. Huang, and B. E. Logan. *Bioresource Technology*, 140:399 – 405, 2013.

17. F. Müller, C. A. Ferreira, D. S. Azambuja, C. Alemán, and E. Armelin. *The Journal of Physical Chemistry B*, 118(4):1102–1112, 2014.

18. J.-Y. Nam, R. D. Cusick, Y. Kim, and B. E. Logan. *Environmental Science & Technology*, 46(9):5240–5246, 2012. PMID: 22463373.

19. J.-S. Park, J.-H. Choi, J.-J. Woo, and S.-H. Moon. 300(2):655 – 662, 2006.

20. R. Pattle. *Nature*, 174:660, 1954.

21. B. B. Sales, O. S. Burheim, S. Porada, V. Presser, C. J. Buisman, and H. V. Hamelers. Extraction of energy from small thermal differences near room temperature using capacitive membrane technology. *Environmental Science & Technology Letters*, 1(9):356–360, 2014.

22. R. A. Tufa, E. Rugiero, D. Chanda, J. Hnàt, W. van Baak, J. Veerman, E. Fontananova, G. Di Profio, E. Drioli, K. Bouzek, et al. *Journal of Membrane Science*, 514:155–164, 2016.

23. W. J. van Egmond, U. K. Starke, M. Saakes, C. J. Buisman, and H. V. Hamelers. *Journal of Power Sources*, 340:71–79, 2017.

24. D. Vermaas, M. Saakes, and D. Nijmeijer. *Environmental science & technology*, 45(16):7089–7095, 2011.

25. J. Weinstein and F. Leitz. *Science*, 191(4227):557–559, 1976. cited By 183.

26. G. L. Wick. *Energy*, 3(1):95–100, 1978.

27. X. Zhu, W. He, and B. E. Logan. *Journal of Membrane Science*, 494:154 – 160, 2015.

Appendix

A Verification of conductivity measurement method

FKS-50 and FAS-30 are soaked in NaCl and tested the same way as the KNO_3-soaked membranes. The conductivity results are shown in Fig. 9 and 10.
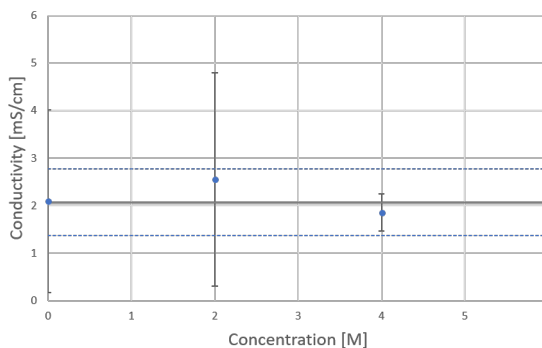

Figure 9. Conductivity of FKS-50 at 25 °C, with mean and double standard deviation.

The conductivity of Na^+ in FKS-50 was found to be 2.1 ± 0.7 mS cm^{-1} at 25 °C which is in the range of what Fuel Cell Store give in their datasheet for the given membrane (8).
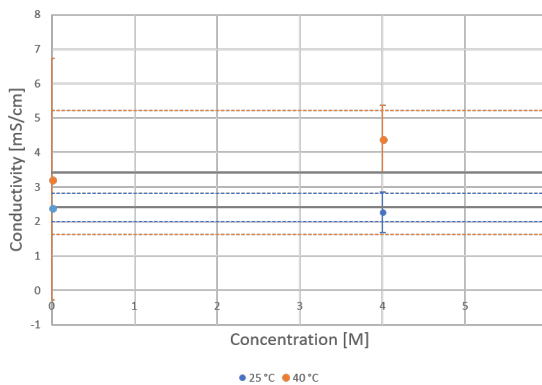

● 25 °C ● 40 °C

Figure 10. Conductivity of FAS-30 at 25 °C and 40 °C, with mean and double standard deviation. Fuel Cell Store reported 3-7 mS cm^{-1} at 25 °C.

The conductivity of of Cl^- in FAS-30 was found to be 2.4 ± 0.4 mS cm^{-1} and 3.4 ± 1.8 mS cm^{-1} at 25 °C and 40 °C respectively, which is within the lower range of what Fuel

Cell Store give in their datasheet for the given membrane. This means that our method does not overestimate the conductivity compared to the test provided in the datasheet.

B   Variable used in modelling cell potential and power density

TABLE II. Values used to calculate open circuit potential and unit cell resistance in RED

Variable name	Value
Mean permselectivity [-]	0.9
Temperature[K]	298 and 313
Activity coefficient [-]	1
Channel height [m]	1.00×10^{-4}
Resistivity 0.200 g KNO_3/100g H_2O 25 °C [Ω m^2]	1.67e-04**
Resistivity 0.200 g KNO_3/100g H_2O 40 °C [Ω m^2]	1.84e-06*
Resistivity 21.4 g KNO_3/100g H_2O 25 °C [Ω m^2]	6.83e-06**
Resistivity 21.4 g KNO_3/100g H_2O 40 °C [Ω m^2]	5.18e-08*
Resistivity 38.3 g KNO_3/100g H_2O 25 °C [Ω m^2]	5.12e-06**
Resistivity 38.3 g KNO_3/100g H_2O 40 °C [Ω m^2]	3.66e-08*
Resistivity 45.6 g KNO_3/100g H_2O 40 °C [Ω m^2]	3.46e-08*

*Measured for concentrations 0, 0.2, 2, 13.64, 21.36, 31.93 and 45.56 g / 100 g H_2O. Linear regression is used to find the resistance at the correct concentration.
**Found from (12). Linear regression is used to find the correct value.